12-1985

Investigation of Electronic Holography using SPICE Computer Simulation Experiments

Monish Ranjan Chatterjee
University of Dayton, mchatterjee1@udayton.edu

INVESTIGATION OF ELECTRONIC HOLOGRAPHY USING SPICE COMPUTER SIMULATION EXPERIMENTS

by

Monish Ranjan Chatterjee

A thesis submitted in partial fulfillment of the requirements for the degree of Doctor of Philosophy in Electrical and Computer Engineering in the Graduate College of The University of Iowa

December 1985

Thesis supervisor: Professor Adrianus Korpel

Graduate College
The University of Iowa
Iowa City, Iowa

CERTIFICATE OF APPROVAL

PH.D. THESIS

This is to certify that the Ph.D thesis of

Monish Ranjan Chatterjee

has been approved by the Examining Committee for the thesis requirement for the Doctor of Philosophy degree in Electrical and Computer Engineering at the December 1985 graduation.

Thesis committee: _____
Thesis supervisor

_____
Member

_____
Member

_____
Member

_____
Member

D E D I C A T I O N

Dedicated to the memory of my Mother,
My Mentor and Guiding Light.
To my Father,
My Rock of Gibraltor.
To Grandma,
For her love, caring and understanding.

ACKNOWLEDGMENTS

I would prefer to keep this brief, as acknowledgments tend to be as hackneyed as the award shows. Yet, the friendship, guidance and help I have received during my work on this report have been so invaluable that I simply must mention the following names at the very least.

My foremost gratitude goes to Professor Korpel, my adviser throughout graduate school. In retrospect, I realize how fortunate my fellow advisees and I have been to have had the opportunity to benefit from Professor Korpel's scientific insight, creative acumen, inexhaustible zest for research, and incorruptible professionalism. In my own case, graduate school has been a period of great stimulation interspersed with humbling moments of self-evaluation. I am indebted to Professor Korpel for his forebearance and support through some difficult times.

I would like to thank the members of my thesis committee for their time and encouragement. In particular, I wish to thank Professors Reddy, Lonngren, Vogel, and Malik for their ready accessibility and willingness to help over the years.

Mere words of thanks cannot measure my indebtedness to my brother Manas and his wife Sharmila; my sister Mamata and her husband Samir; my favorite aunts Anima and Nilima; and everyone else whose good wishes sustained me. Their love is not forgotten.

The friendships I have made here are truly global, and led to some great moments. Poon, from Hong Kong, introduced me to the fanfare of college football in between doses of Feynman diagrams and astrophysics. My long time colleague and roommate Partha enmeshed me to the life in Iowa City in the great blizzards of 1980. Ron, my best American friend, discussed endlessly the imminence of a nuclear holocaust, and his appreciation of ethnic cuisines. Willy, from Belgium, showed me the logical solution of the cube puzzle at the miracle angle of 54 degrees! Gaetano, from Italy, made me taste the worst cup of "espresso" ever percolated. Solomon, from Hong Kong, patiently suffered through my incompetence in basketball and automobiles. And Mathews, from India, gave me some trade secrets in starting out as a teacher of EE.

This page would not be complete without mentioning Shirley, Carma, and Tung-Mei- a trio of the most helpful, cheerful and friendly secretaries anywhere. They always made things much easier.

Finally, I would like to thank two special friends : Sharon, who, with her poetic vision and irrepressible curiosity, showed me where the colors and the songs were in Nature, and with whose intense love for life outside the classroom my innermost feelings became resonant; and Sheila, whose youthful candor gave me a better perspective on the adult world.

TABLE OF CONTENTS

LIST OF FIGURES

LIST OF TABLES

CHAPTER I

INTRODUCTION

Since the discovery of the spin-echo by Hahn [1] in 1950, the study of nonlinear echoes has evolved continuously into a very wide research area ranging from photon and cyclotron echoes to echoes in piezoelectric crystals and powders. In recent years, short- and long-term echoes in various nonlinear systems have been studied by several groups [2,3,4,5]. Table 1.1 summarizes the echo systems and their principal characteristics. A comprehensive review of the investigations in this field can be found in [6].

The short-term or dynamic echo (also called a 2-pulse echo) arises in a system due to one or more of the following nonlinearities :

(a) Nonlinear excitation,

(b) Anharmonicity,

(c) Energy-dependent collisions or loss.

It has been established that the mechanism for echo generation resides in the parametric interaction of a collection of resonators or eigenmodes with an applied electric field in the presence of an odd-order nonlinearity.

The nonlinearity is commonly manifested in the excitation amplitude, or, in some cases, in an amplitude-dependent shift of the oscillator or mode frequencies. In either case, the result is that the system, excited at t=0 by a "write-in" pulse, followed at t=τ by a "recall" pulse, undergoes phase conjugation in the frequency domain, which, in the time domain, leads to a physical reversal of the signal in space and time, thereby producing at t=2τ an "echo" of the "write-in" pulse.

The twin processes of phase conjugation and time reversal are the underlying mechanisms in virtually all dynamic echo systems, from spin echoes to echoes in piezoelectric powders. Phase conjugation can be brought about only by the presence of a nonlinearity in the system. Thus, the principles of phase conjugation and time reversal apply to all three types of nonlinearities mentioned earlier, although the variation of the echo amplitude with the pulse separation is different for each type of nonlinearity. In some cases, however, the description of the echo by phase conjugation and time reversal is more mathematical than physical.

Fig.1.1 gives a convenient physical picture of how phase conjugation automatically leads to time reversal and hence an "echo". Thus, when the phases $\exp(j\phi_\tau)$ of the

oscillators in an ensemble are conjugated at $t=\tau$ to $\exp(-j\phi_\tau)$, it is easy to see that at $t=2\tau$, the oscillators rephase, thereby generating an "echo" of the original signal pulse.

A large number of theories and models have been suggested to explain static and dynamic echo phenomena. These range from models based on precessing magnetic spins and dipoles to electroacoustic interaction and particle orientation [7,8,9,10]. However, most theories have been unable to integrate the various aspects of nonlinear echoes under a common principle. Thus, while appearing to explain the dynamic 2-pulse echo fairly well, the electroacoustic interaction model, for example, cannot readily account for the virtually indestructible static echo.

In 1978, Korpel proposed a parametric theory to explain the dynamic echo [11]. In this theory, the system of independent oscillators or propagating eigenmodes is visualized as a "Fourier Space", where the spectral components of an input signal are preserved physically by the individual particles or modes. When excited by an input pulse, the individual oscillators or modes respond independently to different frequencies, and continue to do so even after the macroscopic signal loses phase coherence and decays due to the finite system bandwidth. Thus,

effectively, the Fourier transform of the signal pulse is now "stored" in the system. The "recall" pulse triggers a nonlinear mechanism by which a parameter in the system (static electric field across a crystal [9] or capacitance in an oscillator) is made to vary at 2ω, where ω is the resonant frequency of the oscillator. It can be shown readily that the above process leads to an echo pulse at $t=2\tau$ following two delta pulses applied at $t=0$ and $t=\tau$ respectively.

The merit of the parametric formalism lies in the fact that in addition to explaining dynamic pulse echoes, it may also be extended to any general signal e(t) of finite duration. If $\phi(\omega)$ is the frequency spectrum of e(t), it may be shown that, for a cubic nonlinearity, the spectrum of the parametrically generated signal $E'(t)$ is proportional to $\phi^2\phi^*$, where the star denotes complex conjugate. In the time domain, this corresponds to a triple product involving convolution and correlation. In particular, if e(t) consists of an arbitrary, finite-duration signal $e_1(t)$ and a delta pulse, then $E'(t)$ is shown to represent a delayed, time-reversed version of the signal $e_1(t)$ itself. It is also interesting to note that the triple product formalism is analogous to the one used in Fourier holography, if $\phi(\omega)$ is taken to represent the sum of the reference wave and the signal wave.

Furthermore, the parametric formalism can be used to analyze the long-term or memory echo as well. By assuming that the coupling factor K to the individual oscillators is modified by the input signal e(t) as $\Delta K \propto |\phi(\omega)|^2$, the recalled signal $E''(t)$ can be shown to involve a convolution and correlation triple product of e(t) and $e_r(t)$, where $e_r(t)$ is the recall pulse applied at t=T. If e(t) consists of two well-separated functions $e_1(t)$ and $e_2(t-\tau)$, the useful part of the recalled signal in this case will be a non-time-inverted replica of e_2 centered at $t=T+\tau$, whenever e_1 is a delta pulse.

The implications of the above results are significant, and hence our efforts to investigate in detail the various aspects of the parametric formalism from both short- and long-term perspectives. From the mathematics of the parametric formalism, as well as the physics of nonlinear echoes, it is clear that such phenomena can be used in novel methods of signal processing, like convolution, correlation, frequency-selective storage, pulse compression, wavefront reconstruction, and, most of all, permanent storage and recall of arbitrary analog signals.

In many ways, the parametric formalism is strikingly similar to the principles of optical holography. Thus, analogous to optics, both the phase and amplitude of the

spectral components of a signal E_1, are stored by recording the pattern of interference with a signal E_2. The original signal is then reconstructed by using an appropriate "read-out" signal. Hence, the parametric formalism may be called "electronic holography".

The convolution and correlation triple product as formulated by Korpel for a memory echo is, curiously enough, identical to that suggested by Gabor [12,13] in his follow-up papers to Longuet-Higgins' work on "holographic model of temporal recall" [14]. Intrigued by the behavioral problem of recall and recognition, Longuet-Higgins suggested a model consisting of a bank of resonators whose coupling constants were to be altered by an amount proportional to the energy in the spectral components to be stored. When working on this specific problem, neither Longuet-Higgins nor Gabor appear to have been aware of the then emerging field of nonlinear echoes. Korpel, on the other hand, was unaware of the Longuet-Higgins and Gabor papers when deriving his parametric theory of short- and long-term echoes. The above represents a remarkable concurrence of ideas, and actually demonstrates that electronic holography is more universal than just a possible storage and recall mechanism of the brain.

In the initial stages of our investigation, our thoughts were to construct physical models of actual systems, using nonlinear electronic resonators. Korpel's own experiments with electronic holography [11] prior to 1978 using 20 parallel LC circuits tuned 25KHz apart around 2MHz, with varactor diodes as the nonlinear elements, proved to be quite encouraging. These experiments with relatively few resonators clearly demonstrated that 2- and 3-pulse echoes could be generated in accordance with the principles of electronic holography. However, due to the limited number of resonators used, the experiments could not demonstrate the generalized properties of electronic holography, like time-inverted and non-time-inverted recall of arbitrary signals.

We later conjectured that trying to build and test 100 or more nonlinear circuits involved insurmountable complexities. In light of today's advanced VLSI and other integrated circuit technologies, one might be tempted to perform echo experiments with such circuitry. However, it must be realized that a successful echo experiment requires a high density of resonators tuned to a wide band of frequencies, with each resonator having a highly selective frequency or amplitude-dependent nonlinear element. Tailoring a nonlinear element to a specific type of

nonlinearity is a prohibitively difficult task. Hence we eventually decided not to pursue echo experiments via electronic hardware.

Our next attempt was to explore the possibilities of carrying out novel echo experiments in acoustic media with comprehensible acoustic modes over a broad range of frequencies. These investigations took many months of experimental testing, with mostly negative results.

In our work with PZT transducers of different shapes, sizes and electrode structures, mode spectrum (using frequency sweeps) and tone burst experiments indicated that although a high density of modes was present, the resonances, in general, appeared in clusters separated by regions of relatively few resonance peaks. The main cluster was usually around the thickness resonance f_T of the device. Subsequent clusters appeared to be more pronounced near odd-order harmonics (though progressively weaker) of f_T. Fig.1.2 shows a typical mode spectrum plot.

For the purpose of nonlinear signal storage, it is desirable to have a large number of resonances which are as uniformly distributed as possible. Most of the resonance experiments yielded spectral and temporal data that were hopelessly mangled and incomprehensible. The resonances were spurious and non-uniform, and modes were hard to identify.

These results were perhaps to be expected, considering the extremely complicated ω-k patterns for the various modes that may be excited in elastic plates and cylinders, as shown in Fig.1.3 [15].

The only resonance experiments that appeared to produce meaningful results consisted of tone burst and d.c. bias experiments with thin PZT-5 plates. The typical plate dimensions were $75\times35\times0.25mm^3$, and the frequency range was between 1KHz to about 10MHz. Fig.1.4 shows the diagram of a typical PZT-5 plate used in the resonance experiments. The typical ω-k characteristics of some of the lowest order modes in a plate are shown in Fig.1.5. The preliminary experiments with short bursts (~5μs) in the range 1KHz-5MHz showed essentially two "clean" modes: a longitudinal (plate) mode, and (presumably) a shear mode. The modes (particularly the shear) appeared to be dispersive, since the burst arrival times varied with the frequency. The horizontal shear mode in principle is not dispersive but could become so at low frequencies due to the finite transverse plate dimensions. For very low frequencies, the modes would seem to break up, while for frequencies above 5MHz, they would disappear (this could be due to the large attenuation at high frequencies). An experimental plot of group velocity v_g as a function of frequency indicated that the longitudinal

plate mode was essentially non-dispersive over 200KHz-2MHz, with v_g~3200m/sec. The shear mode, however, was clearly dispersive in the same range, since v_g was found to vary from 1600m/sec to 2150m/sec.

To test if a strong R.F. pulse would induce nonlinearity in the modes (which is required for an echo experiment), a d.c. bias was applied to the sample across a separate pair of electrodes. With the bias varied from 0-400V (resulting in a maximum field of 16kV/m, close to the breakdown field) across the plate, there was negligible change in the amplitude of both the plate and the shear modes. However, on an expanded time scale, a change in the arrival times of both modes could be clearly observed. The velocity change was found to be 1.5% for the plate mode and 2.3% for the shear mode. Thus, it was evident that the bias induced weak nonlinearities.

At this stage in our investigations, we decided to change directions and conduct design and execution of model experiments to test the theoretical foundations of electronic holography by using the SPICE simulation program. This, to our surprise, led us to discover that SPICE is indeed suitable for simulating large scale systems, with accurately controlled nonlinear parameters. It therefore seems possible that SPICE may be used effectively to

simulate a wide variety of other nonlinear experiments as well.

To check how well SPICE could control a nonlinear parameter, we started with simple experiments of which the outcomes were known beforehand. Later on, however, with more complicated inputs and circuits, SPICE predicted completely unexpected responses. It was subsequently confirmed that these responses were not computer artifacts but instead reflected the real physics of the situation. These findings attest to the reliability of SPICE in describing complicated systems accurately.

Using SPICE experiments, it has been possible to verify most of the important aspects of electronic holography. The generation and properties of dynamic echoes under different types of nonlinearities have been extensively tested, and some new information has been garnered in the process. The case of pulse and generalized memory echoes has also been tested, and the results have been fairly satisfactory. Most of all, the simplicity with which the intriguing concept of memory echoes has translated into the circuit implementation on SPICE, and the closeness of the results to predicted behavior have been somewhat of a pleasant surprise.

Since the SPICE computer modeling experiments have been the main thrust of this research, we devote the remaining chapters in this thesis to detailed discussion of those experiments. The organization is as follows.

In chapter II we discuss dynamic echoes with anharmonic nonlinearity. We start with simple modeling experiments which are later extended to more complex nonlinear circuits. The effects of instability, the generation of linear echoes, and the nonlinear echo dependence on the pulse separation τ and the pulse amplitudes A_1 and A_2 are discussed. The results are compared with the analytic theory developed in the appendices. Both pulse and general signal excitations are discussed, and the unexpected splitting of the echo at high level excitation is reported. Finally, time-inverted recall (with exact analog as well as sampled inputs) and non-time-inverted recall of arbitrary signals (it is shown that the latter are not feasible in the dynamic domain) are discussed in some detail.

Chapter III details dynamic echo experiments with nonlinear coupling. We discuss briefly how efforts at creating nonlinear excitation configurations proved to be futile (once again, we learned through SPICE why such configurations would not work), and led us finally to the

simpler and useful output coupling configuration. The gradual build-up from single to multiple circuits, and the echo dependence on τ, A_1 and A_2 are then discussed. Time-inverted recall experiments are also reported.

Chapter IV is a relatively short chapter in which we discuss, for the sake of completeness, the case of dynamic echoes with nonlinear damping. It is shown how an input nonlinearity configuration automatically leads to a predominantly nonlinear damping environment. Although the SPICE experiments in this case have been relatively inconclusive, we attempt to study theoretically the feasibility of generating dynamic echoes using nonlinear loss. We show by comparing the theoretical results with the SPICE experiments that with the parameters chosen, generation of the echo under nonlinear loss is not possible since at least one of the important conditions is violated.

Long-term or memory echoes, which are the most intriguing of all nonlinear echo phenomena, have been studied by using electronic holography principles on SPICE. The results are presented in chapter V. We restrict ourselves to an ensemble of linear resonators similar in structure to that used for nonlinear coupling. It is shown how, very simply, by altering the individual circuit coupling parameter in accordance with the amplitude squared

of the corresponding spectral component in the input, it is possible to realize memory echoes with practically no limit to the recall time. This is perhaps the most versatile phenomenological implementation of the memory echo in the sense that it treats pulse as well as arbitrary input signals, and places no restriction on the recall time, in contrast to previous explanations for "anomalous persistence" based on acoustic holograms, particle orientation or plastic deformation [16,17,18]. Time-inverted and non-time-inverted memory echoes of arbitrary inputs are also realized with electronic holography principles. We also present, as a general signal processing demonstration, the case of a static echo correlator.

Chapter VI concludes this document by evaluating the overall SPICE performance, its feasibility, limitations, speed and costs of implementation. The merits of the parametric formalism and electronic holography in explaining most aspects of nonlinear echoes are also briefly overviewed.

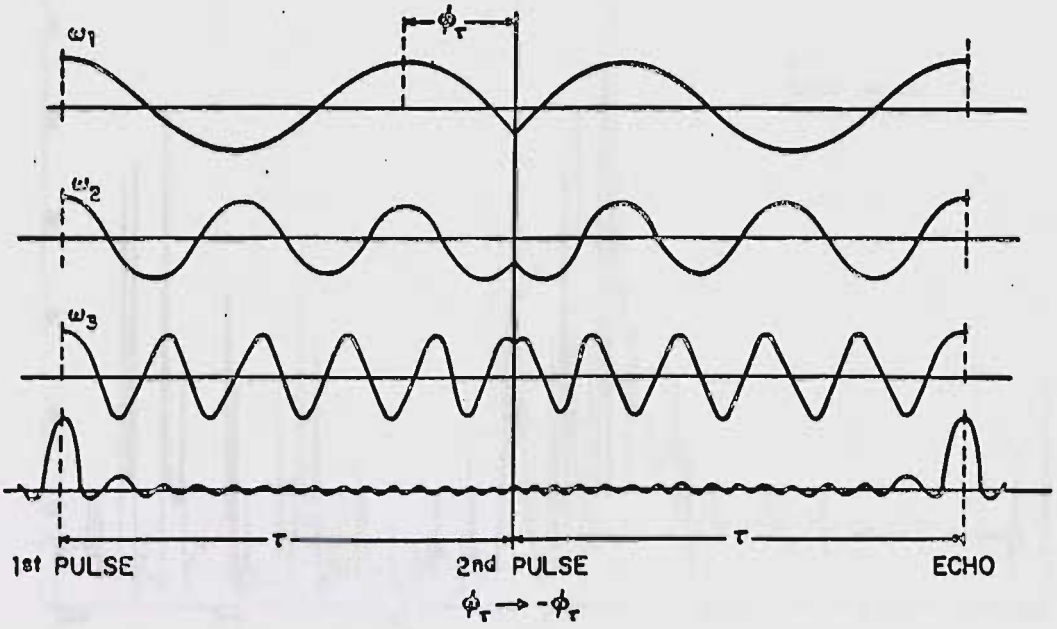

Figure 1.1. Illustration of phase conjugation concept. Only three frequency components are shown (after Korpel and Chatterjee [6]).

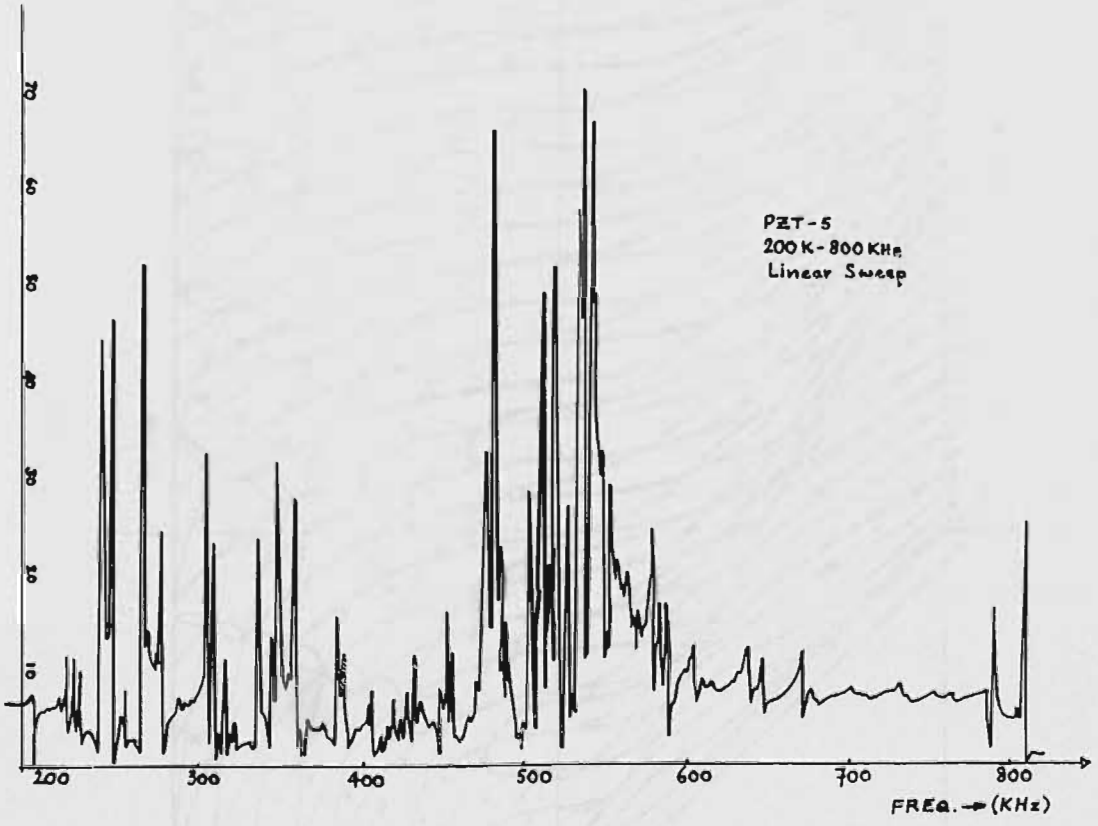

Figure 1.2. Typical mode spectrum plot for PZT-5 plate.

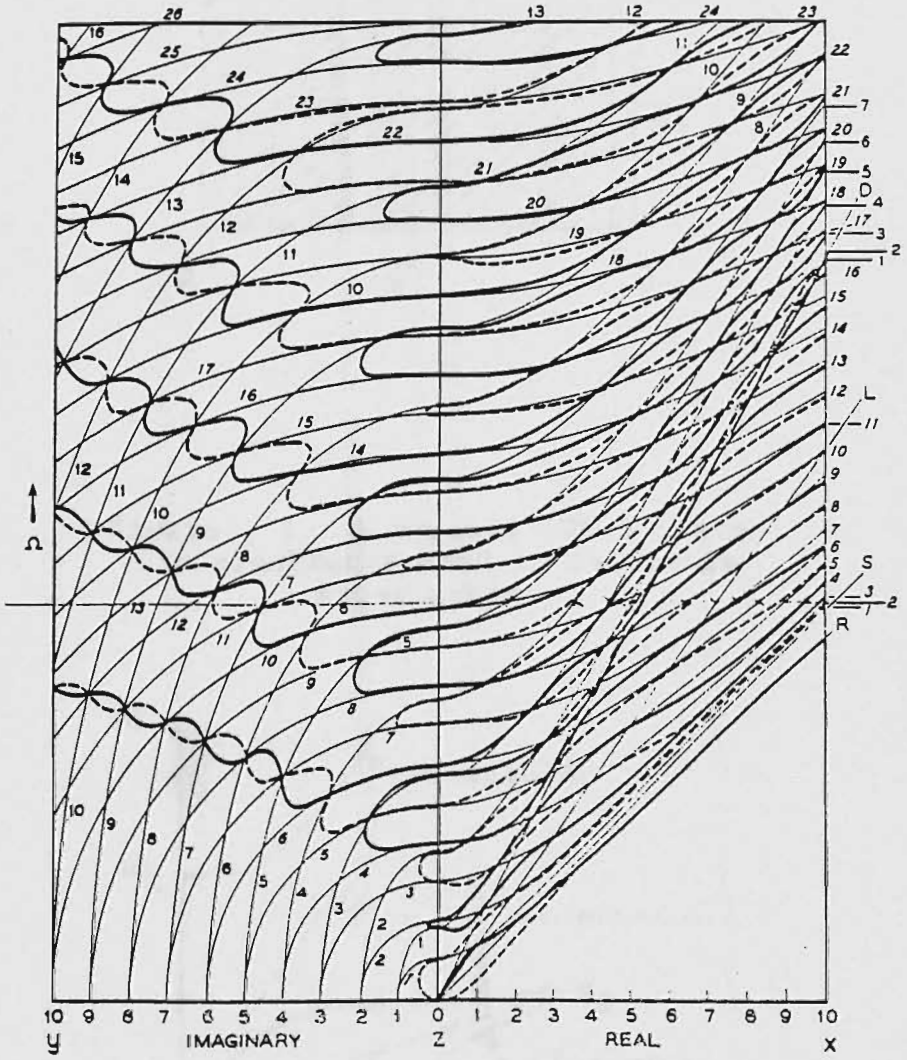

Figure 1.3. Frequency spectrum of longitudinal and flexural modes in an infinite plate having a Poisson's ratio of 0.31 (after Meeker and Meitzler [15]).

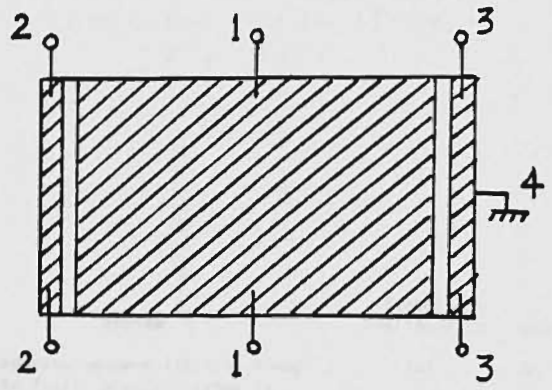

Figure 1.4. A typical PZT-5 plate with electrodes used in resonance experiments.

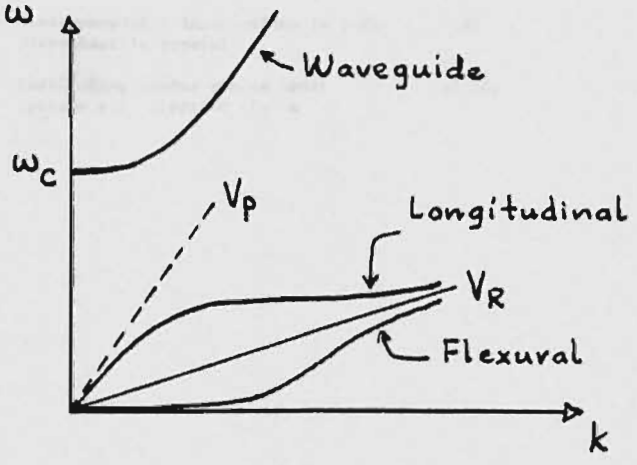

Figure 1.5. Typical ω-k characteristics of the lowest order modes in a plate.

Table 1.1
Types of echoes and their characteristics (from ref. [6]).

Type	System	Probable Nonlinearity	Possible Nonlinear Effects
Spin echo	Precessing nuclear spins in a magnetic field; electron spins in ferromagnetic materials	(a)	(a) Nonlinear excitation (b) Anharmonicity (c) Nonlinear damping (d) Permanent plastic deformations/change of coupling constants due to nonlinear stress and strain in oscillators
Photon echo	Oscillating electric dipoles of Cr^{3+} ions in ruby crystal and of SF_6	(a)	
Ferrimagnetic echo	Precessing magnetic spins with moderately high coupling	(b)	
Cyclotron echo	Gyrating free electrons of a plasma in a magnetic field	(b),(c)	
Molecular echo	Rotating molecules in a gas; oscillating electric dipoles in NH_3	(a)	
Plasma wave echo	Streaming free electrons in a plasma	(a),(b)	
Fluxoid echo	Fluxoid excitations in type II superconductors	(b)	
Phonon echo in crystals	Electroacoustic interactions in bulk piezoelectric crystals	(a)	
Phonon echo in powders	Oscillating powder grains under intense r.f. electric fields	(b),(d)	

CHAPTER II

DYNAMIC ECHOES WITH ANHARMONIC NONLINEARITY

II.1 SPICE Modeling of a Single Nonlinear Circuit and an Ensemble of Linear Circuits

II.1.1 Modeling a Nonlinear Capacitor

To start our SPICE modeling experiments, we decided to first set up a relatively simple test model as a primary element upon which we could base more complicated circuits later. A convenient test model that was set up on SPICE is shown in Fig.2.1(a). C_0 is a linear capacitor placed in series with a nonlinear dependent voltage source f(V). The source f(V) is related to the voltage V between the nodes 1 and 1' through a polynomial series. A nonlinear dependent voltage source is a very useful tool for nonlinear circuit modeling on SPICE.

If we let

$$f(V)=a_3V^3, \tag{2.1}$$

where a_3 is a constant, we can show in a few simple steps (see Appendix A) that the arrangement in Fig.2.1(a)

represents an amplitude-dependent large signal capacitance C_{ls} given by:

$$C_{ls}=C_0[1-(3/4)a_3|V_0|^2], \qquad (2.2)$$

where V_0 is related to V through $V=V_0\sin\omega_c t$, and we assume that the system in which C_{ls} is to be used will be tuned close to ω_c so that all higher harmonics of ω_c will be rejected.

Note that (2.2) indicates a change in the capacitance C_0 given by:

$$\Delta C=-(3/4)a_3|V_0|^2C_0 \ . \qquad (2.3)$$

Thus, if one were to use the above nonlinear capacitor in an RLC resonator, then the resonant frequency of the resonator would change by an amount that could be easily predicted and verified. An expected step response for such a circuit with $a_3|V_0|^2=1$ is shown in Fig.2.1(b).

The test model of Fig.2.1(a) was set up on SPICE with an input $V=V_0\sin\omega_c t$. The current I through the capacitor was plotted. The total current (i.e. not rejecting third harmonic terms) expected from Fig.2.1(a) is given by:

$$I=\omega_c C_0 V_0[(1-(3/4)a_3|V_0|^2)\cos\omega_c t+(3/4)a_3|V_0|^2\cos3\omega_c t]. \qquad (2.4)$$

The result obtained showed harmonic distortion in the current as expected from (2.4). The theoretical current

and the SPICE output are plotted in Fig.2.1(c) and (d) respectively. Note that the plots agree fairly well.

II.1.2 SPICE Experiment with Nonlinear RLC Circuit

The nonlinear capacitor model of Fig.2.1(a) was next used in a parallel RLC circuit, excited by a current step. For use in SPICE, the circuit of Fig.2.2(a) was replaced by its Thevenin equivalent (Fig.2.2(b)), with the current step replaced by a voltage step V_{dc} in series with a resistor R.

The nominal parameters of the linear equivalent of Fig.2.2 are:

$$\text{(i)} \quad \omega_0=[(1/LC_0)-(1/4R^2C_0^2)]^{1/2}, \tag{2.5}$$

where ω_0 is the damped resonant frequency.

$$\text{(ii)} \quad V_{out}=(I_{dc}/\omega_0C_0)e^{-(t/2RC_0)}\sin\omega_0t, \tag{2.6}$$

where $I_{dc}=V_{dc}/R$.

$$\text{(iii)} \quad |V_{out}|_{max}=V_{dc}/\omega_0C_0R=V_{dc}/Q_0, \tag{2.7}$$

where
$$Q_0=\omega_0C_0R, \tag{2.8}$$
is the resonant Q of the circuit.

For a nonlinear circuit the capacitance and hence the resonance frequency depends on the voltage. For a relatively

slow decay one may then expect that the frequency of oscillation changes monotonically during the decay.

For the SPICE experiment, the following parameters were chosen:

C_0=58pF

L=0.14mH

R=200K

V_{dc}=10V

$f(V)=a_3V^3$, a_3 variable

Q_0~129.

With these values, $|V_0|_{max}$ in (2.6) was estimated to be about 0.1V.

Now the linear (small signal,ss) and nonlinear (large signal,ls) resonance frequencies can be written as:

$$f_{0,ss}=1/2\pi(LC_0)^{1/2}\sim 1.77\text{MHz}, \qquad (2.9a)$$

and $$f_{0,ls}=1/2\pi(LC_{ls})^{1/2}=f_0(C_0/C_{ls})^{1/2}, \qquad (2.9b)$$

provided that $$R>(1/2)(L/C_0)^{1/2}. \qquad (2.9c)$$

Note that according to (2.9b), the frequency $f_{0,ls}$ depends on the voltage $|V_0|$, and hence on time. We, however, concentrate on its value near t=0, where the voltage is a maximum.

Using (2.9a-c), the values of $f_{0,ss}$ and $f_{0,1s}$ for different values of a_3 were numerically computed, assuming $|V_0|_{max} \sim 0.1V$.

The circuit of Fig.2.2(b) was then set up on SPICE, and run for different values of a_3. From the decaying oscillatory nature of the linear step response (as in (2.5)), it is clear that the nonlinear capacitor will change from C_{1s} near t=0, to the steady-state value of C_0 as $t \to \infty$, when the response goes to zero. Thus, if the SPICE model works right, the frequency of the response near t=0 should follow (2.9b), and as $t \to \infty$, it should approach the small signal value of (2.9a). From the actual response plots, it was found that for $a_3 < 27$, the experimental values of f_{1s} were within +10% of the theoretical values. The values of f_{ss} were almost exactly as predicted. The results are summarized in Table 2.1a. Note that from (2.2) and (2.9), f_{1s} will be larger than f_{ss} if a_3 is positive, while the reverse will be true if a_3 is negative. Since a_3 was chosen positive in the SPICE experiment, f_{1s} was indeed found to be greater than f_{ss}, as expected. Fig.2.3 shows a typical step response from SPICE.

In summary, the following observations were made:

(a) For $0 < a_3 < 27$, the system outputs were as predicted. The frequencies, decay times and amplitudes were reasonably accurate.

(b) For $29<a_3<49$, and for $a_3>56$, the system gave an error message that read "INTERNAL TIMESTEP TOO SMALL FOR TRANSIENT ANALYSIS".

(c) For $a_3=28$, the system output was a positive ramp, as in Fig.2.4(a).

(d) For $a_3=56$, the system output was a negative ramp, as in Fig.2.4(b).

II.1.3 Instability in Model Circuit

The failure of the model circuit for certain values of a_3 led us to conclude that the circuit becomes unstable under certain conditions. At first glance, it seems obvious from (2.2) that if

$$a_3|V_0|^2>4/3, \tag{2.10}$$

then the value of C_{1s} becomes negative, and as far as the SPICE analysis is concerned, the circuit becomes physically meaningless.

Using a phasor analysis at one frequency, we can derive another instability (jump effect) [19] condition given by:

$$a_3|V_0|^2>4/3Q_0. \tag{2.11}$$

However, since (2.11) only applies to a sinusoidal input, it probably cannot be used to define instability to a step input.

From the SPICE experiments, a check on the $a_3|V_0|^2$ product at the transition from stable to unstable indicated that:

(a) With R=200K, Q_0=129,

$$a_3|V_0|^2 \sim 0.16, \text{ in the range } 0<a_3<27.$$

(b) With R=20K, Q_0=12.9,

$$a_3|V_0|^2 \sim 0.2, \text{ in the range } 0<a_3<0.35.$$

The above experimental values indicated that the exact description of the instability was different from (2.10) or (2.11). Fortunately, it turned out that during subsequent theoretical and experimental investigations, the origin of the instability became clear. We discuss this next.

When the nonlinear parallel RLC circuit of Fig.2.2(b) was excited by a triangular pulse, the closest approximation to a delta pulse on SPICE (with 50ns rise and fall times, and a 10ns plateau), all stable outputs exhibited the damped oscillatory behavior of Fig.2.5. In all cases, it was found that whenever (for a given input and a_3) the product $a_3|V_0|^2$ exceeded about 0.25, the system became

unstable. The experiment was done over an input voltage range of 0.2V to 100V, and a range of a_3 between -10^2 and $+10^{15}$. It was also observed that for negative values of a_3, the system was never unstable (see Table 2.1b). To find a satisfactory explanation for this problem, we used an analysis based on injected charge, which we discuss next.

II.1.4 Stability Analysis of Nonlinear Capacitor from Injected Charge Approach

For the nonlinear capacitor of Fig.2.1(a), it may be shown that (see Appendix B), for $a_3>0$, there is a maximum limit to the amount of charge that can be injected into the device. This charge, Q_{imax}, is given by:

$$Q_{imax}=2C_0/(3(3a_3)^{1/2}),\ a_3>0. \qquad (2.12)$$

and it occurs when

$$a_3|V_{oi}|^2=1/3, \qquad (2.13a)$$

where V_{oi} is the output voltage of the corresponding nonlinear resonator.

Thus, for $a_3>0$, the system becomes unstable when

$$a_3|V_{oi}|^2>1/3, \qquad (2.13b)$$

which is close to the value found in the SPICE experiments (see Table II.1b).

On the other hand, when a_3 is negative, there is no theoretical limit to the amount of charge that can be injected. Thus, for $a_3<0$, the SPICE experiments should not be unstable for any pulse amplitude or duration. Fig.2.6 shows a qualitative plot of Q_i vs. V_{oi} for different signs of a_3.

For a triangular pulse input, the following input voltage and injected charge conditions for stability can be derived: (unstable if)

$$V_{inp}>RQ_{imax}/[(1/2)(t_r+t_f)+t_w], \qquad (2.14)$$

or, equivalently,

$$Q_{in}>Q_{imax}, \qquad (2.15)$$

where V_{inp} is the peak pulse amplitude, and t_r, t_f, and t_w are the pulse rise, fall and duration time respectively.

From the nonlinear SPICE experiments, it was verified that all the unstable outputs satisfied the conditions (2.14) and (2.15). In subsequent nonlinear echo experiments, it was found that the stability condition (2.15) would strictly have to include the total injected charge from all the applied pulses, for a multiple pulse input. This will be discussed in section II.2.

II.1.5 Step and Pulse Response of Linear Parallel RLC Circuit

In order to build up an appropriate nonlinear echo model with multiple electronic resonators, it is necessary to analyze the step and pulse response of a linear RLC circuit, and verify the results on SPICE. The experimental results for both inputs have been discussed in the preceding pages. The theoretical results are presented here for completeness.

Case A: Step Input

The key results may be summarized as follows:

$$\omega_n=1/(LC_0)^{1/2}=\text{undamped natural frequency.} \qquad (2.16a)$$

$$\omega_0=(1/(LC_0)-1/(4R^2C_0^2))^{1/2}=\text{damped frequency.} \qquad (2.16b)$$

$$\zeta=(1/2R)(L/C_0)^{1/2}=\text{damping factor.} \qquad (2.16c)$$

$$T_d=2RC_0=\text{decay time.} \qquad (2.16d)$$

$$V_0(t)=(2\zeta I_0R/(1-\zeta^2)^{1/2})e^{-\zeta\omega_n t}\sin\omega_0 t. \qquad (2.16e)$$

$$R>(1/2)(L/C_0)^{1/2}. \qquad (2.16f)$$

$$Q_0=\omega_0C_0R=(1-\zeta^2)^{1/2}/2\zeta. \qquad (2.16g)$$

Case B: Pulse Input

The closest approximation to a rectangular pulse on SPICE is a narrow triangle with a plateau at the apex. Using a triangle pulse of height V and base width 2T as input, we can show that the response of a linear parallel RLC circuit will be:

$$V_0(t)=(VL/RT)(1-e^{-t/2RC_0}(\cos\omega_0 t-(1/2Q_0)\sin\omega_0 t))u(t)$$

$$-2VL/RT(1-e^{-(t-T)/2RC_0}(\cos\omega_0(t-T)-(1/2Q_0)\sin\omega_0(t-T)))u(t-T)$$

$$+VL/RT(1-e^{-(t-2T)/2RC_0}(\cos\omega_0(t-2T)-(1/2Q_0)\sin\omega_0(t-2T)))\times u(t-2T), \qquad (2.17)$$

where ω_0 and Q_0 are defined in (2.16).

It can be shown by using some algebraic manipulations that if we let $Q_0\to\infty$, $t>2T$, and $2T<<2\pi/\omega_0$, then the solution in (2.17) reduces to the form:

$$V_0=(VT/RC_0)e^{-t/2RC_0}\cos\omega_0 t, \qquad (2.18)$$

where VT is the area of the triangle. Note that (2.18) is identical to a delta function response. This is to be expected as the applied pulse is much shorter than one cycle of the resonance frequency.

A typical analytical plot of (2.17) is shown in Fig.2.7(a). It shows an oscillatory behavior, with an initial rise in the amplitude after the first cycle. This compares fairly well with the typical SPICE output shown in Fig.2.7(b). Note that the SPICE plot corresponds to a small nonlinearity parameter a_3 (~.01), and a pulse amplitude of 100V, while the analytical plot corresponds to a_3=0, and a pulse amplitude of 10V. This accounts for the difference in the amplitude scales in the two plots.

II.1.6 Analysis of N Parallel RLC Circuits Excited by a Common Source

A natural extension of the one resonator nonlinear circuit is the case of N resonators with a resonant frequency separation Δf_c. A block diagram representation of the system is shown in Fig.2.8.

For the macroscopic response of the system in Fig.2.8, we can write:

$$V_0(\omega)=T(\omega)V_{in}(\omega), \tag{2.19}$$

where
$$T(\omega)=\sum_{i=1}^{N} T_i(\omega), \tag{2.20}$$

and
$$T_i(\omega)=j\omega L_i/(R(1-\omega^2 L_i C_0)+j\omega L_i). \tag{2.21}$$

The above system may be solved in two ways. One way is to find the exact impulse response by adding up the individual impulse responses of the resonators. The second way is to approximate each transfer function in (2.21) for large Q by a sum of delta functions, and solving the resulting system by Fourier analysis.

Case A: Exact impulse response

Using a Laplace transform approach, we can show that the exact impulse response of the system in Fig.2.8 is given by:

$$V_0(t)=(A/RC_0)e^{-t/2RC_0}\sum_{i=1}^{N}(\cos\omega_i t-(1/2Q_{0,i})\sin\omega_i t), \quad (2.22)$$

where A is the area of the impulse, and

$$Q_{0,i}=\omega_i RC_0, \quad (2.23a)$$

$$\omega_i=((1/L_iC_0)-1/4R^2C_0^2)^{1/2}=\omega_c-((N+1)/2)\Delta\omega_c+i\Delta\omega_c, \quad (2.23b)$$

ω_c=center frequency of the ensemble,

$$\Delta\omega_c=\text{frequency separation}=\omega_{i+1}-\omega_i, \quad (2.23c)$$

and N=number of resonators (taken to be odd for symmetry).

If we assume in (2.22) that $Q_{0,i}>>1$, then using a few simple algebraic steps, we can express it as follows:

$$V_0(t)=(A/RC_0)e^{-t/2RC_0}((\sin N\Delta\omega_c t/2)/(\sin\Delta\omega_c t/2))\cos\omega_c t. \tag{2.24}$$

Note that the carrier frequency in (2.24) is exactly the center frequency of the ensemble.

Case B: Approximation for $Q_0\to\infty$

If we assume that $Q_{0,i}\to\infty$ for each resonator in the ensemble, then we can approximate the transfer function of each resonator by the sum of two delta functions. Thus, if for each resonator,

$$RC_0\to\infty,\ (BW)_i\to\infty, \tag{2.25}$$

then $$T_i(\omega)\sim(\pi/RC_0)(\delta(\omega-\omega_i)+\delta(\omega+\omega_i)), \tag{2.26}$$

where $\delta(\omega+\omega_i)$=the limit of the function sketched in Fig.2.9 when $RC_0\to\infty$.

The validity of the limiting form of $T_i(\omega)$ as in (2.26) is demonstrated in Appendix C.

As a further check, we find that if we use (2.26) to find the response of the network to a delta function of height A, we obtain:

$$V_0(t)=(A/RC_0)\cos\omega_i t, \tag{2.27}$$

which is in agreement with (2.22) when $Q_0 \to \infty$.

Using (2.26) we can write the overall transfer function as:

$$T(\omega) \simeq \sum_{i=1}^{N} (\pi/RC_0)(\delta(\omega-\omega_i)+\delta(\omega+\omega_i)). \qquad (2.28)$$

If we let the input $V_i(t)=A\delta(t)$, then (2.29)

$$V_0(t)=(A\pi/RC_0)F^{-1}\left(\sum_{i=1}^{N}(\delta(\omega-\omega_i)+\delta(\omega+\omega_i))\right), \qquad (2.30)$$

where F^{-1} denotes inverse Fourier transform.

It is simple to show from (2.30) that:

$$V_0(t)=(A/RC_0)((\sin N\Delta\omega_c t/2)/(\sin\Delta\omega_c t/2))\cos\omega_c t. \qquad (2.31)$$

Note that (2.31) is identical to (2.24) except for the $\exp(-t/2RC_0)$ factor. However, if we recall that (2.31) was derived assuming $Q_{0,i} \to \infty$, it is obvious that the exponential decay factor is missing because $RC_0 \to \infty$ as $Q_{0,i} \to \infty$. Hence, both methods yield identical results.

Equations (2.24) and (2.31) are analogous to the diffraction pattern due to N point sources with constant spatial separation, and to the electric field pattern of N locked modes with zero relative phase in a laser [20,21]. Hence, the impulse response of N electronic resonators with

fixed resonant frequency separation is a good electrical analog of the above optical phenomena. Fig.2.10 shows a plot of the $(\sin N\Delta\omega_c t/2)/(\sin\Delta\omega_c t/2)$ factor in (2.31). From the plot, we can draw the following conclusions:

(a) The envelope of the response consists of a periodic array of major peaks occuring at:

$$t=kT,\ k=0,1,2,.... \tag{2.32}$$

where $$T=1/\Delta f_c=2\pi/\Delta\omega_c, \tag{2.33}$$

is the separation between the peaks. These major peak responses are known as the "linear echoes" of an ensemble.

(b) Between adjacent linear echoes, the response contains (N-1) zeroes, and its amplitude is smaller than 1/N of the largest linear echo amplitude.

(c) Due to the finite bandwidth, the linear echoes undergo an exponential decay with a time constant of $2RC_0$.

(d) The width of the linear echo, measured between the center and the first zero (or, equivalently, between $2/\pi$ points) is given by:

$$t_{LE}=1/N\Delta f_c. \tag{2.34}$$

(e) In addition to the major peaks, there are also minor peaks or sidelobes that occur at:

$$t=(n+1/2)/N\Delta f_c,\ n\neq 0,kN, \tag{2.34a}$$

where k and n are integers, and these peaks have the same width as the major peaks. The important difference between the major and the minor peaks is that they have an amplitude ratio of N. Thus, in the normalized plot in Fig.2.10, the major peaks have an amplitude of N(=5), while the minor peaks have an amplitude of 1. From this, we can infer that in order to suppress the sidelobes (to reduce interferences in nonlinear echo experiments), we should make N as large as possible.

A SPICE experiment was performed with 21 linear parallel RLC circuits with the following parameters:

$N=21$

$\Delta f_c=25KHz,\ 75KHz$

$R=1M$

$C_0=58pF$

$f_c=2MHz$

$T_d=2RC_0=116\mu s$

$(Q_0)_{center}=729.$

From Table 2.2 which summarizes the findings, it is clear that the theoretical and SPICE results compare very well in terms of linear echo width, time of occurence and amplitude. Fig.2.11(a)-(c) show typical linear echoes obtained from SPICE. Fig.2.11(a) and (b) show the first and second linear echoes respectively for N=21, while Fig.2.11(c) shows the first linear echo for N=101.

Thus, it has been possible to model 21 (and later 101) linear resonators on SPICE, and the results have compared favorably with theory. The amount of computer time required for SPICE calculations with 21 linear resonators was less than 10 minutes for a circuit time of 85μs. We will discuss further the limitations and usefulness of SPICE in the analysis of large scale circuits in chapter VI.

II.2 Electronic Holography on SPICE Using an Ensemble of Nonlinear Circuits

Having successfully modeled 101 linear resonators on SPICE, we next extended our approach to explicit forms of nonlinearity in the system, and also theoretically analyzed the details of the specific nonlinear echo processes against which the SPICE experiments could be tested. In the remainder of this chapter, we discuss the theoretical derivations and SPICE experiments pertaining to nonlinear echoes in the presence of anharmonic nonlinearity.

II.2.1 Nonlinear Echo Generation by Anharmonic Nonlinearity

Case A: Nonlinear response to two delta pulses

Suppose the system under consideration consists of a large number (N) of resonators, each with bandwidth W equal to $1/RC_0$, and spread between $\omega_c-W_b/2$ and $\omega_c+W_b/2$. Let the input excitation consist of two delta voltage pulses of areas A_1 and A_2 applied at t=0 and $t=\tau$ respectively. The linear macroscopic response of the system is now given by:

$$V_1(t)=\mathrm{Re}[A_1 W\Sigma_{i=1}^{N} e^{j\omega_i t}+A_2 W\Sigma_{i=1}^{N} e^{j\omega_i (t-\tau)}], \tag{2.35a}$$

$$=\mathrm{Re}((NA_1W/W_b)\Sigma_{i=1}^{N} e^{j\omega_i t}(W_b/N)+(NA_2W/W_b)\Sigma_{i=1}^{N} e^{j\omega_i (t-\tau)}(W_b/N)), \tag{2.35b}$$

which, for large N, may be approximated as:

$$V_1(t)\sim(NW/W_b)\mathrm{Re}(A_1\int_{\omega_c-W_b/2}^{\omega_c+W_b/2} e^{j\omega t}d\omega+A_2\int_{\omega_c-W_b/2}^{\omega_c+W_b/2} e^{j\omega(t-\tau)}d\omega), \tag{2.36a}$$

$$=NW(A_1\,\mathrm{sinc}f_b t\cos\omega_c t+A_2\,\mathrm{sinc}f_b(t-\tau)\cos\omega_c(t-\tau)), \tag{2.36b}$$

where $f_b=W_b/2\pi$ and $\mathrm{sinc}(x)=\sin(\pi x)/\pi x$.

Note that we have assumed high Q resonators so that exponential decay factors may be ignored.

For an individual resonator at frequency ω the effective excitation amplitude at $t=\tau$ is given by:

$$a=|A_1W+A_2We^{-j\omega\tau}| \tag{2.37a}$$

$$=W(A_1^2+A_2^2+2A_1A_2\cos\omega\tau)^{1/2}. \tag{2.37b}$$

Note that the dimension of "a" in (2.37) is <volts> for voltage pulse inputs.

Now, suppose that at $t=\tau$, the individual resonators undergo a frequency shift (which, as we will show later, can be brought about by a cubic nonlinearity parameter in the nonlinear capacitor model) given by:

$$\Delta\omega=-\alpha a^2 , \tag{2.38}$$

where α is assumed to be a constant, and "a" is defined by (2.37).

Using (2.37) and (2.38) in (2.36), we can now write the nonlinear macroscopic response for $t>\tau$ as:

$$V_{NL}(t)=(NW/W_b)\mathrm{Re}\left(A_1\int_{\omega_c-W_b/2}^{\omega_c+W_b/2} e^{j(\omega+\Delta\omega)t}\,d\omega\right.$$

$$\left.+A_2\int_{\omega_c-W_b/2}^{\omega_c+W_b/2} e^{j(\omega+\Delta\omega)(t-\tau)}\,d\omega\right). \tag{2.39}$$

From (2.39), we can show after some algebra (see Appendix D) that:

$$V_{NL}(t)=NWRe(A_1 e^{-j\alpha W^2(A_1^2+A_2^2)t} \sum_{n=-\infty}^{\infty} (-j)^n \times$$

$$\times J_n(b_1) e^{j\omega_c(t+n\tau)} sincf_b(t+n\tau)$$

$$+A_2 e^{-j\alpha W^2(A_1^2+A_2^2)(t-\tau)} \sum_{n=-\infty}^{\infty} (-j)^n \times$$

$$\times J_n(b_2) e^{j\omega_c(t+(n-1)\tau)} sincf_b(t+(n-1)\tau)), \quad (2.40)$$

where $J_n(b_1)$ and $J_n(b_2)$ are Bessel functions of order n and arguments b_1 and b_2, and

$$b_1=2\alpha W^2 A_1 A_2(t), \quad (2.41a)$$

$$b_2=2\alpha W^2 A_1 A_2(t-\tau). \quad (2.41b)$$

Note that the two terms in the parentheses in (2.40) consist of infinitely many sinc functions centered at $t=-n\tau$ and $t=(1-n)\tau$ respectively. For negative n, these will represent "echo" responses centered at $t=-n\tau$ and $t=(1-n)\tau$ respectively. For positive n, these terms will represent echo-like responses that occur virtually before $t=2\tau$, and

may physically extend into the observation region ($t>2\tau$). Now, for certain selected conditions, sinc functions occuring at the same time will be widely different in amplitude and neighboring ones will be well separated if $1/f_b >> \tau$. If, in addition, we assume that $A_2 >> A_1$, then (2.40) will essentially predict "multiple" nonlinear echo responses at $t=m\tau$, $m=2,3,...$ Such multiple echoes have in fact been reported in the literature [2] .

Specific Example: Dynamic 2-pulse echo

Let us, in particular, examine the case when $A_2 >> A_1$, and concentrate on the 2-pulse nonlinear echo at $t=2\tau$. From (2.40), this echo appears in the first term for n=-2, and in the second term for n=-1. However, near $t=2\tau$, these terms are different only in the amplitudes A_1 and A_2, and with $A_2 >> A_1$, the first term may be neglected. Thus, the echo can be written as (n=-1) :

$$V_{NL}^{2\tau}(t)=NWRe(jA_2 e^{-j\alpha W^2 (A_1^2+A_2^2)(t-\tau)} e^{j\omega_c(t-2\tau)} \times$$

$$\times J_{-1}(b_2)\,\mathrm{sincf}_b(t-2\tau)), \qquad (2.42a)$$

$$=NWA_2 \sin(\omega_c(t-2\tau)-\alpha W^2 (A_1^2+A_2^2)(t-\tau))\times$$

$$\times J_1(b_2)\,\mathrm{sincf}_b(t-2\tau). \qquad (2.42b)$$

Note that (2.42b) represents a sinc function centered at $t=2\tau$, which is the 2-pulse anharmonic nonlinear echo.

For small b_2, i.e. $2\alpha W^2 A_1 A_2 \tau << 1$, and assuming that the response has a narrow spread around $t=2\tau$, (2.42b) can be approximated as :

$$V_{NL}(t) \sim N\alpha W^3 A_1 A_2^2 \tau \sin(\omega_c(t-2\tau) - \alpha W^2 (A_1^2 + A_2^2)(t-\tau)) \times$$

$$\times \text{sincf}_b(t-2\tau). \qquad (2.43)$$

Upon examining (2.42b) and (2.43), we may note that they illustrate the following well known properties of an anharmonic nonlinear echo [6] :

(a) For small τ, the echo amplitude is related to the pulse amplitudes as :

$$V_{DE} \propto A_1 A_2^2.$$

(b) The dynamic echo initially grows linearly with τ, and then decreases for large values of τ. Note that in an actual finite bandwidth, finite Q experiment, the decay of the nonlinear echo would be brought about not only by the $J_1(b_2)$ factor in (2.42b), but also by an exponential decay factor due to the envelope decay of the resonator ensemble. This will be treated later when an actual circuit model is set up.

Case B : Nonlinear response to a general signal followed by a "recall" pulse

This situation, under certain specific conditions, should result in a time inverted recall of a general input.

Let the general signal be given by:

$$V_{in}(t)=\mathrm{Re}(g(t)e^{j\omega_c t})=\mathrm{Re}((1/2\pi)\int_{-\infty}^{\infty} G(\Omega)e^{j(\omega_c+\Omega)t}\,d\Omega), \quad (2.44)$$

where $G(\Omega)$ is the spectrum of the (complex) envelope $g(t)$.

The response of a single resonator at $\omega_i=\omega_c+\Omega$ to this input may be written as :

$$V_i(t)=\mathrm{Re}((1/2\pi)\int_{-\infty}^{\infty} G(\Omega)e^{j(\omega_c+\Omega)t}\,T_i(\omega_c+\Omega)d\Omega), \quad (2.45)$$

where T_i is given by (2.21). We will however use the approximate expression (2.26) to gain some rapid insight into the problem. In that case we have:

$$V_i(t)=\mathrm{Re}((W/2\pi)\int_{-\infty}^{\infty} G(\Omega)e^{j(\omega_c+\Omega)t}\,\pi\times$$

$$\times(\delta(\omega_c+\Omega-\omega_i)+\delta(\omega_c+\Omega+\omega_i))d\Omega), \quad (2.46a)$$

where $W=1/RC_0$.

Or, $$V_i(t)=\mathrm{Re}((W/2)G(\omega_i-\omega_c)e^{j\omega_i t}), \quad (2.46b)$$

where we assume that $G(\Omega)$ is narrow enough such that $G(-\omega_i-\omega_c)$ is small compared to $G(\Omega)$ and may be ignored.

Now the linear macroscopic response of a large number (N) of resonators between $\omega_c-W_b/2$ and $\omega_c+W_b/2$ may be written as:

$$V_l(t)=\mathrm{Re}((W/2)\sum_{i=1}^{N} G(\omega_i-\omega_c)e^{j\omega_i t}). \qquad (2.47)$$

For N very large, (2.47) may be written as:

$$V_l(t)=\mathrm{Re}((NW/2W_b)\sum_{i=1}^{N} G(\omega_i-\omega_c)e^{j\omega_i t}(W_b/N)), \qquad (2.48)$$

which when $N\to\infty$ becomes:

$$V_l(t)=\mathrm{Re}((NW/2W_b)\int_{\omega_c-W_b/2}^{\omega_c+W_b/2} G(\omega_i-\omega_c)e^{j\omega_i t}\,d\omega_i). \qquad (2.49)$$

Now, if the spectral content of G is smaller than W_b then we may write:

$$V_l(t)=\mathrm{Re}((NW/2W_b)\int_{-\infty}^{\infty} G(\Omega)e^{j\Omega t}e^{j\omega_c t}\,d\Omega), \qquad (2.50)$$

which, of course, is proportional to the originally applied function g(t). Now, let us apply both g(t) and $A_2\delta(t-\tau)$ to this linear system. It is readily seen that in this case the linear response is given by:

$$V_1(t)=\mathrm{Re}\left((NW/2W_b)e^{j\omega_c t}\int_{-\infty}^{\infty} G(\Omega)e^{j\Omega t}\,d\Omega\right.$$

$$\left.+(NW/W_b)e^{j\omega_c(t-\tau)}A_2\int_{-W_b/2}^{W_b/2} e^{j\Omega(t-\tau)}\,d\Omega\right). \quad (2.51)$$

Now, in a nonlinear system, there occurs at $t=\tau$, a frequency shift due to the voltage sensitive capacitance, as given by (2.38). The effective excitation across the resonator at $\omega_c+\Omega$ is given by:

$$a=\left|(W/2)G(\Omega)+WA_2e^{-j\Omega\tau}\right|$$

$$=W\left(|G(\Omega)|^2/4+A_2^2+A_2(G(\Omega)/2)e^{j\Omega\tau}\right.$$

$$\left.+A_2(G^*(\Omega)/2)e^{-j\Omega\tau}\right)^{1/2}. \quad (2.52a)$$

As a check, we may note that the dimension of "a" in (2.52) is also <volts>, as in (2.37).

Next, if we assume that:

$$|A_2|>>|G(\Omega)/2|, \quad (2.52b)$$

then, using (2.38), (2.39), (2.52a) and (2.52b) in (2.51), the nonlinear response for $t>\tau$ may be written as:

$$V_{NL}(t)=\mathrm{Re}\left((NW/W_b)A_2e^{j\omega_c(t-\tau)}e^{-j\alpha A_2^2W(t-\tau)}\times\right.$$

$$\times \int_{-W_b/2}^{W_b/2} e^{j\Omega(t-\tau)} e^{-j\alpha(t-\tau)P(\Omega)} d\Omega), \qquad (2.53a)$$

where $P(\Omega)$ is given by :

$$P(\Omega)=(W^2/4)|G(\Omega)|^2+(W^2/2)A_2G(\Omega)e^{j\Omega\tau}+(W^2/2)A_2G^*(\Omega)e^{-j\Omega\tau}. \qquad (2.53b)$$

This is a rather formidable expression and cannot be easily reduced to a closed form without some simplifications. If we now make the additional assumption that :

$$|(t-\tau)\alpha(W^2/2)A_2G(\Omega)|<<1, \qquad (2.54)$$

then we can expand the exponential term inside the integral in (2.53a) to obtain :

$$V_{NL}(t)=Re((NW/W_b)A_2e^{j\omega_c(t-\tau)}e^{-j\alpha A_2^2W^2(t-\tau)}\times$$

$$\times \int_{-W_b/2}^{W_b/2} e^{j\Omega(t-\tau)}(1-j\alpha(t-\tau)P(\Omega))d\Omega), \qquad (2.55)$$

where $P(\Omega)$ is defined in (2.53b).

Using (2.55) and carrying out the necessary algebra, we arrive at an approximate solution for the general input

case which contains the following four terms (see Appendix D for details):

$$\text{Term 1 : } NWA_2\cos(\omega_c(t-\tau)-\alpha A_2^2 W^2(t-\tau))\text{sincf}_b(t-\tau). \quad (2.56a)$$

$$\text{Term 2 : } (N\alpha W^3 A_2(t-\tau)/4W_b)\sin(\omega_c(t-\tau)-\alpha A_2^2 W^2(t-\tau))\times$$

$$\times \int_{-W_b/2}^{W_b/2} |G(\Omega)|^2 e^{j\Omega(t-\tau)} d\Omega. \quad (2.56b)$$

$$\text{Term 3 :}(N\alpha W^3 A_2^2(t-\tau)\pi/W_b)\sin(\omega_c(t-\tau)-\alpha A_2^2 W^2(t-\tau))g(t). \quad (2.56c)$$

$$\text{Term 4 :}(N\alpha W^3 A_2^2(t-\tau)\pi/W_b)\sin(\omega_c(t-\tau)-\alpha A_2^2 W^2(t-\tau))g(2\tau-t). \quad (2.56d)$$

where we have invoked the condition that the spectrum $G(\Omega)$ is narrower than W.

Of the four terms in (2.56), (2.56a) represents a sinc function centered at $t=\tau$. This term will have only a small tail in the region of interest. The term in (2.56b) represents, in the limit as $W_b \to \infty$, a delay of the autocorrelation of the signal envelope. Under the assumption (2.52b), the contribution of this term to the response in the region of interest will be small. The term in (2.56c) represents the original modulated input, with a

different amplitude, and a frequency and phase-shifted carrier. Note that since the recall pulse is applied at $t=\tau$, and the duration of $g(t)$ is necessarily less than τ, this term has negligible effect on the response in the region of interest.

The only term of any interest in the observation region is (2.56d), which is the time inverted anharmonic echo term we seek. Note that according to (2.56d), the time-inverted echo term actually has a linear dependence on t. One would expect this term to distort the recalled signal $g(2\tau-t)$. However, if we assume that $g(t)$ is a sufficiently narrow time-limited signal so that $g(2\tau-t)$ extends over a short interval around 2τ, then the effect of the amplitude distortion will be small.

Thus, it seems reasonable to assume that as long as we do not use very high amplitudes and too large values of τ, and satisfy the conditions (2.52b) and (2.54), the system described so far should yield time inverted anharmonic echoes. As we shall find later, if the condition (2.54) is violated, then we can no longer restrict the expansion in (2.55) upto the linear term, and this may result in undesirable higher order terms that overlap the inverted nonlinear echo at $t=2\tau$, and thereby may cause interferences that spoil the shape of the recalled signal.

Another important factor to take note of is that the result derived above does not contain any "multiple" echo term, as was obtained for the 2-pulse system. This, of course, is easy to explain. The higher order expansion terms that were left out in (2.55) would also result in multiple echoes involving complicated convolutions and correlations of g(t). However, under the assumption (2.54), these terms remain negligible.

We must also note, at this point, that our analysis for the dynamic recall of arbitrary signals can be used to investigate non-time-inverted recall as well. To do this, we use the general mathematical procedure for electronic holography as outlined by Korpel [11] .

It may be shown [11] that the spectrum of a dynamic recalled signal in the presence of a cubic nonlinearity is given by :

$$\phi'(\omega)=\phi^{2}(\omega)\phi^{*}(\omega), \qquad (2.57)$$

where $\phi(\omega)$ is the spectrum of the input of duration T. Equation (2.57) is only valid for t>T.

Now, suppose the input e(t) consists of a delta pulse at t=0 followed by a general signal $e_1(t-\tau)$ applied at $t=\tau$ (the reversal of the above sequence leads to time inverted recall as we have seen before), so that

$$e(t)=\delta(t)+e_1(t-\tau). \tag{2.58}$$

Then, $$\phi(\omega)=1+\phi_1(\omega)\exp(-j\omega\tau). \tag{2.59}$$

Using (2.59) in (2.57), we can show that the only term of interest in the recalled signal in the region $t>\tau$ is given by :

$$\phi'_{nt}(\omega)=\phi_1^2(\omega)\exp(-2j\omega\tau), \tag{2.60}$$

which corresponds to a macroscopic signal given by the autoconvolution of $e_1(t-\tau)$. Thus,

$$E'(t)=e_1(t-\tau) * e_1(t-\tau). \tag{2.61}$$

Equation (2.61) indicates that the domain of nonlinear dynamic echoes precludes non-time-inverted recall of a general signal, although it is possible to do other types of signal processing in the region of interest using this technique.

II.2.2 Response of a Discrete Number of Parallel RLC Circuits to Two Delta Pulses, Without and With Nonlinearity

We next apply the methodology developed in the preceding pages to specific electronic resonator ensembles,

in order to obtain the exact circuit responses under anharmonic nonlinearity.

Case A : Linear response, one resonator

Using (2.18), it follows immediately that for two delta pulses of strengths A_1 and A_2 applied at t=0 and $t=\tau$ to an RLC resonator, the response for $Q_0>>1$ may be written as :

$$V_0(t)=(A_1/RC_0)e^{-t/2RC_0}\cos\omega_0 t+(A_2/RC_0)e^{-(t-\tau)/2RC_0}\times$$

$$\times\cos\omega_0(t-\tau)u(t-\tau), \qquad (2.62)$$

where u(t) is a unit step.

Note that (2.62) indicates decaying oscillations, as expected.

Case B : Anharmonic nonlinearity, one resonator

Suppose that for $t>\tau^+$, the resonant frequency of the resonator is changed from ω_0 to $\omega_0+\Delta\omega$, where :

$$\Delta\omega=-\alpha a^2, \qquad (2.38)$$

where α is a constant, and a^2 is defined by :

$$a^2 = A_1'^2 + A_2'^2 + 2A_1' A_2' \cos\omega\tau, \qquad (2.37)$$

where $$A_1' = (A_1/RC_0)e^{-t/2RC_0}, \qquad (2.63a)$$

$$A_2' = (A_2/RC_0)e^{-(t-\tau)/2RC_0}. \qquad (2.63b)$$

Then, assuming that $A_2 >> A_1$ as before, we can show after some algebra, that for $t>\tau^+$, the resonator output can be written as (see Appendix E) :

$$V_0(t) \sim (A_2/RC_0)e^{-(t-\tau)/2RC_0} u(t-\tau) \mathrm{Re}\left(e^{-j\alpha(A_1'^2 + A_2'^2)(t-\tau)} \times \right.$$

$$\left. \times \sum_{n=-\infty}^{\infty} (-j)^n J_n(b) e^{j(\omega_0(t+(n-1)\tau))} \right), \qquad (2.64a)$$

where $$b = 2\alpha A_1' A_2' (t-\tau). \qquad (2.64b)$$

Case C : Anharmonic nonlinearity, N resonators

Let the resonant frequency of the ith resonator be given by :

$$\omega_i = \omega_c - ((N+1)/2)\Delta\omega_c + i\Delta\omega_c. \qquad (2.23b)$$

Then the output due to N independent resonators may be shown to be :

$$V_{0,NL}(t) \sim (A_2/RC_0) e^{-(t-\tau)/2RC_0} \times$$

$$\times \; \mathrm{Re}\left(e^{-j\alpha(A_1'^2 + A_2'^2)(t-\tau)} \sum_{i=1}^{N} \sum_{n=-\infty}^{\infty} (-j)^n J_n(b) \times \right.$$

$$\left. \times \; e^{j(\omega_c - ((N+1)/2)\Delta\omega_c + i\Delta\omega_c)(t+(n-1)\tau)} \right) u(t-\tau) \; . \qquad (2.65)$$

Note that in (2.65), the summation over i of the exponential terms involving the $(t+(n-1)\tau)$ factor corresponds to a delta function at $t=(1-n)\tau$, in the limit as $N \to \infty$. For finite N, these terms still represent pulse-like responses at $t=(1-n)\tau$. Hence, in a parallel RLC resonator model, for negative n, these terms potentially represent multiple anharmonic echoes at $t=m\tau$, $m=2,3,\ldots$. However, the amplitudes and phases of the response plots are now more complex, but are essentially perturbations around the nominal amplitude A_2 and the center frequency ω_c of the ensemble.

Using some mathematical manipulations, we can show that (2.65) can be written as (see Appendix E) :

$$V_{0,NL}(t) \sim (A_2/RC_0) e^{-(t-\tau)/2RC_0} \; u(t-\tau) \times$$

$$\times \mathrm{Re}\left(e^{-j\alpha(A_1'^2 + A_2'^2)(t-\tau)} \sum_{m=2}^{\infty} J_{1-m}(b)(-j)^{1-m} \times \right.$$

$$\left. \times e^{j\omega_c(t-m\tau)} (\sin(N/2)\Delta\omega_c(t-m\tau)/\sin(1/2)\Delta\omega_c(t-m\tau))\right). \quad (2.66)$$

Specific Example : 2-pulse nonlinear echo (m=2)

Letting m=2 in (2.66), we can show after some algebra :

$$V_{0,NL}^{2\tau}(t) \sim (A_2/RC_0) e^{-(t-\tau)/2RC_0} u(t-\tau) \times$$

$$\times J_1(b)(\sin(N/2)\Delta\omega_c(t-2\tau)/\sin(1/2)\Delta\omega(t-2\tau)) \times$$

$$\times \sin(\omega_c(t-2\tau) - \alpha(A_1'^2 A_2'^2)(t-\tau)) . \quad (2.67)$$

Comparing this with (2.42b) we see that for $N \to \infty$ we get essentially the same response around $t=2\tau$. However, an important difference is that (2.67) predicts periodic "linear" echoes at $t=2\tau+n/\Delta f_c$. By putting $t=2\tau$ in (2.67), we can derive an explicit expression for the amplitude of the envelope near $t=2\tau$, as a function of τ.

This leads to :

$$\text{amp}(V_{0,NL}(2\tau)) \sim -(A_2/RC_0)e^{2\tau} e^{-\tau/2RC_0} \times$$

$$\times J_1((2\alpha A_1 A_2 \tau/R^2 C_0^2)e^{-3\tau/2RC_0}) \; . \qquad (2.68)$$

Note that (2.68) is an explicit representation of a 2-pulse anharmonic echo as a function of the pulse separation τ. A plot of (2.68) (shown later) shows that the response goes to zero both as $\tau \to 0$, and as $\tau \to \infty$. This is quite satisfactory in terms of observed results.

Case D : N anharmonic resonators, SPICE circuit model

The amplitude dependence of $\Delta\omega$ in (2.38) so far has been heuristic. However, if we are to model a real nonlinear circuit using a nonlinear capacitor model, $\Delta\omega$ must be derived explicitly from the form of the voltage-dependent nonlinearity assumed for the capacitor. Interestingly enough, it turns out that a cubic voltage nonlinearity actually leads to an amplitude-squared dependence on $\Delta\omega$, which is exactly what we want. This result is derived in Appendix F. It is the link between the heuristic concept of electronic holography and anharmonic resonators discussed previously, and the actual working circuit model programmed on SPICE.

The essential results of Appendix F are :

(i) Large signal capacitance

$$C_{ls}=C_0(1-(3/4)a_3|V_0|^2) . \qquad (2.2)$$

(ii) Change in capacitance

$$\Delta C=-(3/4)a_3|V_0|^2 C_0. \qquad (2.3)$$

(iii) Input instability criteria (for triangular input)

$$a_3|V_0|^2 < 0.25 \text{ (experimental)}, \qquad (2.69a)$$

and,

$$V_{in}^2 < R^2 C_0^2 /a_3\Delta T^2 . \qquad (2.69b)$$

where ΔT is the base width of the pulse.

(iv) Anharmonic frequency shift

$$\Delta\omega=(3/8)a_3|V_0|^2 \omega_{ss} , \qquad (2.70)$$

where $\omega_{ss}=1/(LC_0)^{1/2}$ is the small signal resonant frequency.

Eq.(2.70) shows that a cubic voltage nonlinearity has led to an amplitude squared dependence of $\Delta\omega$.

(v) The parameter α

$$\alpha=\alpha(\omega_i)=-(3/8)a_3\omega_i , \qquad (2.71a)$$

where ω_i is the resonant frequency of the ith resonator.

Note that according to (2.71), α is really a function of ω_i instead of a constant. However, if we assume that the fractional bandwidth of the ensemble around the center frequency ω_c is small, then we can show that ω_i can be replaced by ω_c in (2.71a) without much error.

Thus, for small fractional bandwidth, we can write :

$$\alpha \rightarrow -(3/8)a_3\omega_c, \tag{2.71b}$$

for $(N-1)\Delta\omega_c/\omega_c << 1$.

II.2.3 Parameter Estimation for SPICE Nonlinear Echo Experiment

We now need to know the values of the actual circuit parameters before modeling an anharmonic nonlinear echo experiment on SPICE. In Appendix G, the details of the calculations are worked out.

The essential results of Appendix G are :

(i) Linear response amplitude at $t=2\tau$

$$V_L(2\tau) \sim (A_2/RC_0)e^{-\tau/2RC_0}(\sin(N/2)\Delta\omega_c\tau/\sin(1/2)\Delta\omega_c\tau). \tag{2.72}$$

(ii) Nonlinear echo amplitude at $t=2\tau$

$$V_{NL}(2\tau) \sim -(A_2N/RC_0)e^{-\tau/2RC_0} \times$$

$$\times \; J_1((2\alpha A_1 A_2 \tau/R^2 C_0^2)e^{-3\tau/2RC_0}). \qquad (2.68)$$

(iii) Criterion for observing the nonlinear echo above the noise of the tail of the linear echo

$$|J_1((2\alpha A_1 A_2 \tau/R^2 C_0^2)e^{-3\tau/2RC_0})| >> (1/N)(\sin(N\theta)/\sin\theta), \qquad (2.73)$$

where $\theta=\Delta\omega_c\tau/2$.

Also, in order that the nonlinear echo at $t=2\tau$ occurs well before the first linear echo (to avoid the possibility of losing the nonlinear echo in the relatively strong linear echo), we must make sure that :

(iv) $$t \neq nT \;, \qquad n=0,1,2,... \qquad (2.74)$$

where $T=1/\Delta f_c$ is the arrival time of the first linear echo.

(v) Stability requirement

$$\alpha V_{in}^2 < -3R^2 C_0^2 \omega_c^2/8\Delta T^2 \;, \qquad (2.75a)$$

and, $$|\alpha A_2|^2 < (3/32)R^2 C_0^2 \omega_c^2 = M, \qquad (2.75b)$$

where $A_2=\Delta T V_2/2$ is the area of the second pulse.

A set of design parameters (which satisfy the above constraints), using a table of Bessel functions, is listed below :

$\tau=T/3\sim14\mu s.$	$T=1/\Delta f_c=40\mu s$
$R=1M\Omega$	$M=3.963\times10^{-3}$ sec.
$C_0=58pF$	$Q_0\sim729$
$N=21,101$	$J_1(y)\sim0.3$
$f_c=2MHz$	$y=0.631$
$\Delta f_c=25KHz$	$V_2/V_1=A_2/A_1=10$
$V_1=1V,\ V_2=10V$	$T=0.1\mu s$
$a_3\sim950V^{-2}$	$\lvert\alpha\rvert\sim45\times10^{8}V^{-2}s^{-1}$

II.2.4 Observations from SPICE Nonlinear Echo Experiments

With the optimum set of parameters listed above, the system was set up on SPICE. A typical nonlinear resonator section used on SPICE is shown in Fig.2.12. From the SPICE output, it was found that in addition to linear echoes at $t=40\mu s$ and $t=54\mu s$, there was, indeed, a nonlinear echo at $t=2\tau=28\mu s$. In Fig.2.13(a) and (b), we show typical SPICE outputs for the above set of parameters with 21 and 101 resonators respectively.

Table II.3 summarizes the findings from the above experiment, and compares the results with theoretical estimates.

In order to correctly derive the theoretical estimates, it was necessary to consider the loading at the

output of each resonator due to the remaining resonators. It may be shown that this requires a correction to the ideal theoretical values by the following amount :

$$V_{0,actual}=(1/N)V_{0,theory}. \qquad (2.76)$$

Note that both the linear and nonlinear echo amplitudes and times of occurence are in reasonable agreement with theory, especially for small values of τ. In Fig.2.14, the variation of the nonlinear echo amplitude with the pulse separation τ is plotted. Note that for values of τ upto about 20μs, the theoretical and experimental values agree fairly well. However, for τ>20μs, the experimental value starts to deviate drastically. This seems to correlate with the fact that, for large values of τ, the nonlinear echo was found to split up, move away from $t=2\tau$, and in general, behave erratically. On searching the nonlinear echo literature for experimental corroboration of such peculiar behavior, we found that in actual powder echo experiments such abnormal dependence on τ has been reported [4,6].

In addition to the nonlinear echo vs. τ experiments (with V_1:V_2 fixed at 1:10), we also conducted nonlinear echo vs. V_1 and V_2 experiments, keeping τ fixed at 10μs. As can be seen from Fig.2.15(a) and (b), the variation with V_2 is parabolic, and that with V_1 is linear at low amplitudes. At

high amplitudes, the echo starts to saturate. This is correlated, once again, with an unexpected splitting in the nonlinear echo at high pulse levels, which makes the echo amplitude measurement highly inaccurate.

In order to check if the unexpected splitting of the echo at large τ and signal levels was due to some computer artifact, or if it reflected the actual physics of the system, we next considered the analytical result for the above system both with the parameter α held constant (as in 2.71(b)), as well as a variable (as in 2.71(a)). We speculated that the splitting could be due to the approximation involved in assuming α a constant; or, it could be due to the many higher order expansion terms that were neglected in our simplified theory.

Some of the analytical plots (based on (2.40) with $A_2 >> A_1$) of the response vs. τ are shown in Fig.2.16(a)-(f). Fig.2.16(a) and (b) show the plots for a pulse ratio 1:10 and τ=14μs, for α constant and variable, respectively. The analytical expressions used are derived in Appendix G. Note that the plots indicate a nonlinear echo at t=28μs, and a linear echo at t=40μs, as expected. Moreover, the two plots are identical for all intents and purposes. Fig.2.16(c) shows the exact plot for τ=25μs. We find here that the nonlinear echo has indeed "split" into additional humps at

t=55μs, and t=65μs, in addition to the normal one at t=50μs. This compares well with the response obtained from SPICE, as shown in Fig.2.17(a). Fig.2.16(d) shows the exact plot for τ=35μs. In this case, the nonlinear echo is seen to move slightly to the right of t=70μs, and an additional hump appears near t=65μs. This also agrees with observed behavior on SPICE, as shown in Fig.2.17(b). Fig.2.16(e) and (f) show the analytical response for pulse ratio of 6:10 and τ=14μs, with α constant and variable. These plots also indicate that at large signal levels, the nonlinear as well as the linear echoes start to split up or smear out. The effect of α being variable is once again seen not to be significant. We may therefore conclude that the splitting of the echo is related to the overall effect of all the terms in the exact response of the system. Thus, the SPICE program has clearly reflected the actual physics of the complicated nonlinear resonator ensemble. A few other SPICE outputs for large pulse ratios and/or large a_3 values are shown in Fig.2.17(c)-(e). These plots also demonstrate the high level splitting and movement of the nonlinear echo.

For certain combinations of $a_3>0$, V_1, V_2 and τ, we once again encountered the problem of instability in the SPICE nonlinear echo experiments as discussed in sections II.1.2 and II.1.3. It was also verified that the total

injected charge was the parameter that determined the stability of the system for $a_3>0$.

A set of experiments with a_3 negative were performed using SPICE to see if there was any instability. Fig.2.18(a) and (b) show the corresponding variations with τ and V_2 respectively.

From the total set of experiments performed with different combinations of τ, a_3, and V_1:V_2, the following major conclusions can be drawn :

(a) If we let V_1 or V_2 to be zero, no echo appears. Hence, two pulses are indeed necessary for the nonlinear echo (this fortifies the holographic model).

(b) If a_3 is positive, the system is unstable whenever (2.15) is satisfied.

(c) If a_3 is negative, the system is always stable .

(d) If a_3 is too small, e.g. a_3=-100, the nonlinear echo does not appear. This shows that for the echo to be discernable, the nonlinearity must be relatively strong.

(e) The linear echoes appear at $t=n/\Delta f_c$, n=1,2,... The nonlinear echo appears at $t=2\tau$.

(f) The echo width is approximately $1/N\Delta f_c$.

(g) For large values of τ, V_1 or V_2 (or combinations of these), the echo splits up into multiple humps that move away from the normal $t=2\tau$ point (see Fig.2.17(a)-(e)). There

is reason to believe that this is caused by the infinitely many terms in (2.66) which start to contribute in a complicated way to the 2-pulse echo for large values of τ, V_1 or V_2.

II.2.5 Time-Inverted Dynamic Echo of an Arbitrary Input Signal

The last experiment in the current series of investigations consisted of using the SPICE anharmonic echo model to see if, for an input e(t), made up of a finite duration arbitrary signal $e_1(t)$ followed by a "recall" pulse, there does indeed occur a time-inverted echo of $e_1(t)$ located symmetrically to the right of the recall pulse on the time axis. From our discussion in section II.2.1, it appears possible to obtain time-inverted recall (TIR) as long as the excitation amplitudes are not very high, condition (2.54) is satisfied, and the system has sufficient bandwidth to ensure that the undesirable response tails from non-echo terms will not interfere with the echo.

Theoretical explanation for TIR based on the SPICE nonlinear echo model

Suppose that in the conventional 2-pulse dynamic

echo experiment, we replace the first pulse by an arbitrary input consisting of a carrier modulated by a finite duration (t_0) baseband signal. We intend to show that if the second pulse (now the "recall" pulse) is applied at $t=\tau$, then between the times $t=2\tau-t_0$ and $t=2\tau$, there appears a time-inverted "echo" of the input signal, as long as the system remains cubically nonlinear. The rigorous theory for this has, of course, been derived in section II.2.1, but here we present a simpler pulse-echo argument. This situation is shown in Fig.2.19.

To prove the above, we first use the following statement (which is readily proved in a manner similar to the sampling theorem) :

"Given a time-limited r.f. signal of duration t_0 and carrier ω_c, expressed as $f(t)\cos\omega_c t$, the spectral content of the signal will be preserved by the corresponding sampled signal $f(t)\delta_T(t)\cos\omega_c t$ (where $\delta_T(t)$ is a comb-function of frequency $2\omega_c$), except that odd-order harmonics will be generated."

Thus, if we apply the sampled signal to a system whose bandwidth satisfies the condition :

$$BW<<3\omega_c-\omega_B \ , \qquad (2.77)$$

where ω_B is the bandwidth of the baseband signal, then, as far as the circuit is concerned, the sampled signal will be identical to the original r.f. signal.

Hence, we may replace the signal $f(t)\cos\omega_c t$ of Fig.2.20(a) by that of Fig.2.20(b). It is fairly simple to show that when the signal of Fig.2.20(b), followed by a "recall" pulse at $t=\tau$, is applied to the nonlinear system, the individual nonlinear echo due to each pulse will appear at the appropriate instant after the recall pulse. The result is a time-inverted replica of the signal $f(t)\delta_T(t)\cos\omega_c t$, located between the times $t=2\tau-t_0$ and $t=2\tau$ (see Fig.2.20(c)).

With the above and the previous SPICE results in mind, we arrived at the following set of design values for the TIR experiment :

(1) N=number of stages=101

(2) Δf_c=frequency separation=25KHz

(3) f_c=4MHz (doubled to keep the fractional bandwidth small)

(4) TMAX<10ns (to have at least 25 iterations per cycle)

(5) TSTEP=20ns

(6) V_2=recall pulse amplitude=10V

(7) f(t) is taken as a sawtooth with t_0=1μs, and maximum height=2V

(8) a_3=-1000 (negative value chosen for stability)

(9) τ<14μs (we choose $\tau=t_0$+5μs=6μs)

With the above set of parameters, the SPICE experiment yielded an "echo" output that was indeed time-inverted, with the leading edge having a sharper slope (but not instantaneous as in the trailing edge of the input sawtooth, because of the limited bandwidth) than the trailing edge. The response peak was located at the junction of the two slopes, at around 11μs, and the total echo width was about 1μs (see Fig.2.21(a) and (b)). The trailing edge decayed nearly to zero at t=12μs. In Fig.2.21(a) we show an approximate sketch of the TIR response from SPICE alongside the applied input for perspective. In Fig.2.21(b) we show the detailed SPICE response. The trailing edge decayed nearly to zero at t=12μs.

We may note that with the above parameters, the average pulse echo width is about 0.4μs. Thus, for a 1μs r.f. signal, the recalled echo contains only (1/0.4)=2.5 resolvable points. This is rather inaccurate. Yet, it is indeed interesting that the time-inversion property of electronic holography could still be demonstrated.

Note that to obtain more resolution, we can do the following :

(1) Make the pulse echo narrower. This may be done by making N larger or Δf_c larger. If N is made larger, the circuit computation time increases. If Δf_c is made larger, the fractional bandwidth increases. Both of these are undesirable. One way to keep the fractional bandwidth small for larger Δf_c would be to increase f_c further. But this means that TMAX would have to be reduced even further, thereby increasing the computation time. Thus, we cannot work outside an optimum set of values and resolution with the available facilities.

(2) Make the signal width itself longer. This would, of course, have to be limited to a value reasonably less than τ, because, for τ very small, the pulse echo amplitude decreases linearly with τ. Thus, the larger we make the interval $(\tau - t_0)$ between the end of the signal and the recall pulse, the less will be the amplitude distortion.

We did, however, perform a few additional TIR experiments with larger t_0 values. In one case, t_0 was made 3μs (retaining a sawtooth envelope), and τ was 8μs. In this case, once again, a clearly time inverted echo was obtained in the interval 13μs to 16μs, with the peak occuring around 13μs (see Fig.2.22(a) and (b)). In Fig.2.22(a), we once again show the qualitative TIR response alongside the input

for perspective. Fig.2.22(b) shows the actual SPICE output. In the second case, t_0 was made 4μs, with the break in the sawtooth at 3μs. Between 3μs and 4μs, the input was forced to decrease linearly from 2V at 3μs to 0V at 4μs. The intention was to clearly show the inverted slope in the echo. The recall pulse was applied at t=9μs. However, it turned out that in this case the resulting echo, although having a peak at 15μs, did not actually extend from 14μs to 18μs as expected (see qualitative perspective sketch in Fig.2.23(a) and the actual SPICE output in Fig.2.23(b)). Instead, the echo started to show some splitting effects, in which the region to the left of the echo area seemed to be reinforced in amplitude, while part of the normal echo to the right appeared to be blanked out in a manner reminiscent of interference.

It was only much later, while experimenting with TIR in the nonlinear coupling regime, that we found an apparent way of reducing the extent of splitting in the recalled TIR echo. We will discuss the method (which, incidentally, failed in the anharmonic regime) shortly, after first presenting our initial speculations and efforts vis-a-vis the splitting.

To verify if the blanking and reinforcing of the response near the echo area was caused by undesirable

response components or not, we carried out the 2-slope, 4μs TIR experiment with a slight variation. Instead of applying the recall pulse at t=9μs, it was now applied at t=8.875μs, which is exactly one-half carrier cycle (180) removed from its earlier position. In the simplest case, if the "interference" was due to the phase addition of the echo with the tail of the linear response to the 10V recall pulse, then, it would make sense to assume that if the recall pulse were applied a half-cycle earlier (which would also move the linear response by a half-cycle), then the blanked portions of the previous response would be reinforced, and vice-versa, thereby restoring the proper TIR shape of the recalled signal. Amazingly enough, the above procedure indeed made a significant difference in the recalled signal. The blanked portions of the TIR signal were restored, and the unwanted reinforcements were suppressed (see qualitative perspective sketch in Fig.2.23(c) and actual SPICE output in Fig.2.23(d)). However, to the far right of the echo area, there were now very well-defined narrow additional response humps that were separated from the TIR echo. This indicated some still unexplained interference and high-level splitting effects.

The following were thought to be the possible causes for the interference at the time :

(i) The tail of the natural (instantaneous) response to the 10V pulse. Using a rough estimate of the amplitude of this response in the vicinity of the TIR echo, we found that normally this amplitude would be at least a factor 5 to 10 smaller than the nonlinear echo amplitude. Hence, it should not have any significant impact on the TIR echo shape. However, we must also note the following. It was found that in the TIR echo envelope, the linearly decreasing portion was not exactly linear. In fact, it was found to have a fast decay (almost exponential) after reaching the peak. It might be thought that this is due in part to the amplitude distortion caused by the dependence on τ for small τ; however, the distortion order seemed to be reversed. So this does not appear to be a feasible explanation.

(ii) The tail of the autocorrelation of $g(t-\tau)$. Note that as long as (2.52b) is satisfied, and the system bandwidth is large enough, this tail should not affect the TIR echo. From the choice of parameters, (2.52b) is certainly satisfied.

(iii) The fundamental assumption (2.54) for seeing a TIR echo may not have been true under the present condition. To verify if (2.54) was true or not, the value of this term was estimated both for the pulse echo and the TIR echo systems.

Case A : 2-pulse nonlinear echo

In this case, (2.54) takes the form :

$$(t-\tau)\alpha W^{2} A_1 A_2 << 1. \qquad (2.78)$$

Assuming that WA_1 and WA_2 represent the linear responses of one resonator to the input pulses, we obtain the following estimates for them both from theory and from SPICE :

$\tau=10\mu s \quad \Delta T=0.11\mu s$

$V_1=1V,\ V_2=10V,\ a_3=-10^3$

$f_c=2MHz.$

Hence we can show :

$$WA_1 \sim 0.948mV,\ WA_2 \sim 9.48mV.$$

Using (2.71b) and assuming that the $(t-\tau)$ factor is approximately equal to τ, we obtain :

$$\tau\alpha(WA_1)(WA_2) \sim 0.423 \text{ radian.}$$

Note that the above value is not much smaller than 1. However, for a 2-pulse nonlinear echo, (2.78) does not have to be satisfied, since the result derived for this case is exact.

Case B : TIR echo system

Following a computation procedure similar to above,

and assuming that the linear response amplitude of a single resonator to a sawtooth can be taken approximately to be that due to a 2V pulse, we obtain in this case (with f_c=4MHz, ΔT=0.05μs) :

$$\tau\alpha(WA_2)((W/2)G(\Omega))\sim 0.174 \text{ radian.}$$

Note that the above quantity is reasonably small compared to 1. In this case, however, the magnitude of this number is very critical in determining the validity of the results derived for the TIR echo. Thus, if any of the assumptions made in the calculation above fails, then the system response will be quite different from that expected.

(iv) The effect of α not being a constant. As we have discussed earlier, the exact analytical plots for pulse inputs with α constant as well as a variable show little difference in the responses. As such, it seems reasonable to assume that the error due to the approximation in α is not significant, even when a general input is involved.

As a final attempt to reduce the splitting of the TIR echo, we used a series of delta pulses (in this case, triangular pulses) with alternating signs and a sawtooth envelope of total duration 4μs, instead of the usual analog

r.f. sawtooth as input. This was followed by a recall pulse at t=9μs. The reason for trying this was that we had found in later experiments with nonlinear coupling echoes, that with sampled inputs, the recalled TIR signal was fairly close to the expected TIR shape, and there was virtually no splitting. We believed, as a result, that this was probably due to the "cleaner" spectrum of the sampled signal whereby all higher harmonics were rejected by the circuit.

In Fig.2.24 we show the SPICE output for a sampled sawtooth input. It is clear from the plot that the recalled TIR signal in this case is still split up, and does not extend from 14μs to 18μs as expected. Instead, after an initial rise near 14μs, the response rapidly decays, and eventually reappears as an additional hump near 18μs. Thus, we may conclude that the effect of TIR echo splitting is associated with the anharmonic nonlinearity itself (i.e., the assumptions made in the theory for echo generation with such nonlinearity were not stringent enough as many terms were ignored for simplicity), and has nothing to do with the nature of the input, nor is it a computer artifact.

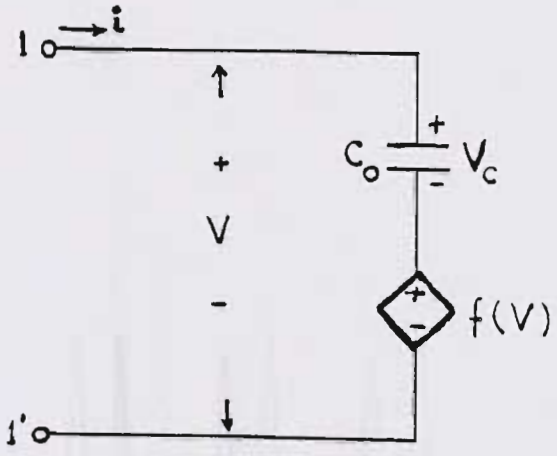

(a) Nonlinear capacitor test model.

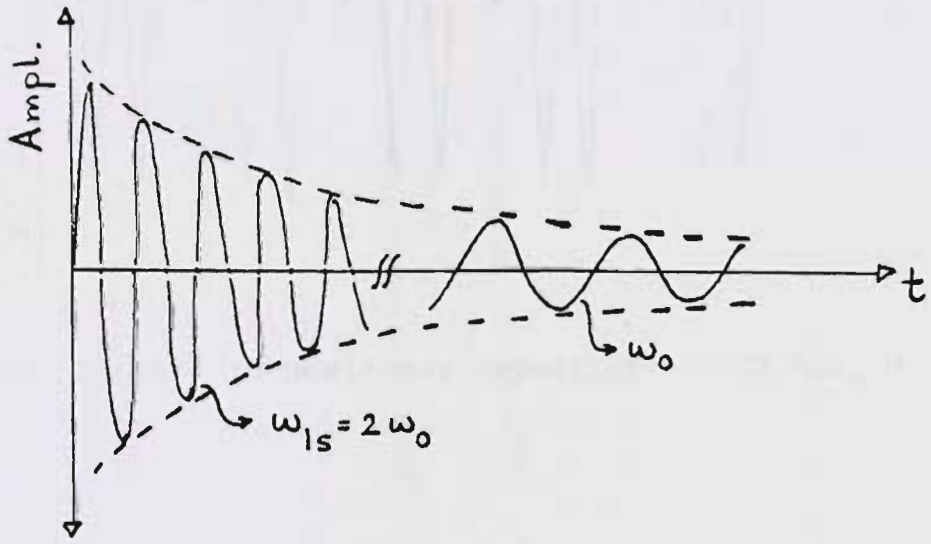

(b) Expected step response of nonlinear RLC resonator for $a_3|V_0|^2=1$.

Figure 2.1. Test experiments with nonlinear capacitor.

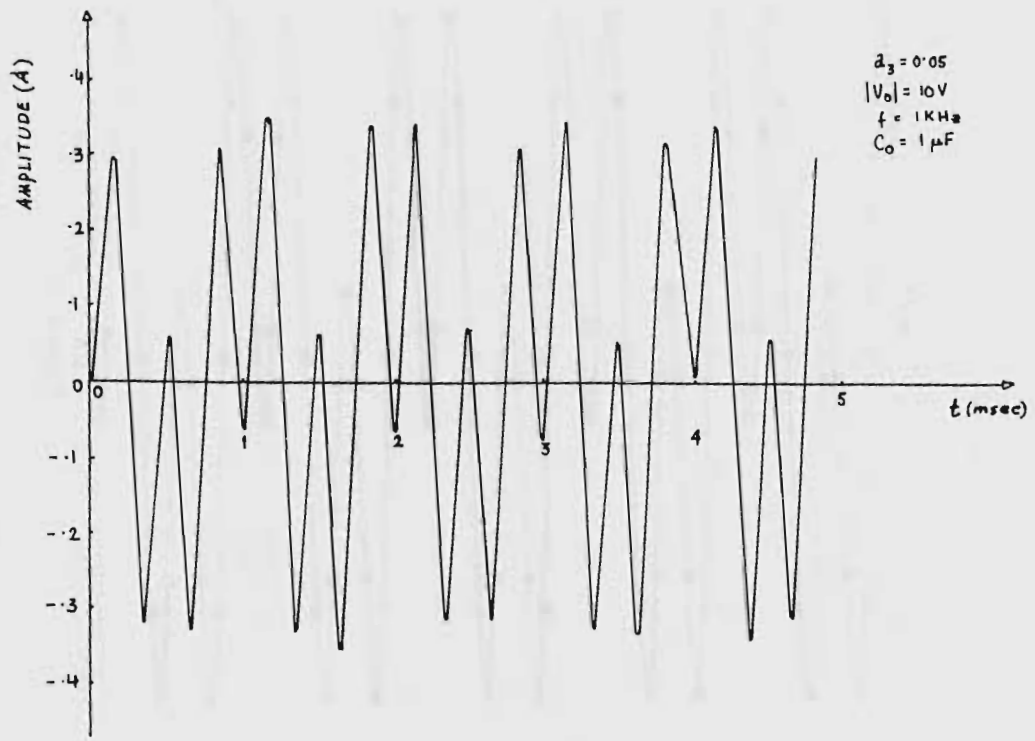

(c) Current in nonlinear capacitor--SPICE output.

Figure 2.1. (continued)

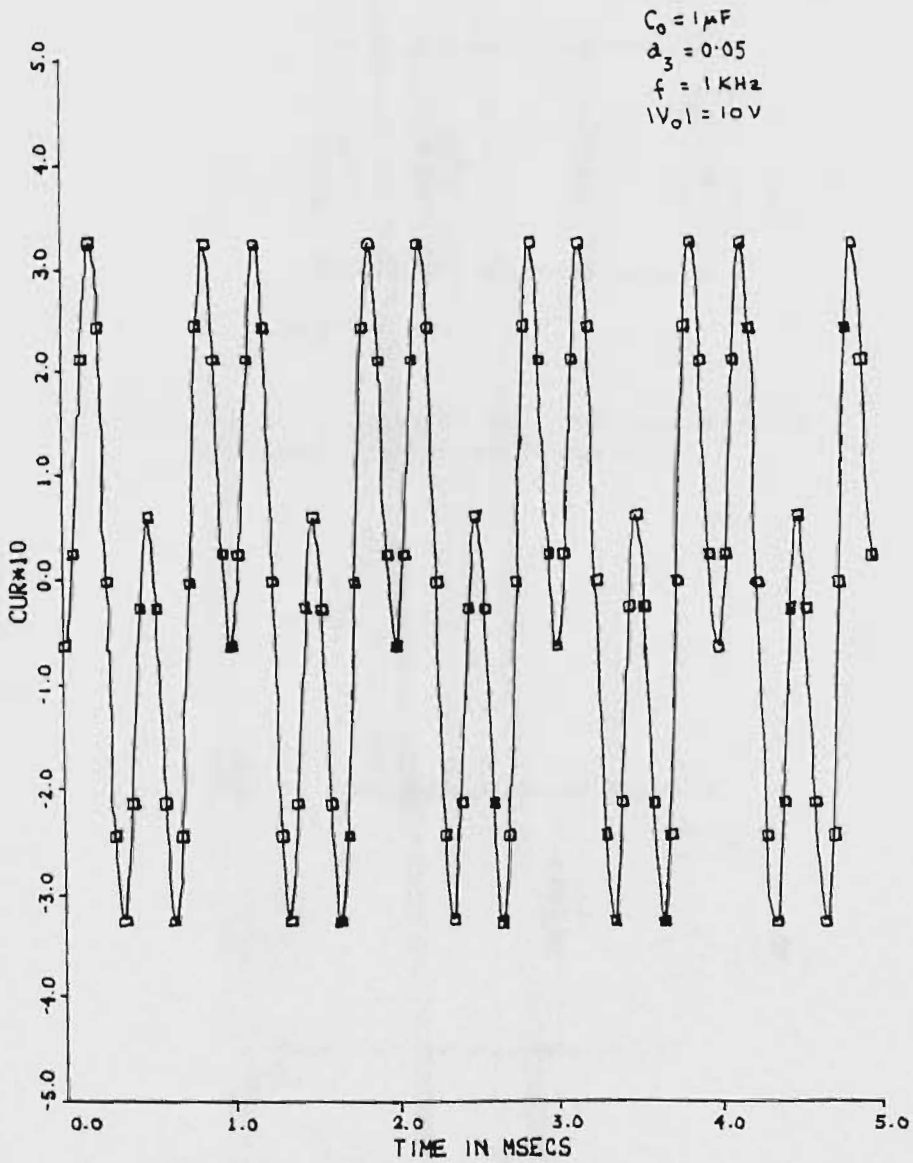

(d) Current in nonlinear capacitor--analytical plot.

Figure 2.1. (continued)

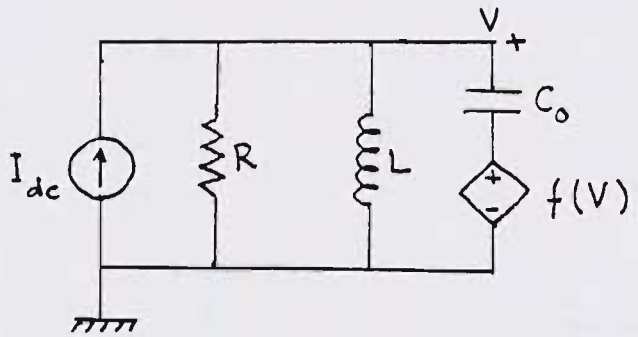

(a) Typical nonlinear RLC resonator with current source excitation.

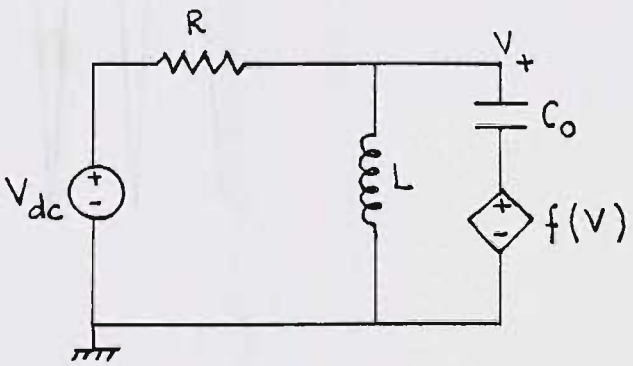

(b) Thevenin form of the circuit in (a).

Figure 2.2. Nonlinear RLC resonator configuration.

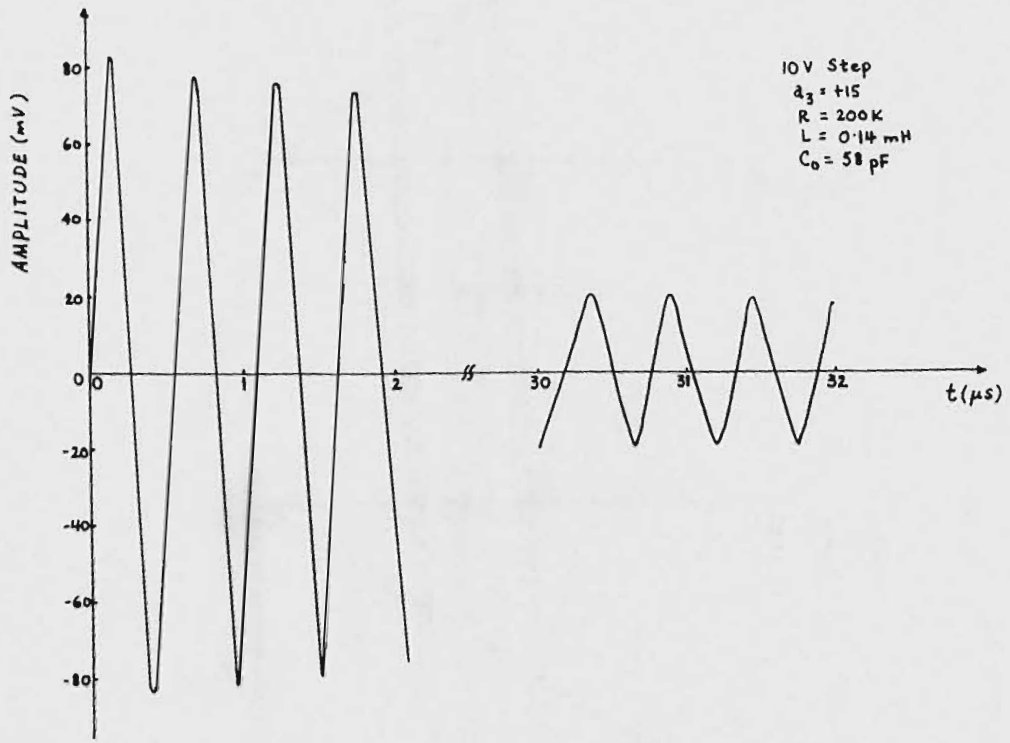

Figure 2.3. Typical step response from SPICE near t=0 and t=∞, showing expected decrease in frequency for lower amplitudes.

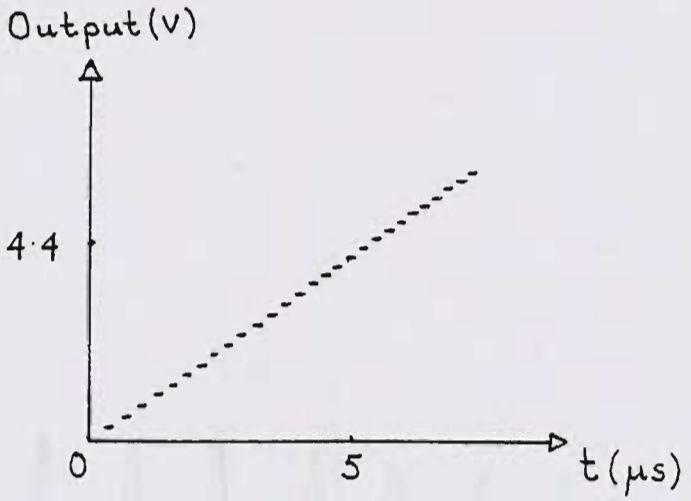

(a) a_3=28.

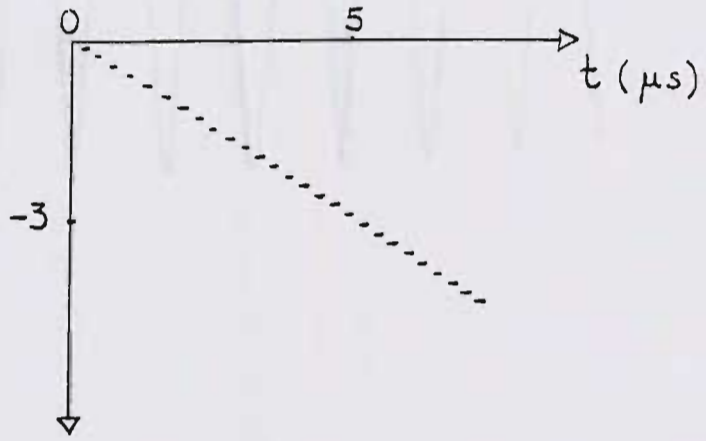

(b) a_3=56.

Figure 2.4. SPICE response of nonlinear resonator to a step input.

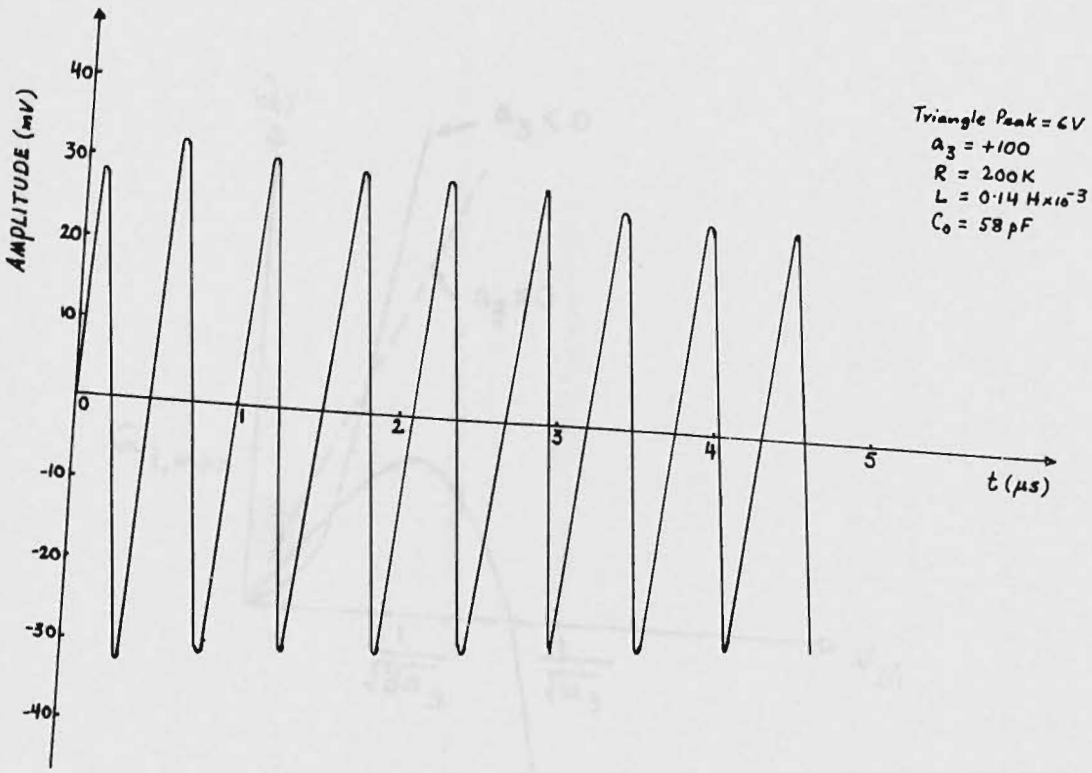

Figure 2.5. SPICE response of nonlinear resonator to triangular pulse, with a_3=100.

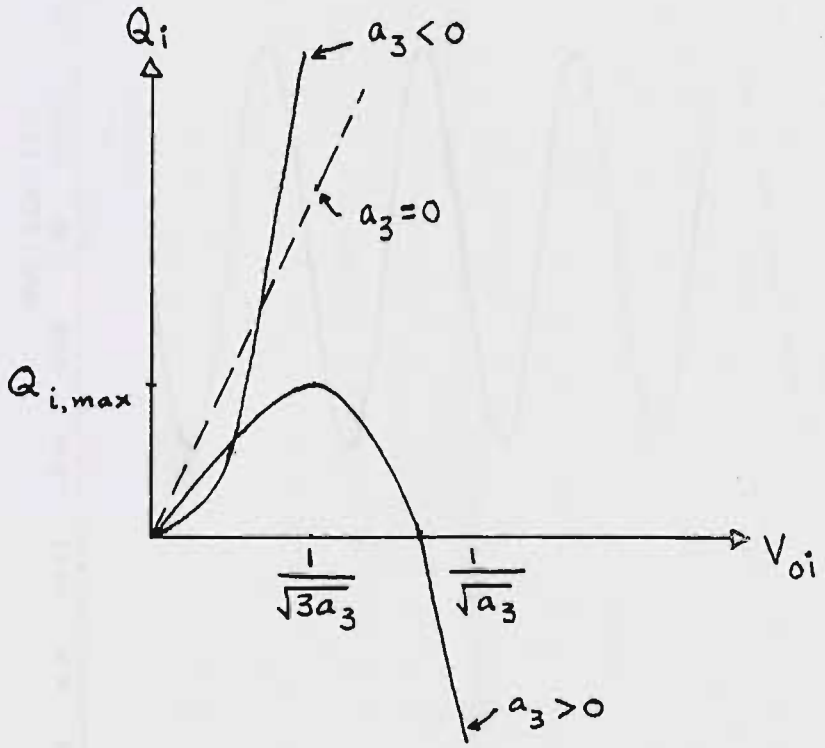

Figure 2.6. Qualitative plot of Q_i vs. V_{Oi}.

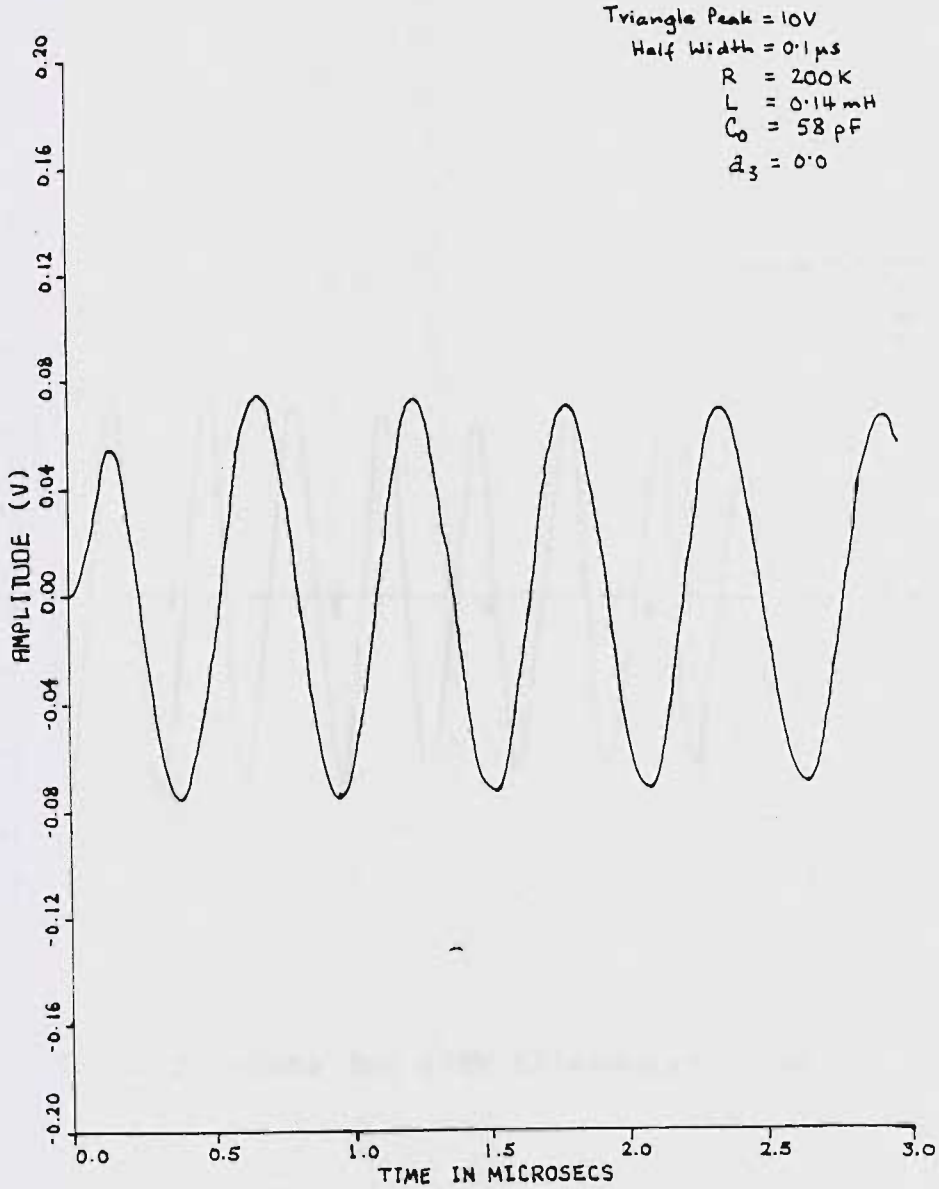

(a) Analytical plot for 10V triangular pulse.

Figure 2.7. Response of nonlinear resonator to a triangular pulse, with a_3=0.

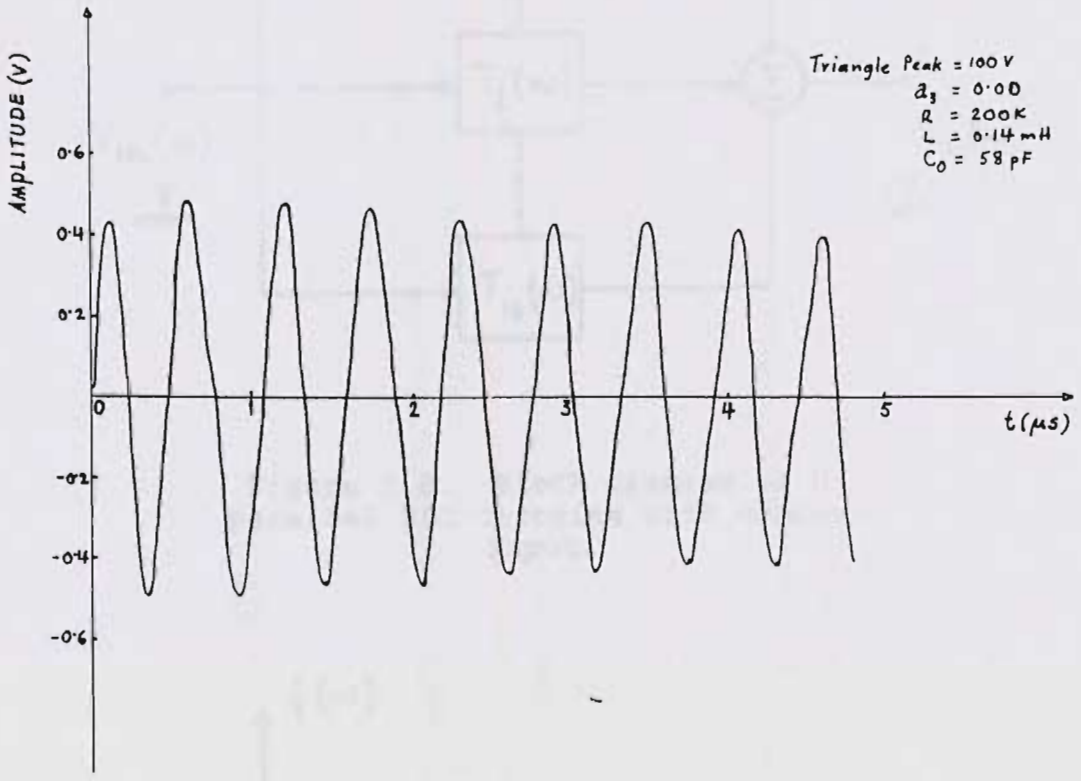

(b) SPICE response for 100V triangular pulse.

Figure 2.7. (continued)

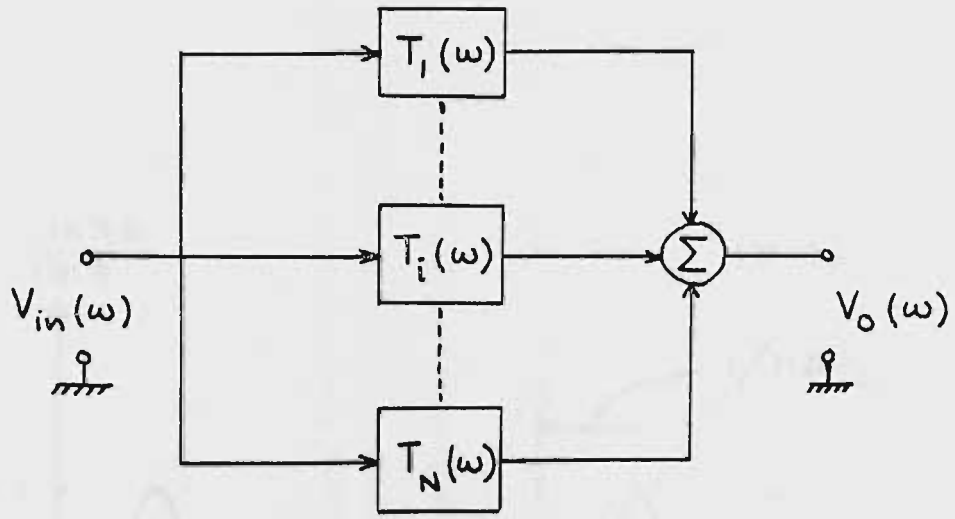

Figure 2.8. Block diagram of N parallel RLC circuits with common input.

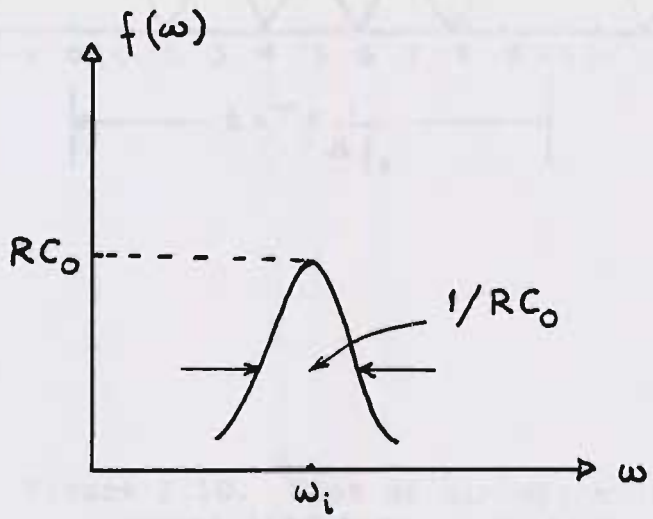

Figure 2.9. Qualitative plot of a function which becomes a delta function as $RC_0 \to \infty$.

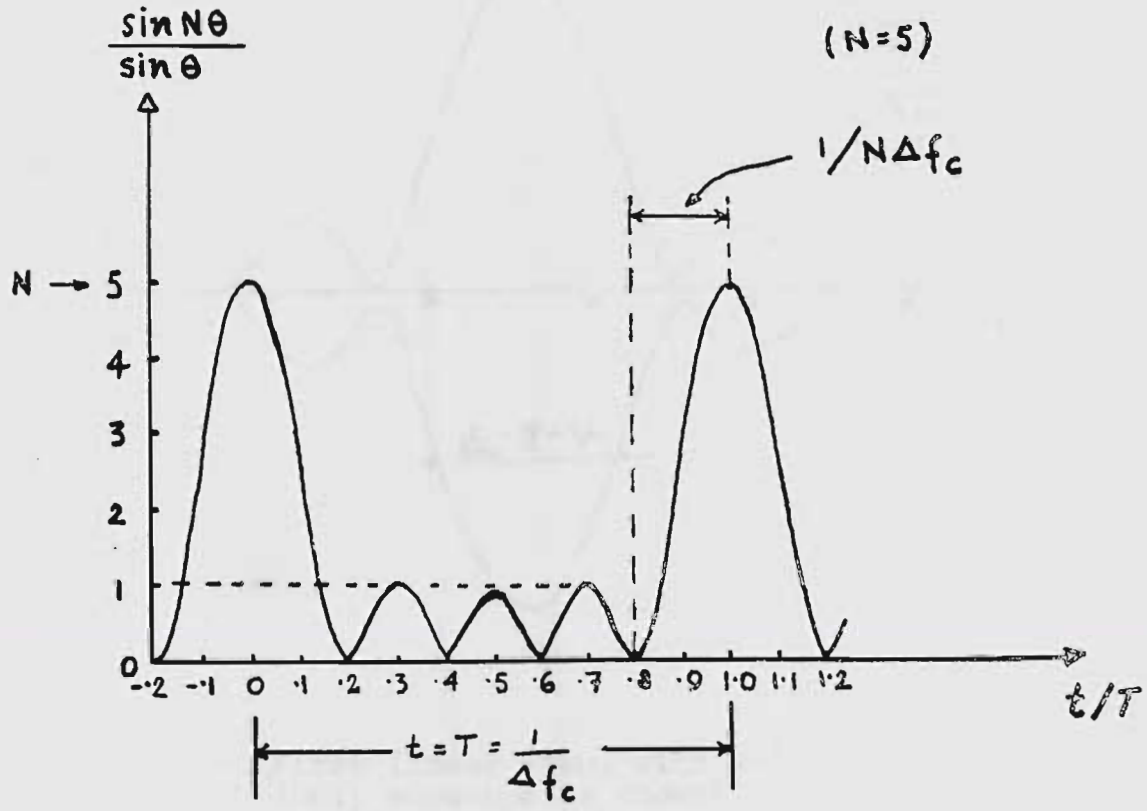

Figure 2.10. Plot of $\sin(N\theta)/\sin\theta$ vs. normalized time ($\theta=\Delta\omega_c t/2$).

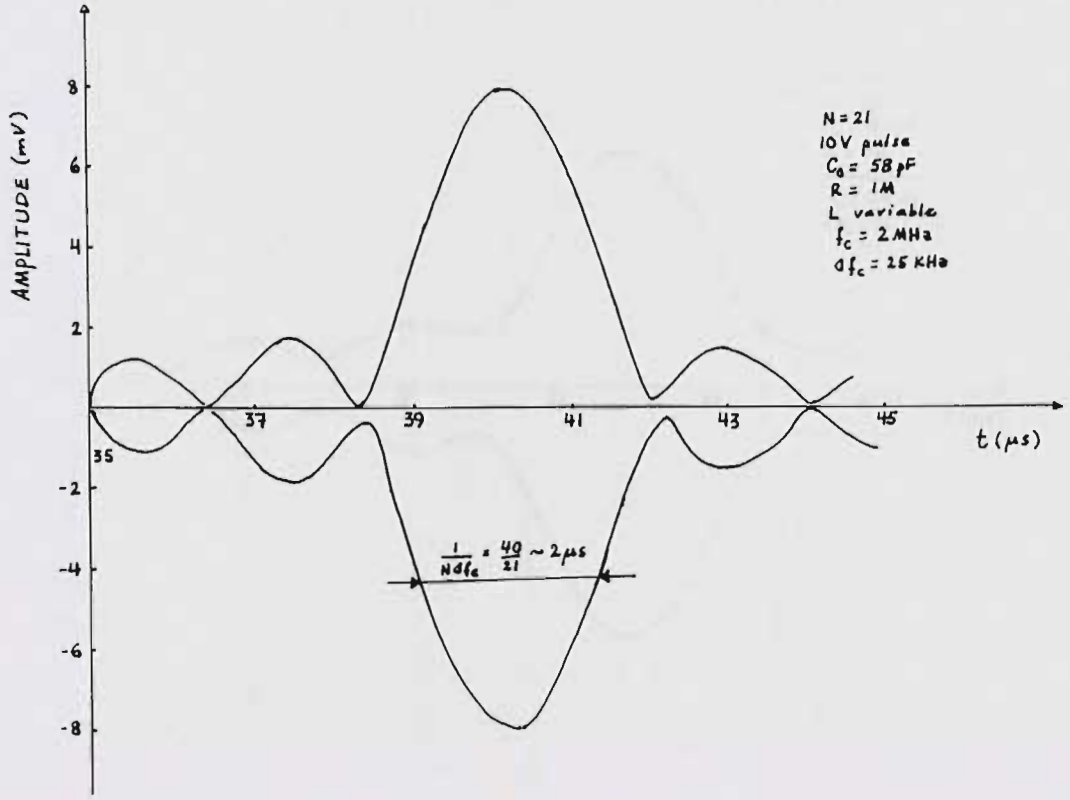

(a) First linear echo, with N=21 (only envelope is shown).

Figure 2.11. Linear echo experiment on SPICE.

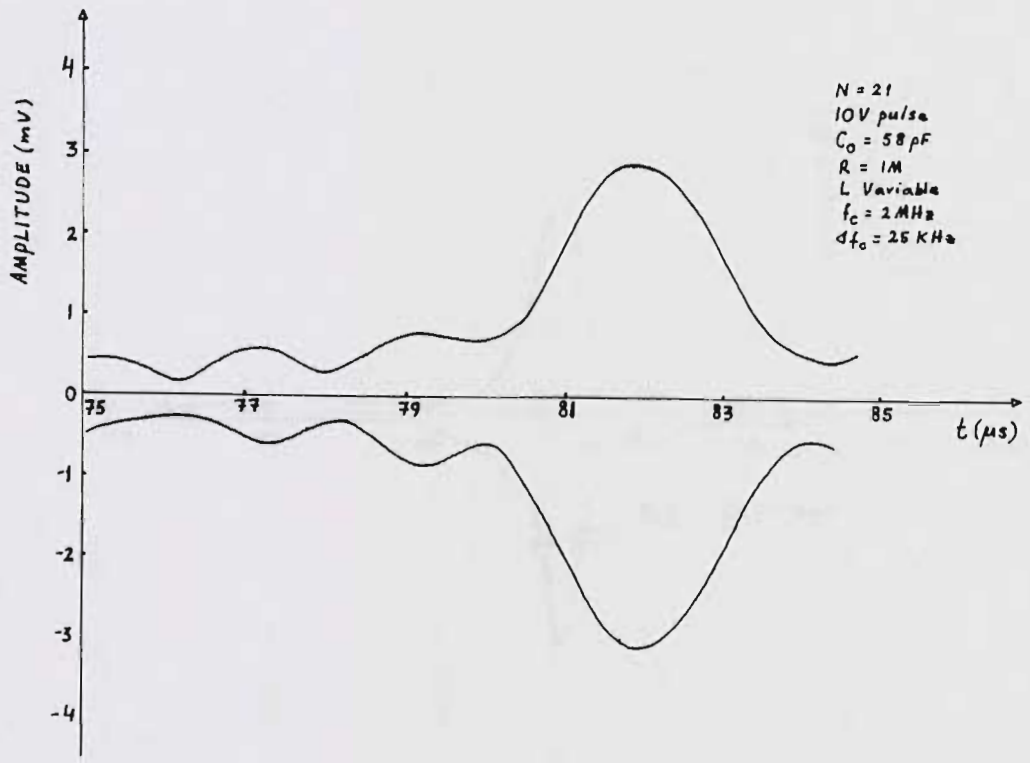

(b) Second linear echo, with N=21
(only envelope is shown).

Figure 2.11. (continued)

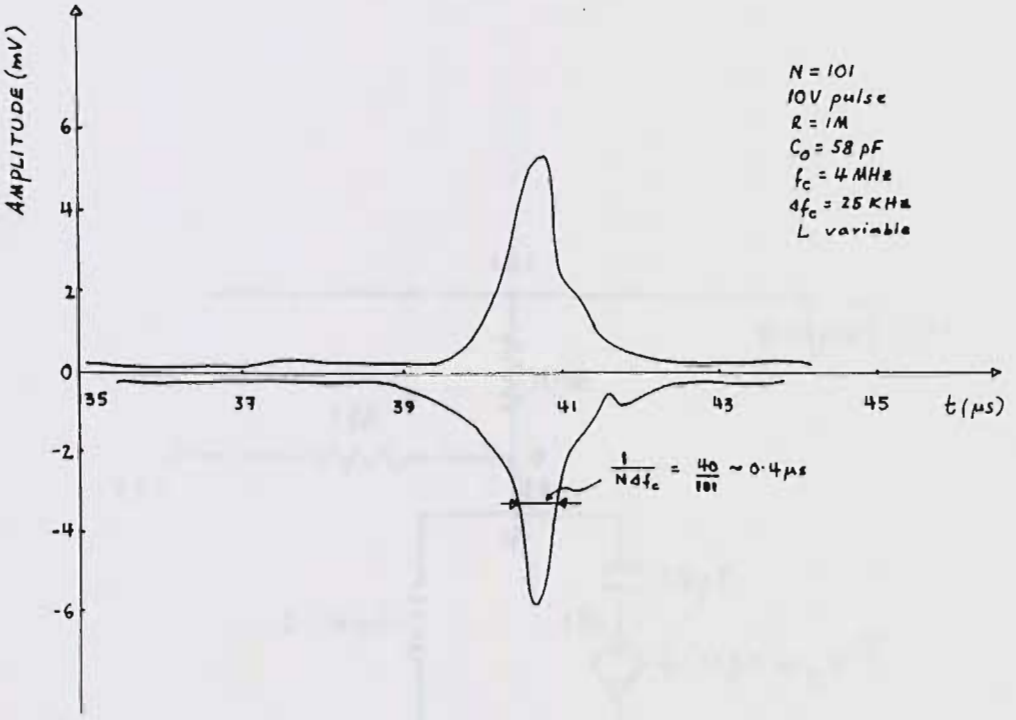

(c) First linear echo, with N=101
(only envelope is shown).

Figure 2.11. (continued)

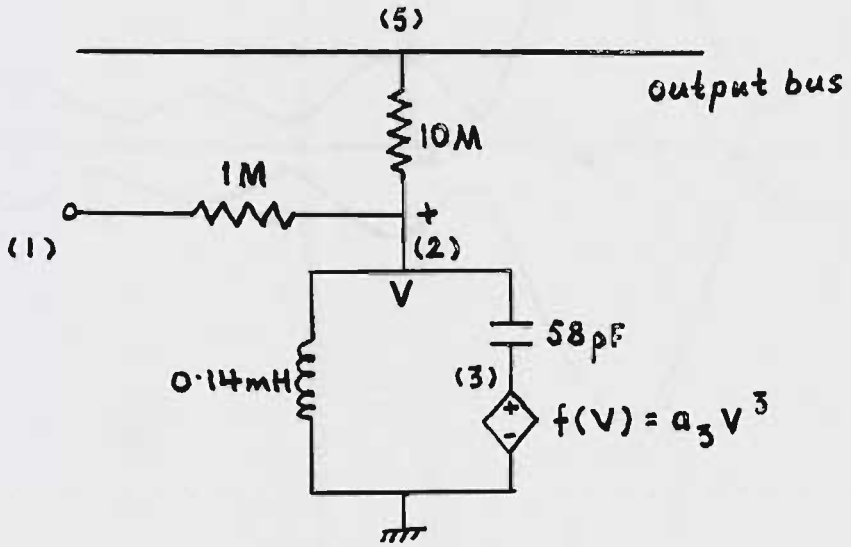

Figure 2.12. Typical nonlinear resonator section used in SPICE.

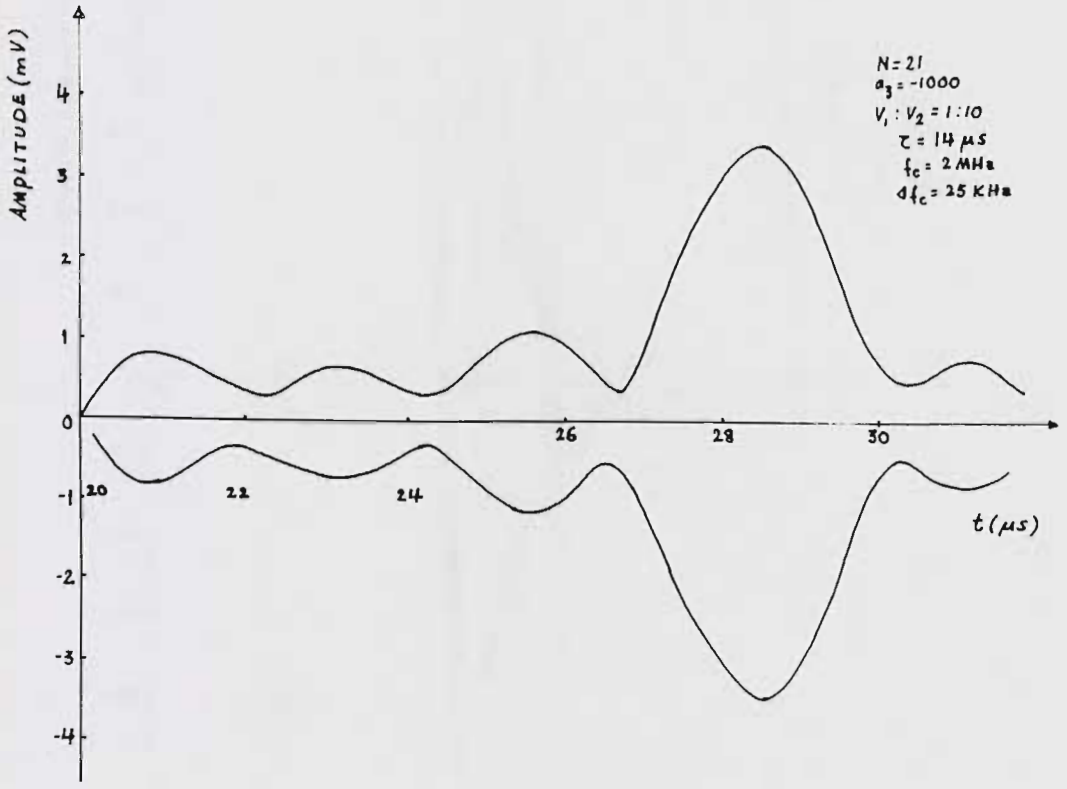

(a) N=21 (only envelope is shown).

Figure 2.13. SPICE anharmonic nonlinear echo experiments.

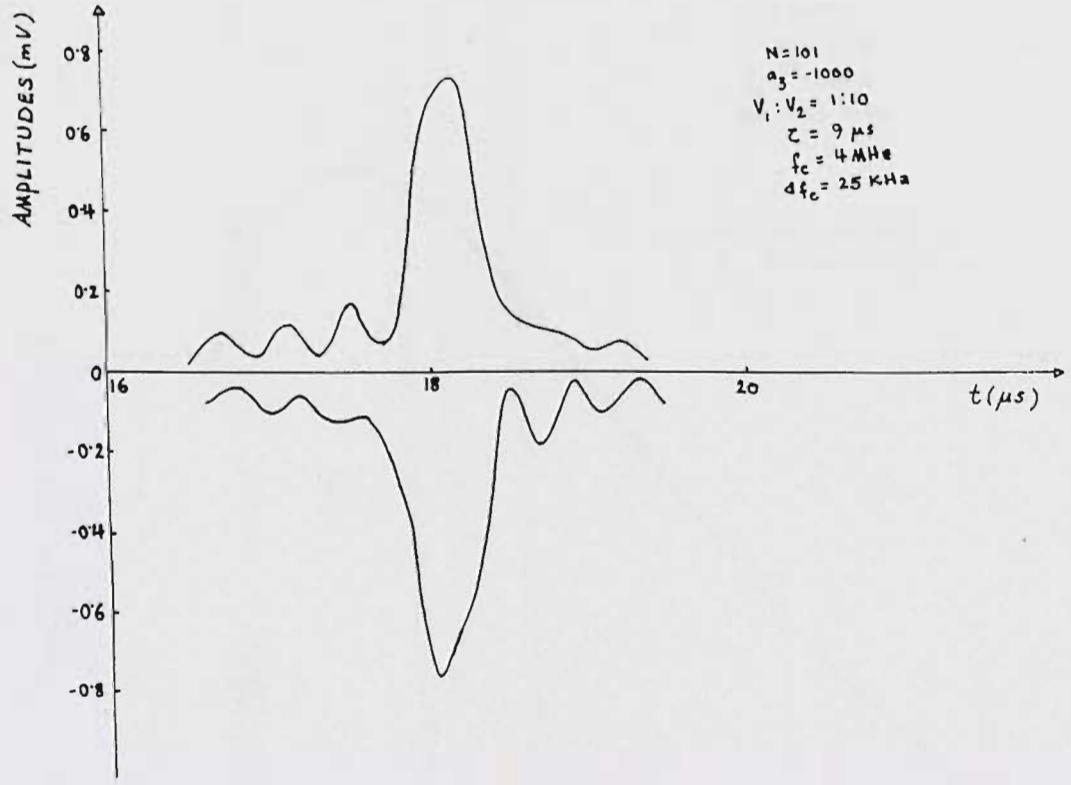

(b) N=101 (only envelope is shown).

Figure 2.13. (continued)

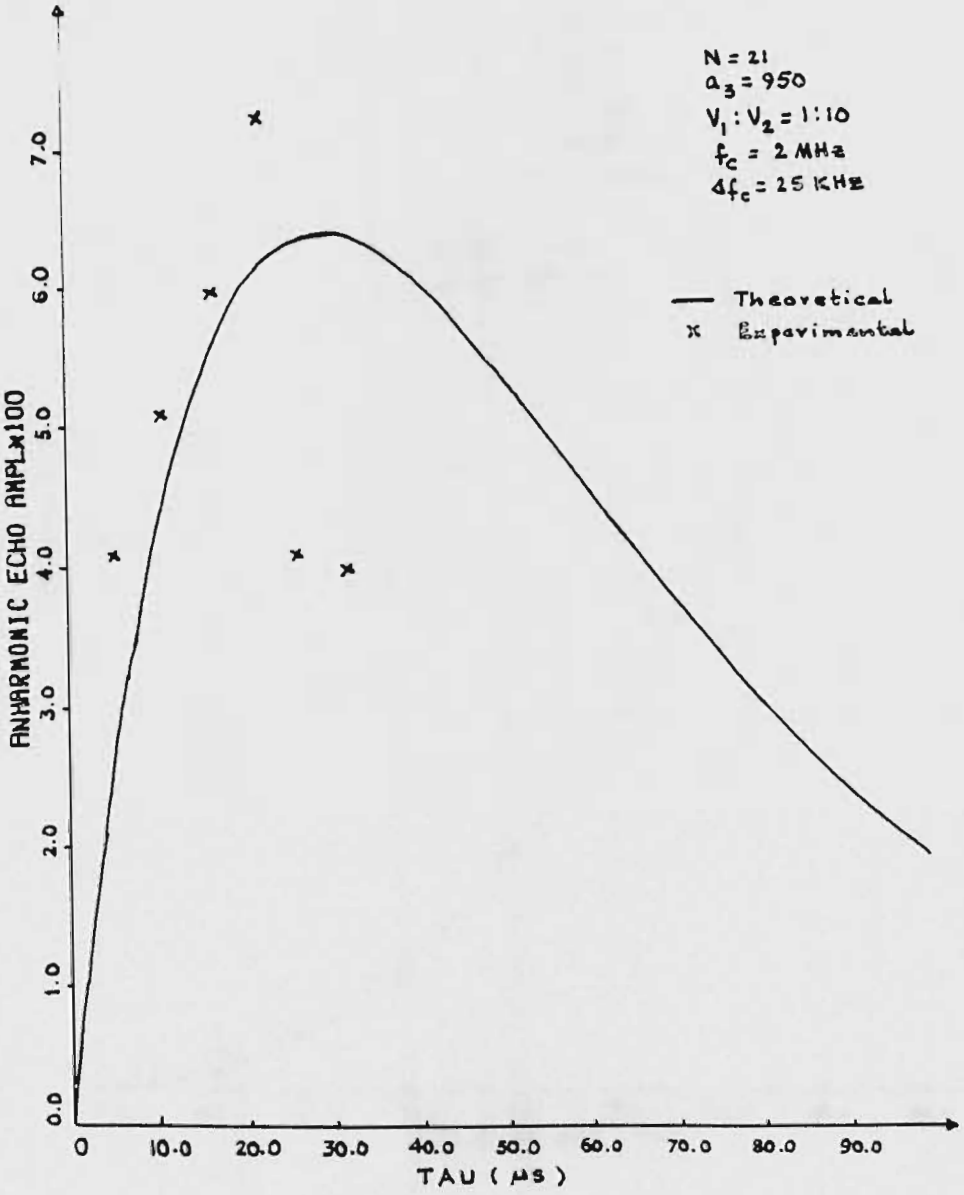

Figure 2.14. Nonlinear anharmonic echo vs. τ, with a_3=950.

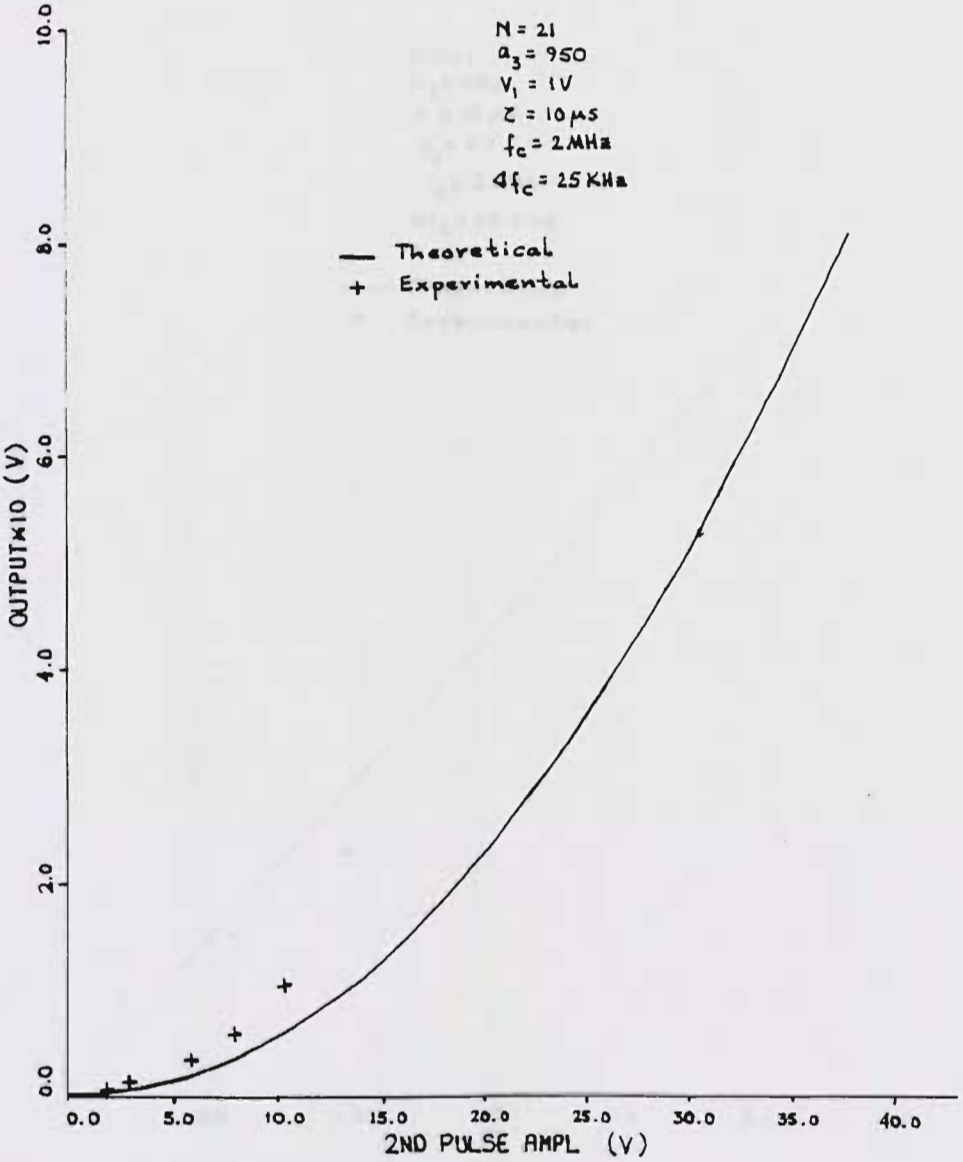

(a) Echo vs. V_2, with a_3=950.

Figure 2.15. Nonlinear anharmonic echo vs. pulse amplitudes.

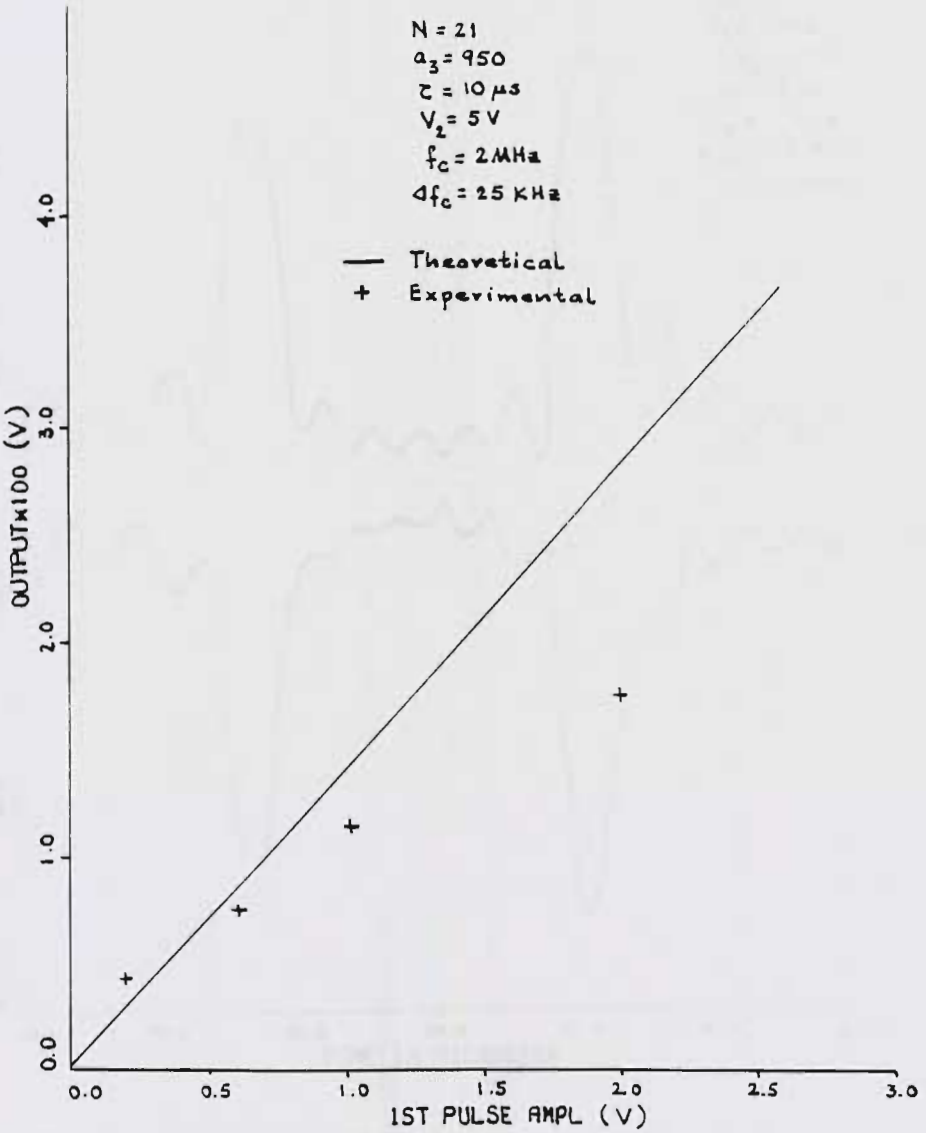

(b) Echo vs. V_1, with a_3=950.

Figure 2.15. (continued)

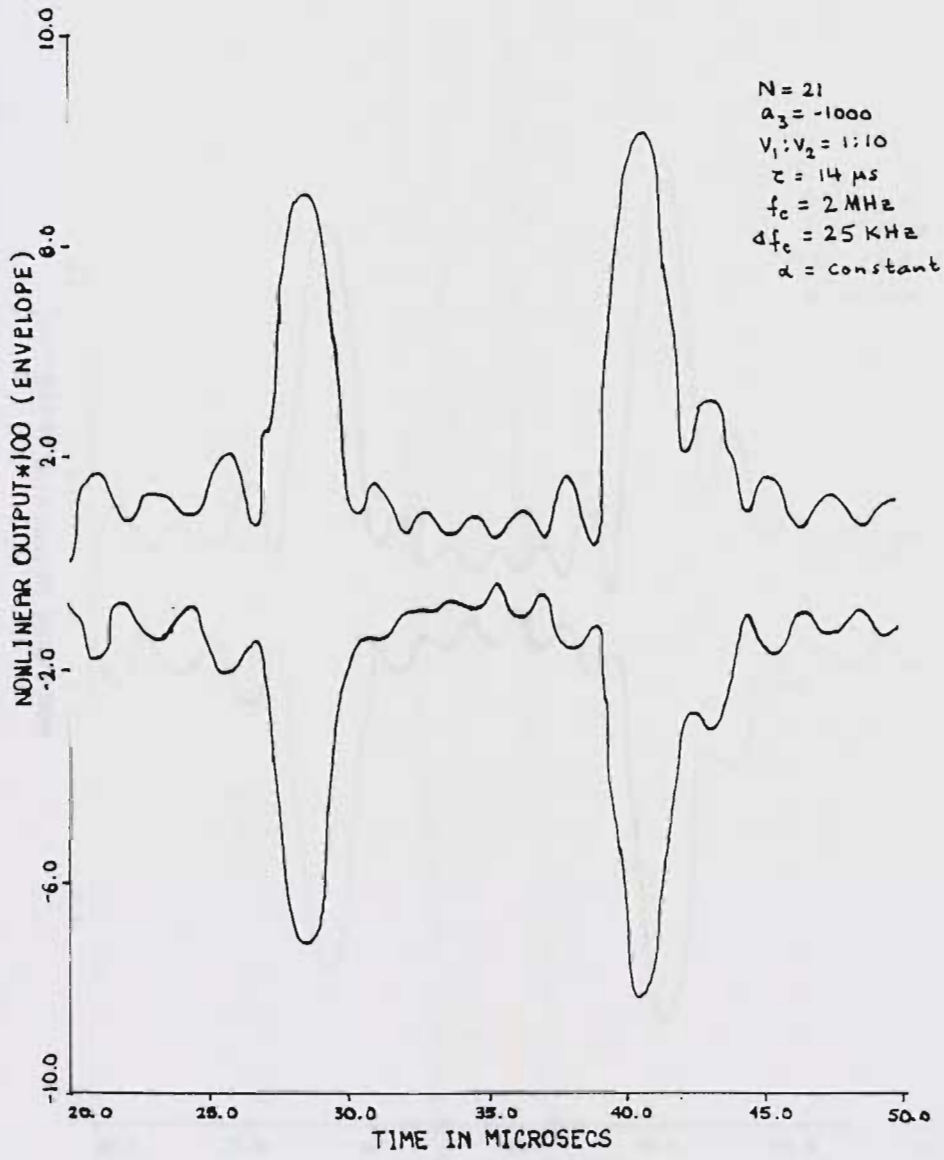

(a) α=constant, τ=14μs, pulse ratio 1:10.

Figure 2.16. Analytical plots of response vs. t, with α constant and variable.

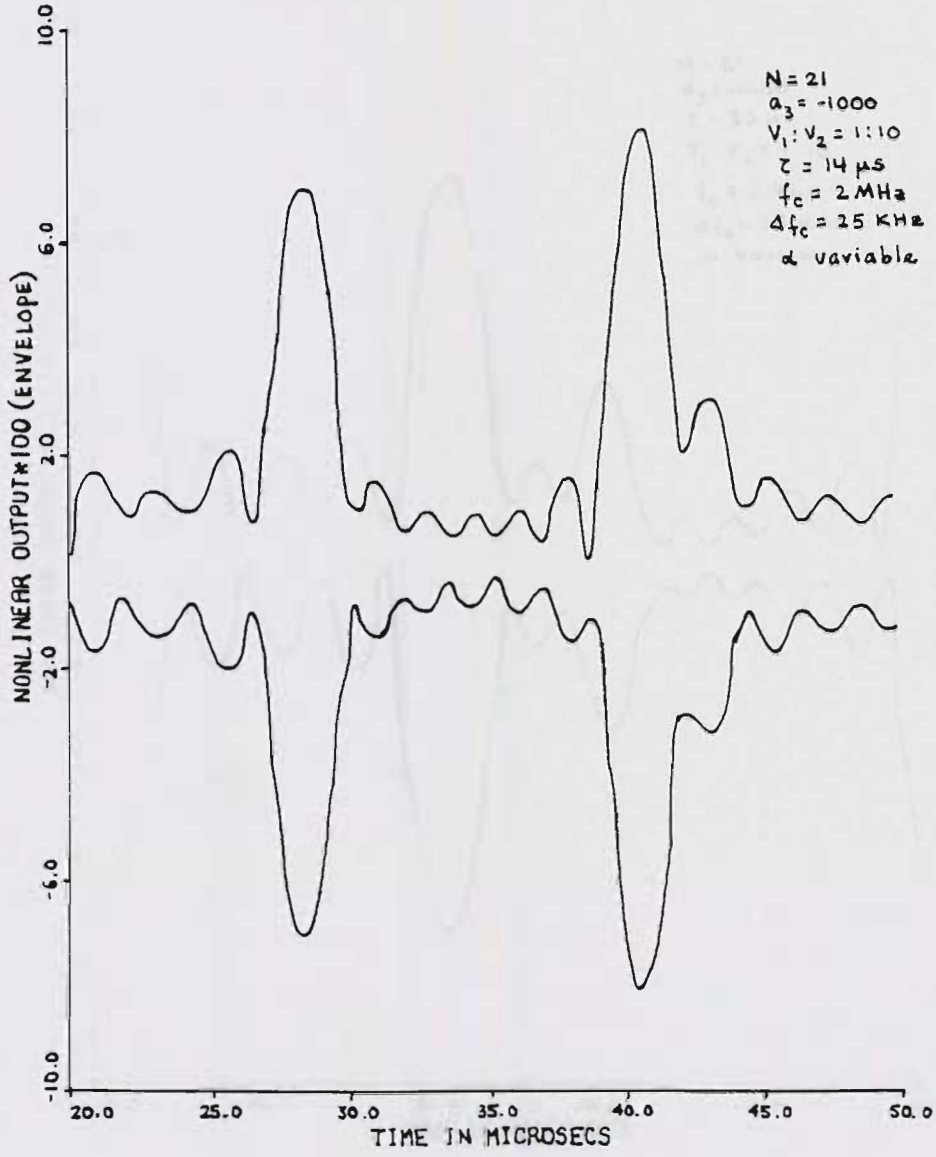

(b) α=variable, τ=14μs, pulse ratio 1:10.

Figure 2.16. (continued)

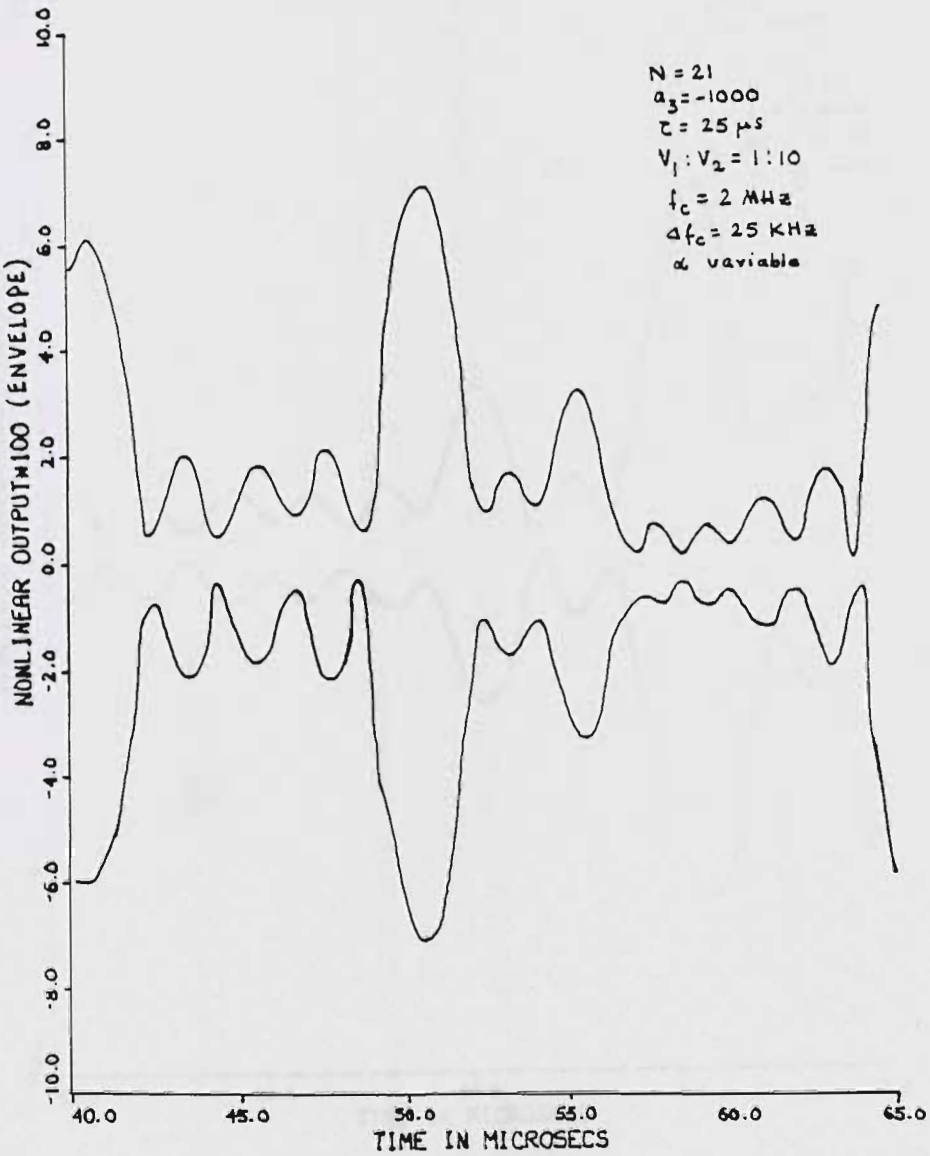

(c) α=variable, τ=25μs, pulse ratio 1:10.

Figure 2.16. (continued)

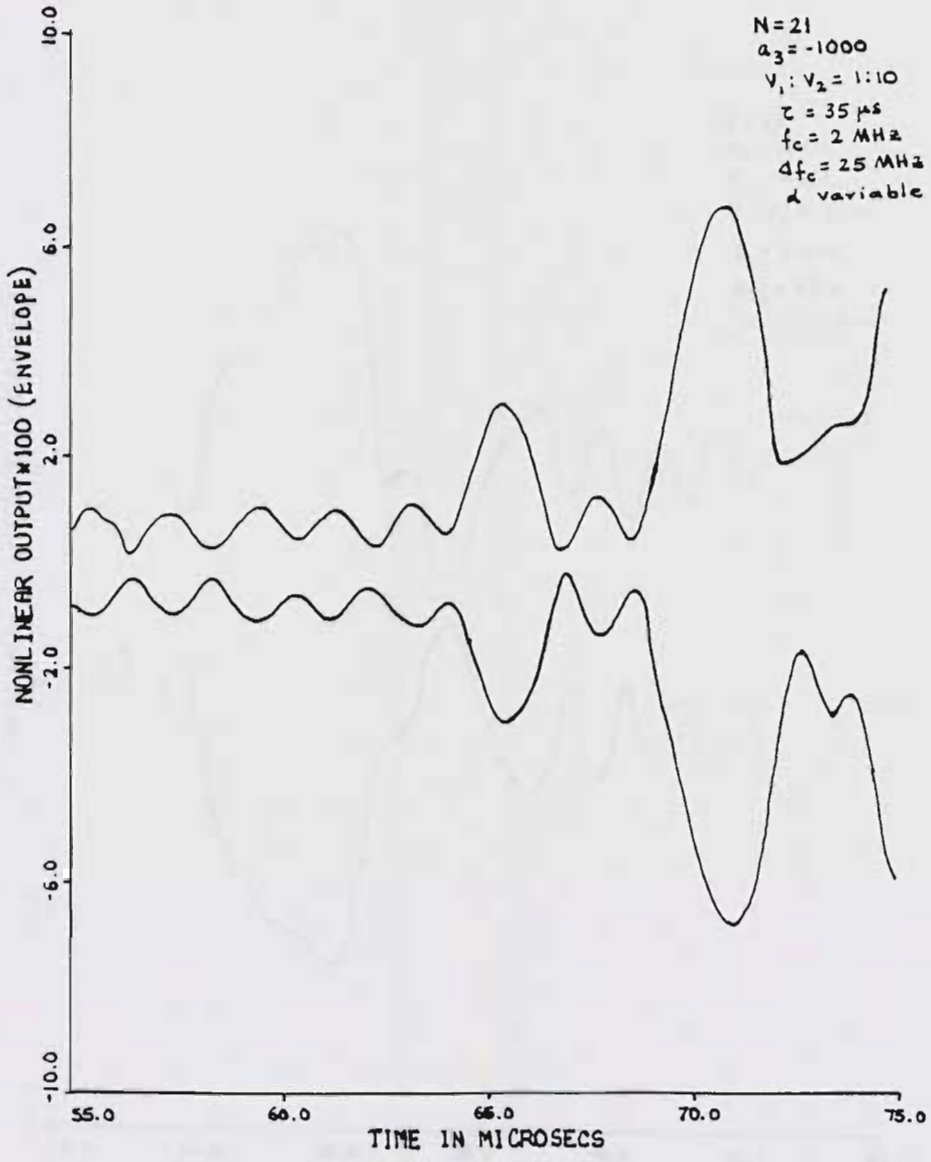

(d) α=variable, τ=35μs, pulse ratio 1:10.

Figure 2.16. (continued)

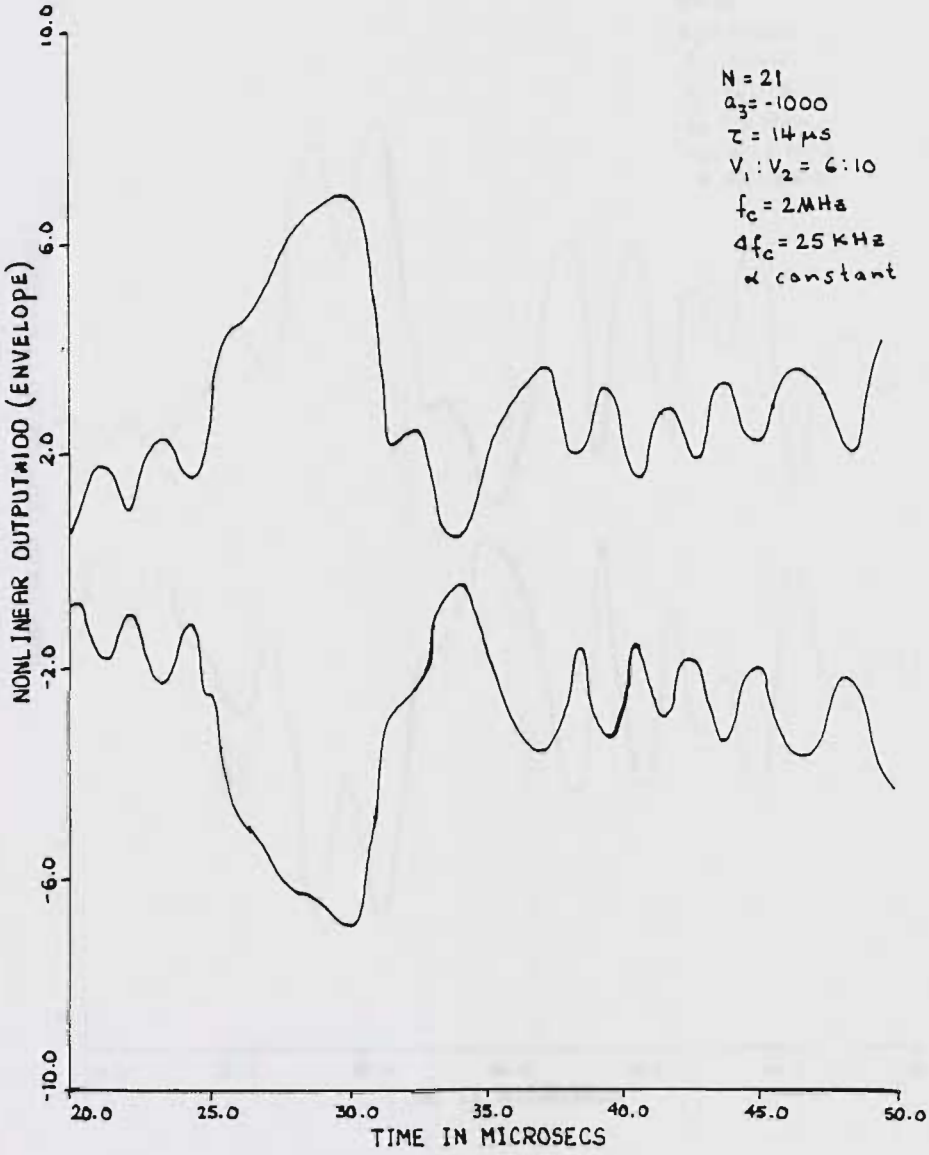

(e) α=constant, τ=14μs, pulse ratio 6:10.

Figure 2.16. (continued)

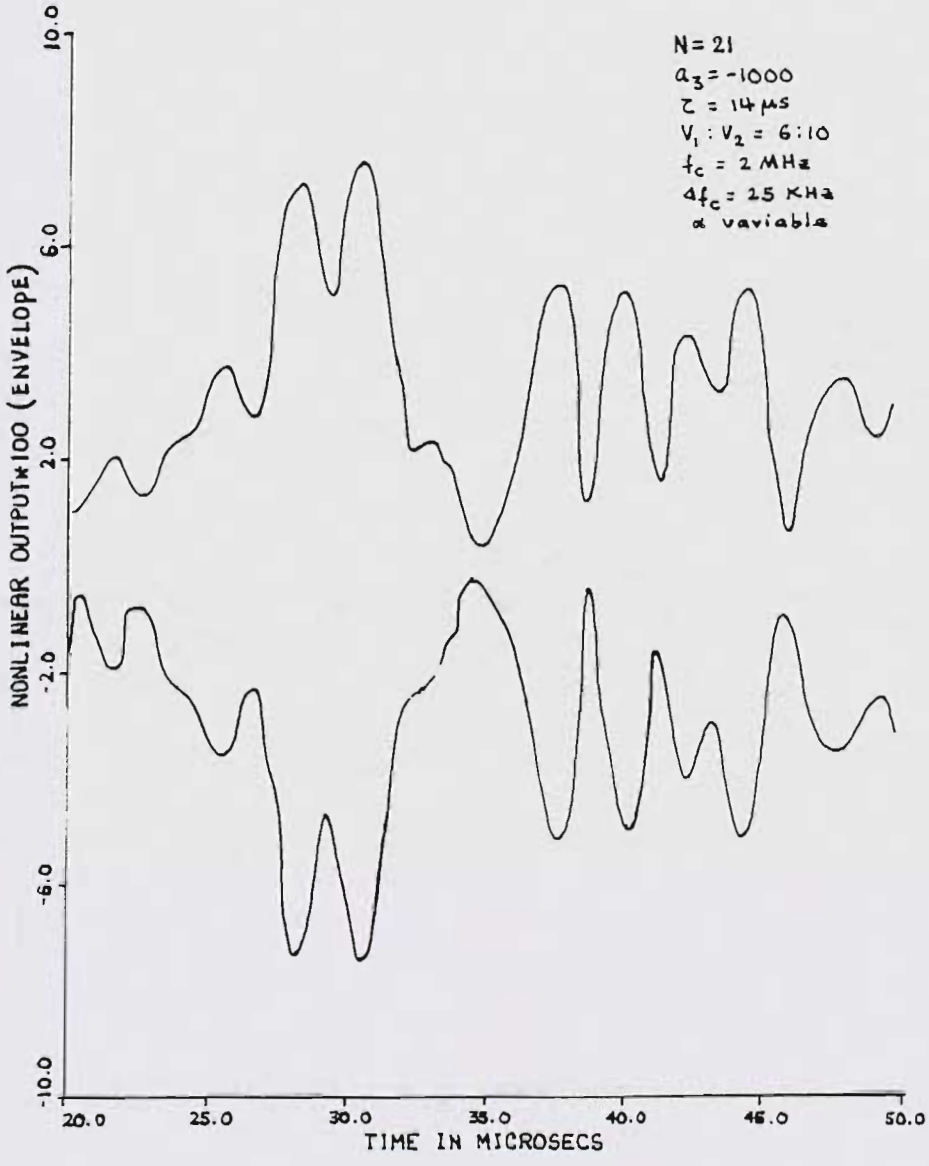

(f) α=variable, τ=14μs, pulse ratio 6:10.

Figure 2.16. (continued)

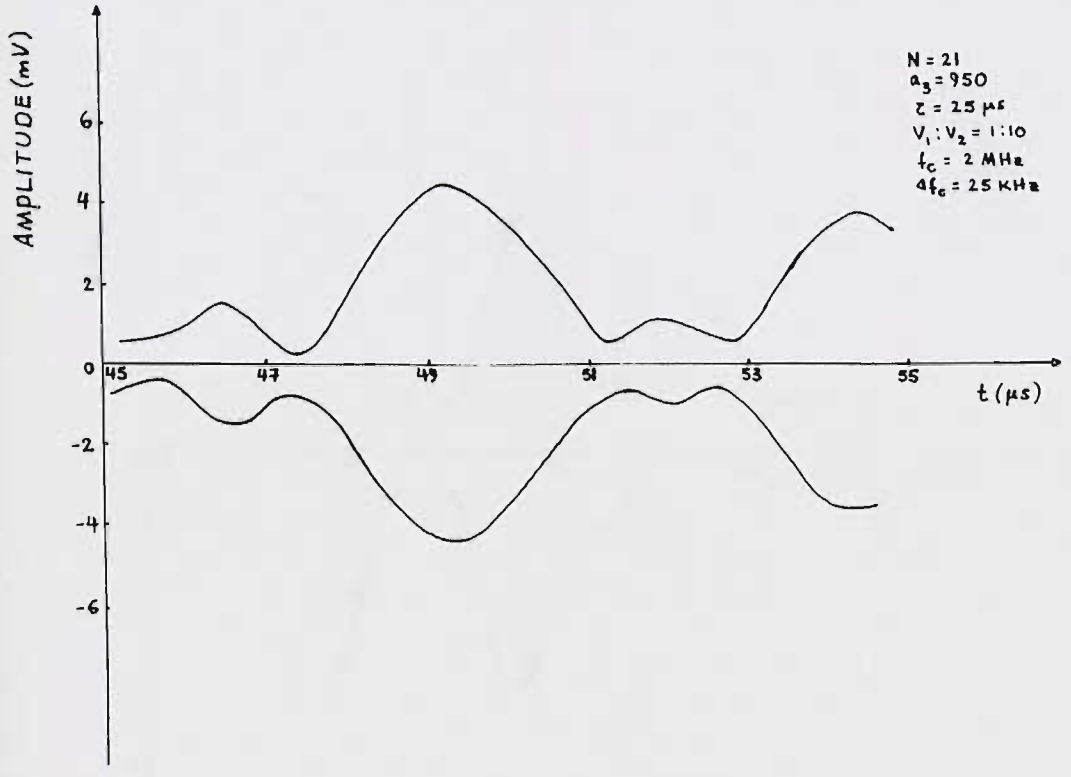

(a) For τ=25μs (only envelope is shown).

Figure 2.17. SPICE outputs showing nonlinear echo splitting and movements.

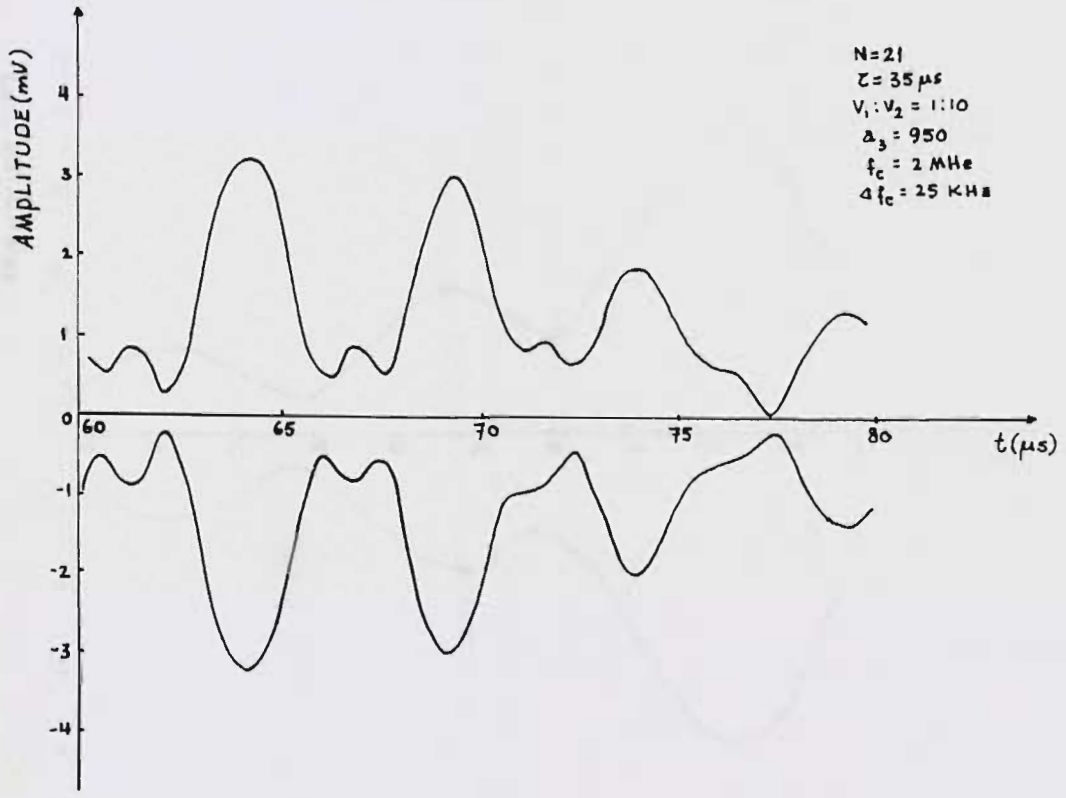

(b) For τ=35μs (only envelope is shown).

Figure 2.17. (continued)

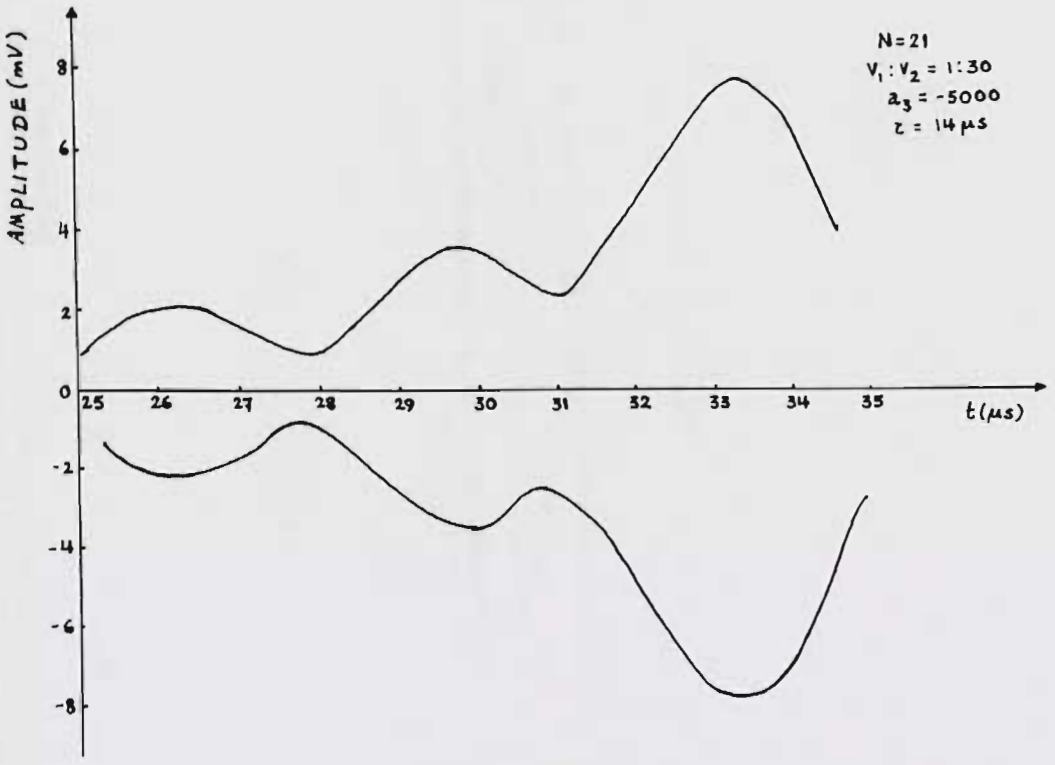

(c) For pulse ratio 1:30, a_3=-5000
(only envelope is shown).

Figure 2.17. (continued)

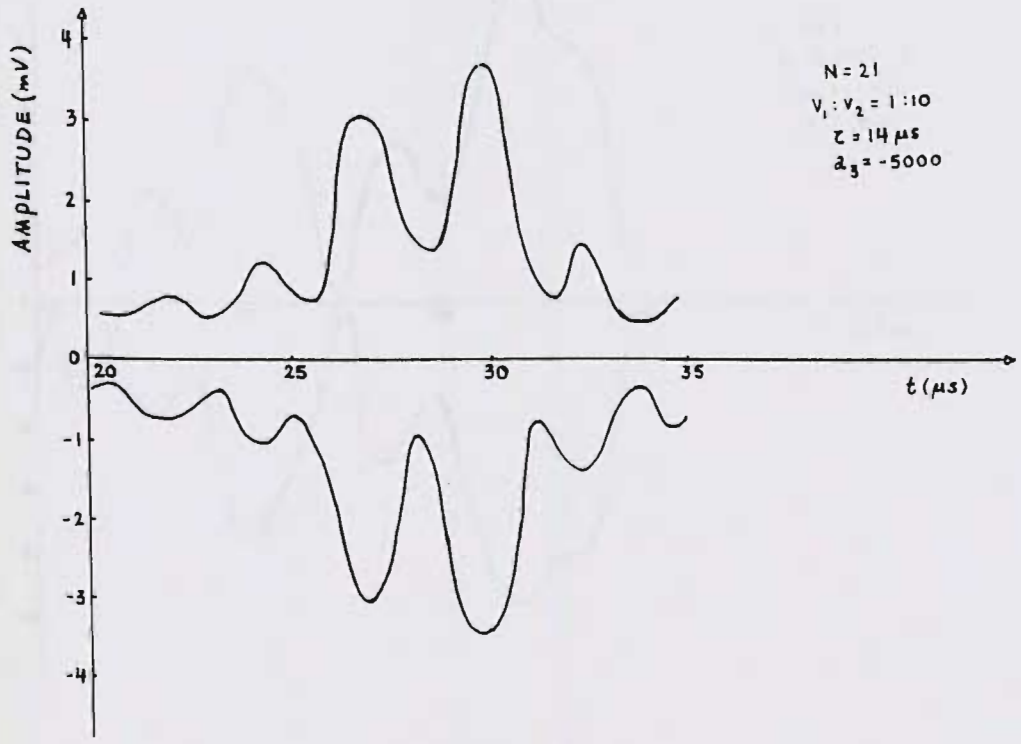

(d) For a_3=-5000 (only envelope is shown).

Figure 2.17. (continued)

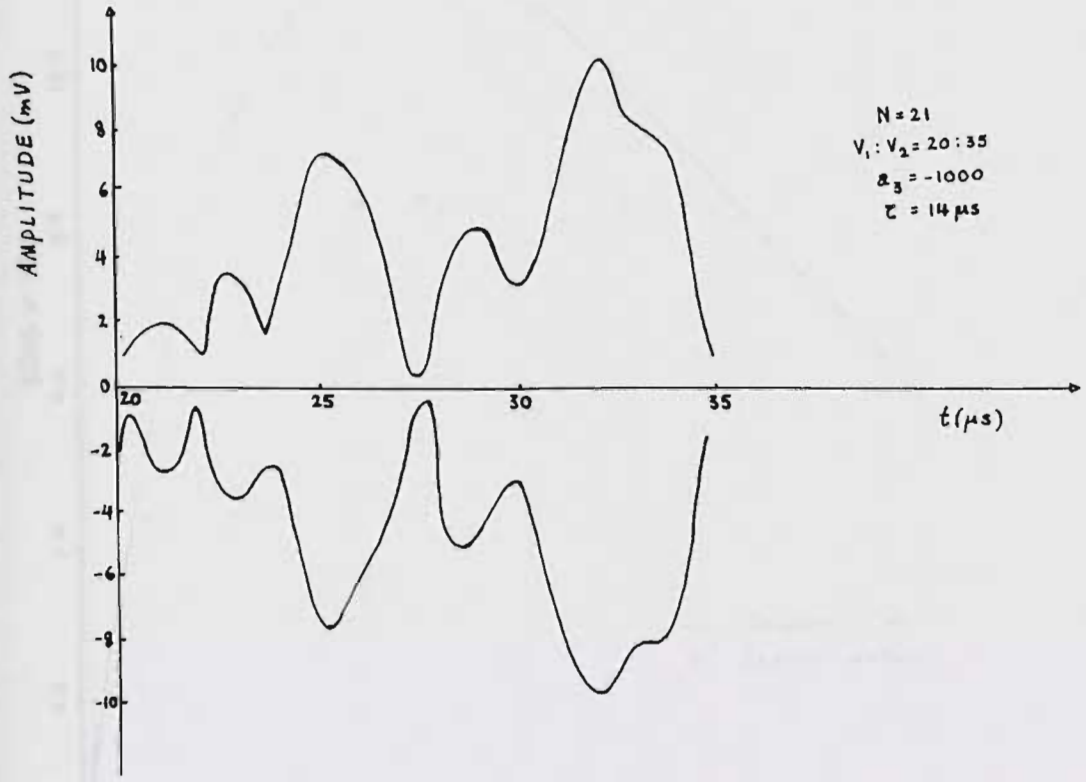

(e) For pulse ratio 20:35 (only envelope is shown).

Figure 2.17. (continued)

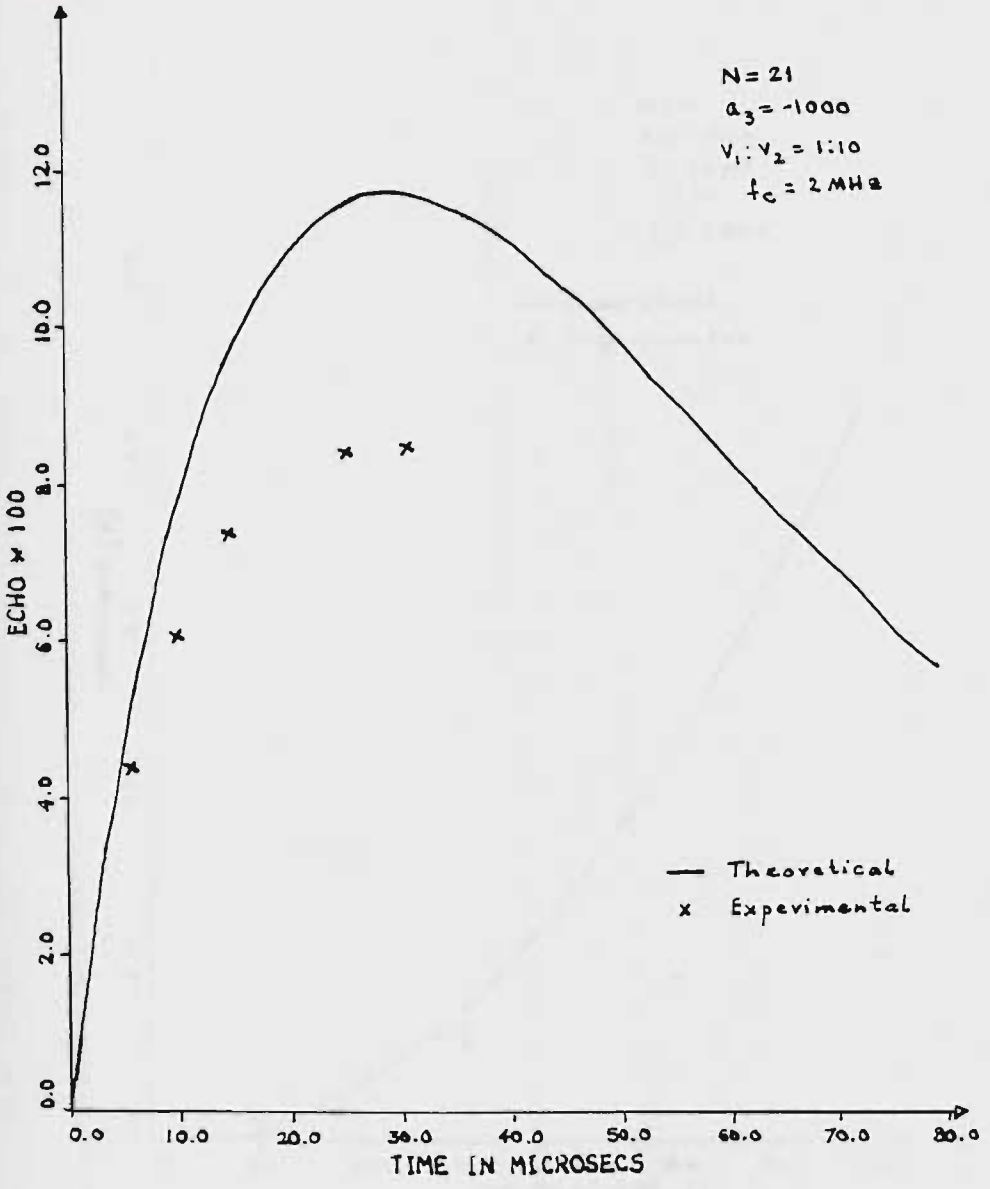

(a) Echo vs. τ, for a_3=-1000.

Figure 2.18. Nonlinear anharmonic echo characteristics for negative a_3.

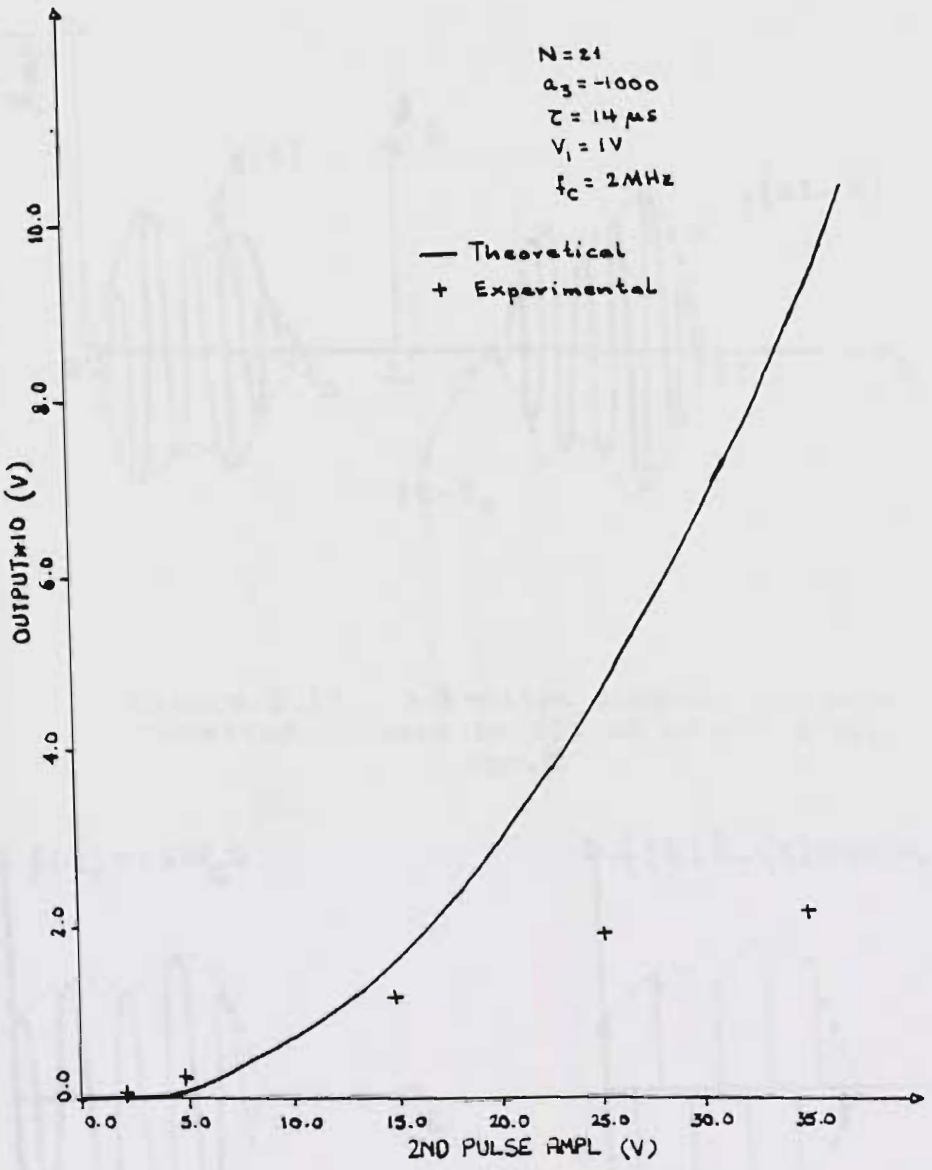

(b) Echo vs. A_2 for a_3=-1000.

Figure 2.18. (continued)

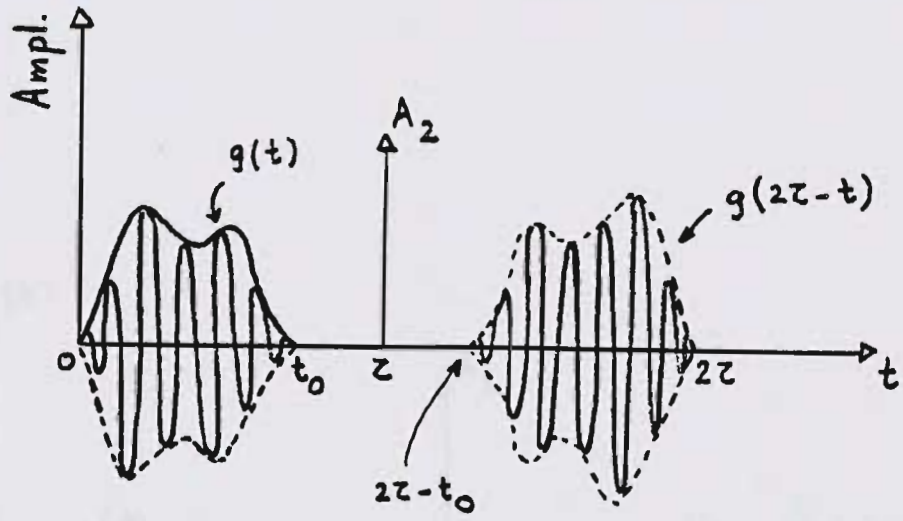

Figure 2.19. Schematic diagram or time inverted dynamic recall of an arbitrary input.

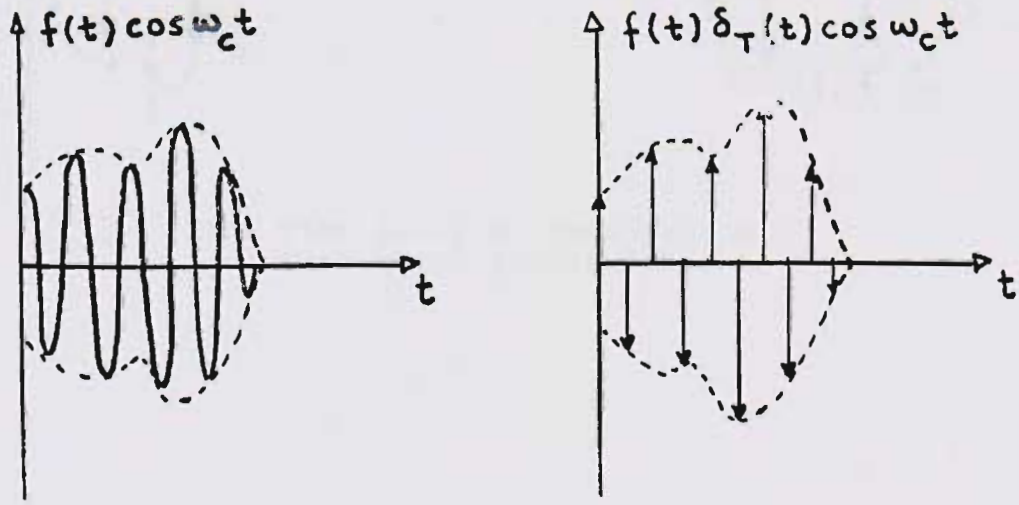

(a) R.f. (b) Sampled

Figure 2.20. Arbitrary finite duration signal and time inverted replication.

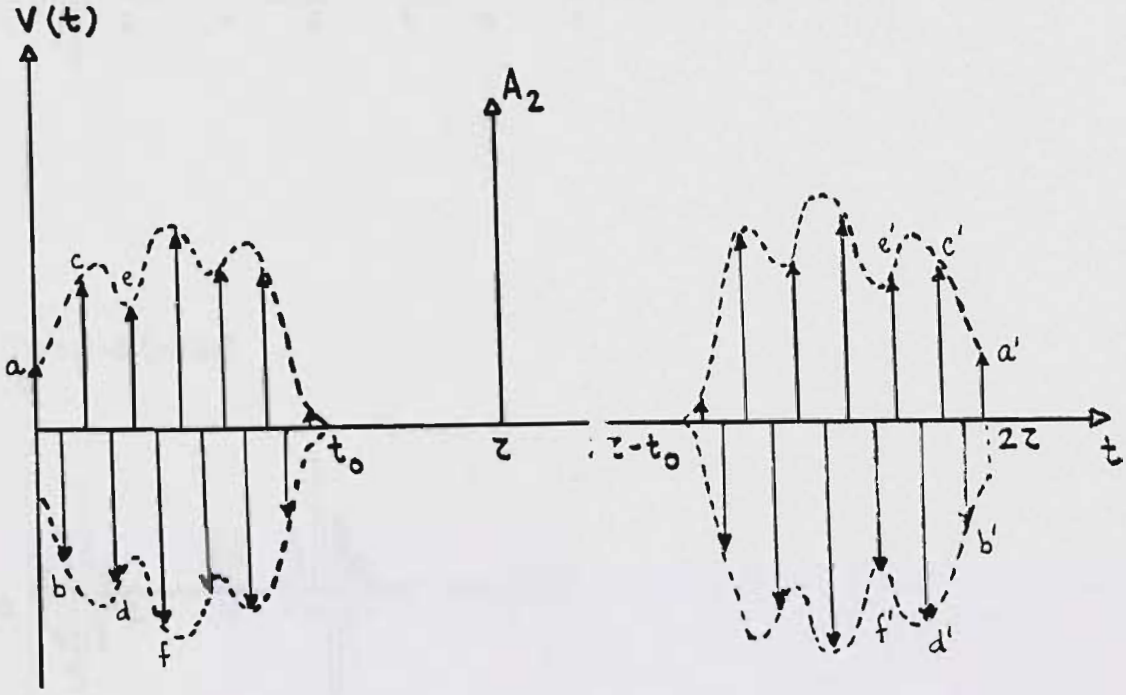

(c) Time inverted replication through nonlinear echo.

Figure 2.20. (continued)

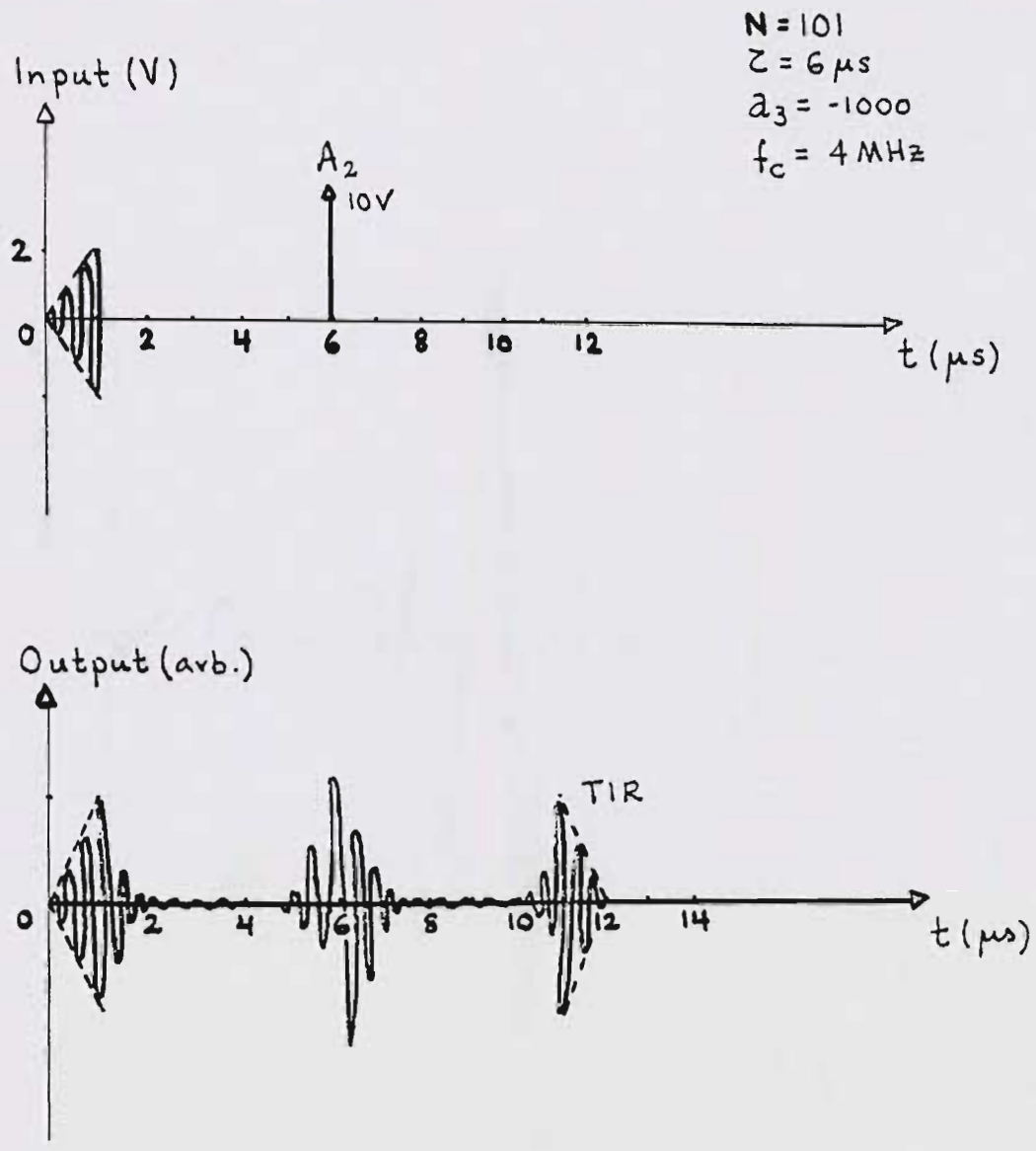

(a) Qualitative sketch.

Figure 2.21. TIR for 1μs r.f. sawtooth input.

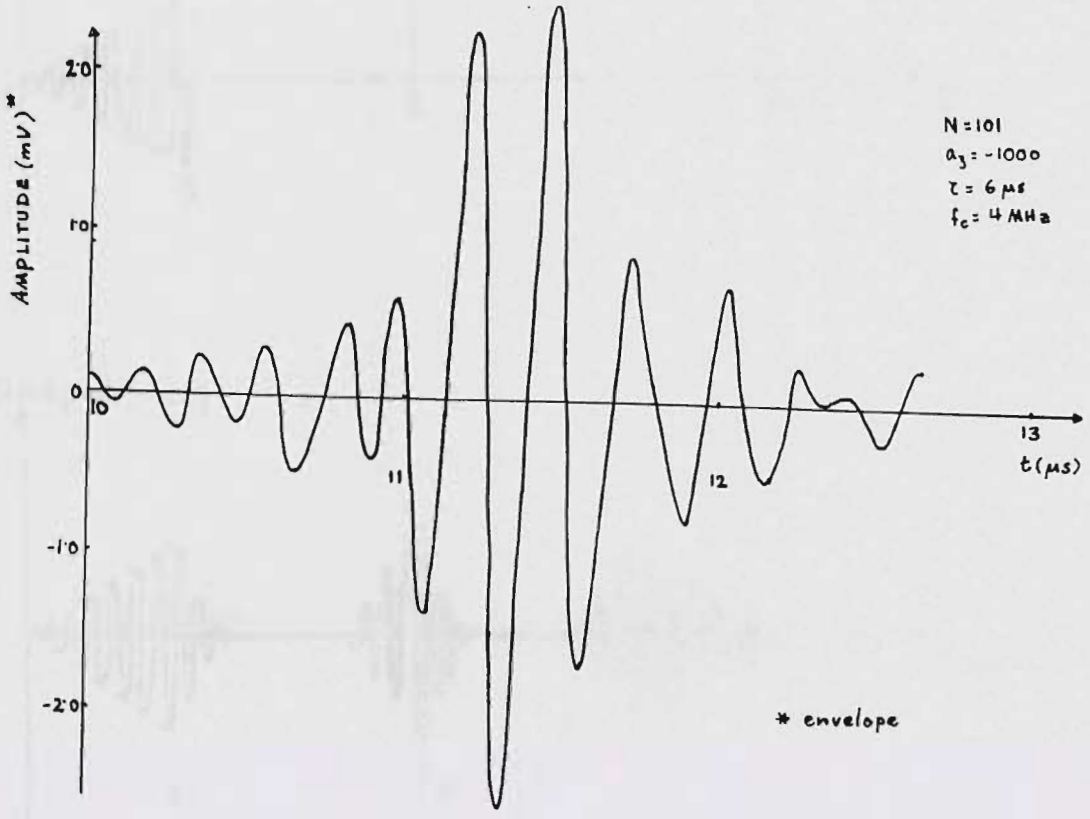

(b) Actual SPICE output.

Figure 2.21. (continued)

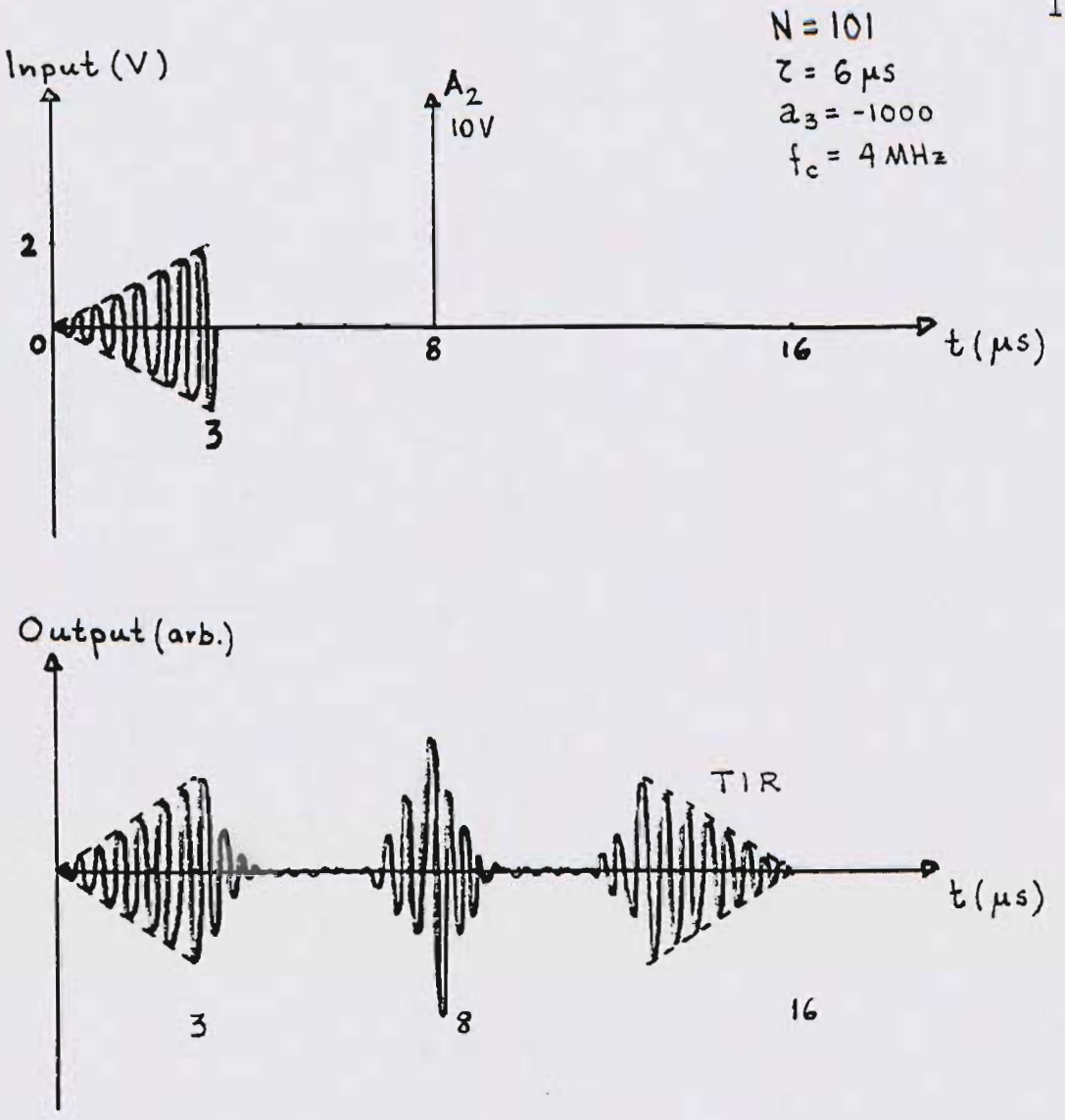

(c) Qualitative sketch.

Figure 2.22. TIR for 3μs r.f. sawtooth input.

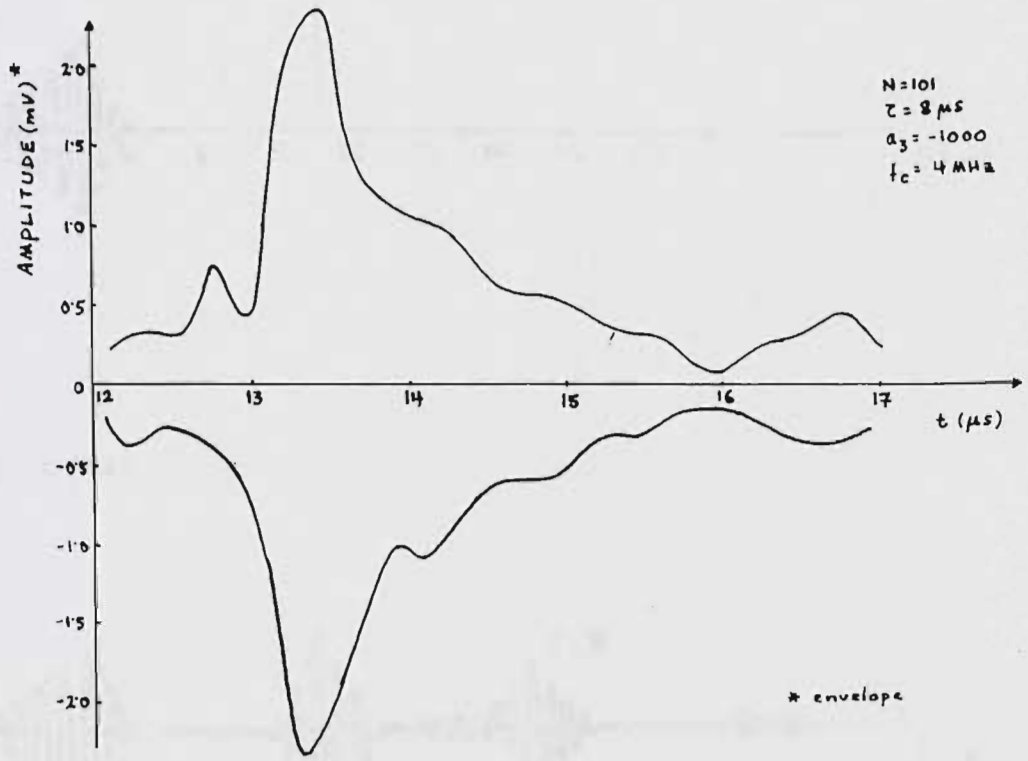

(b) Actual SPICE output.

Figure 2.22. (continued)

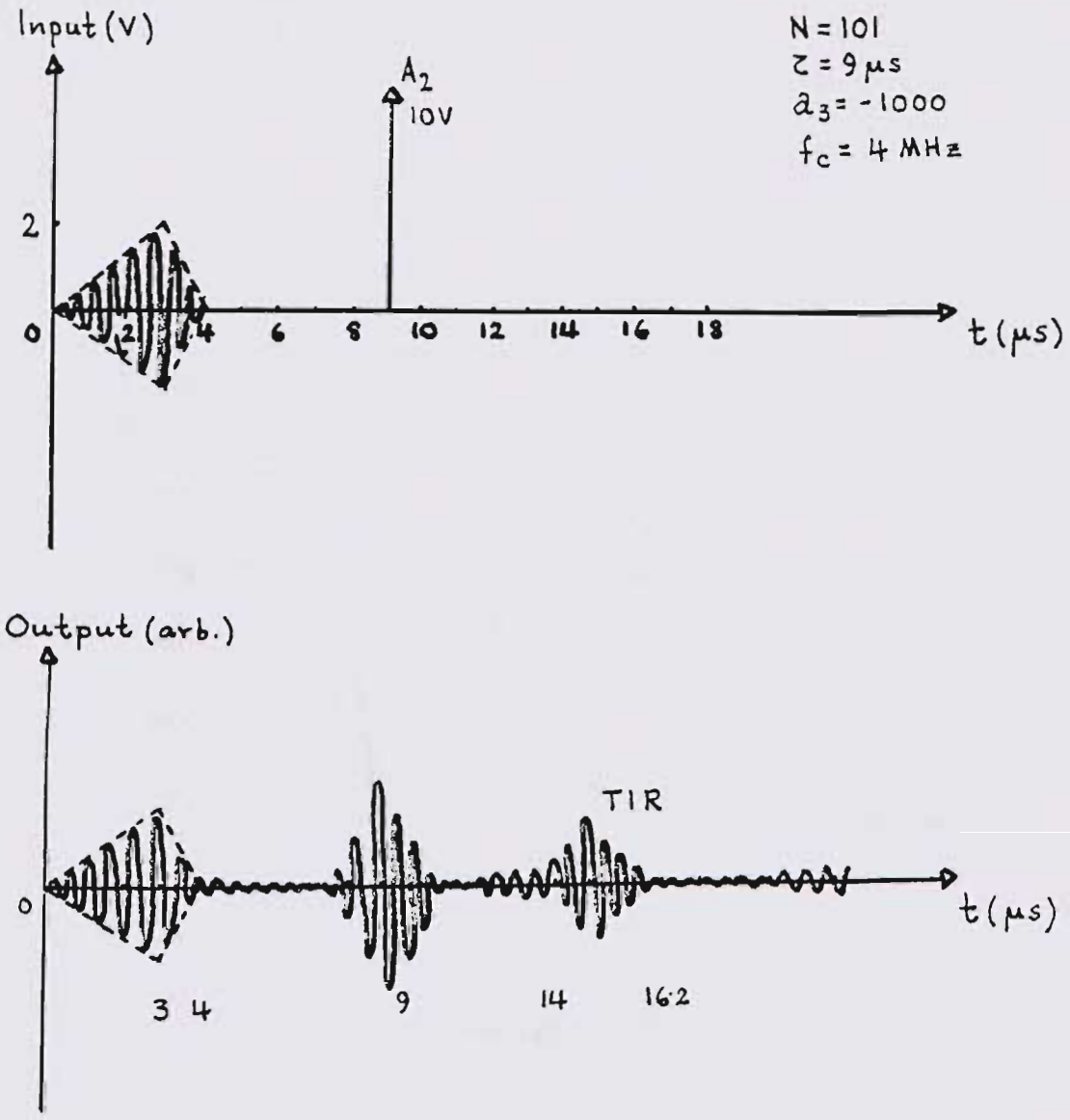

(a) Qualitative sketch.

Figure 2.23. TIR experiments for 4μs r.f. sawtooth input.

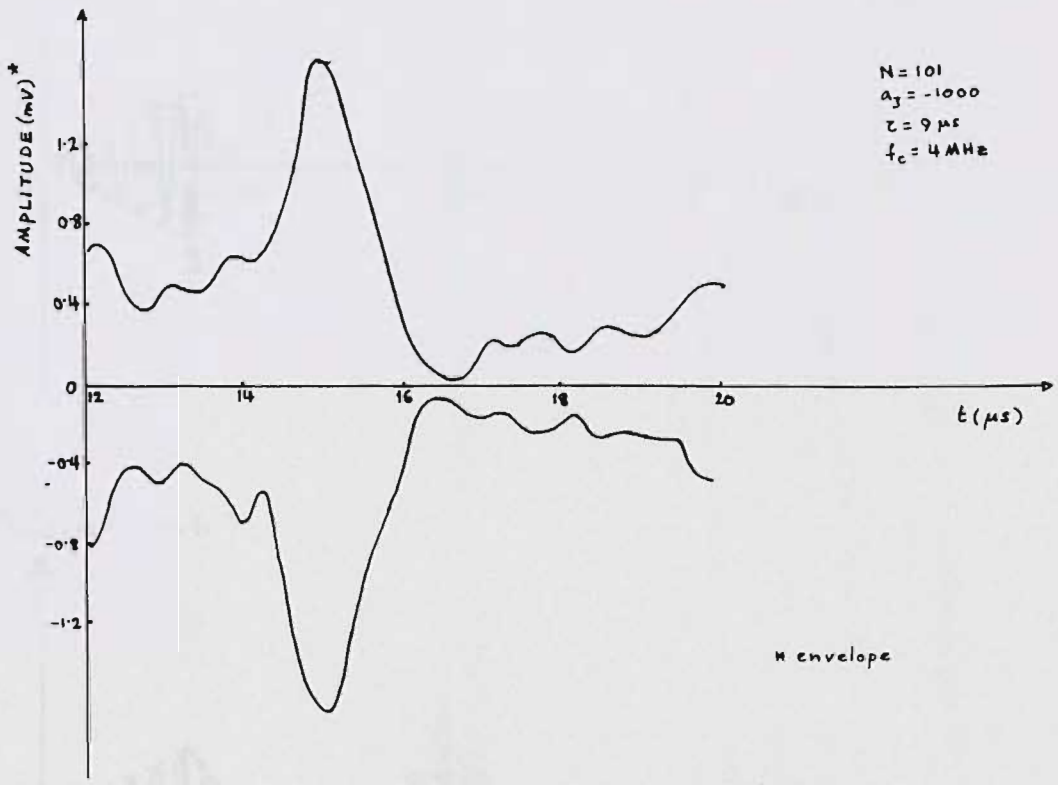

(b) Actual SPICE output.

Figure 2.23. (continued)

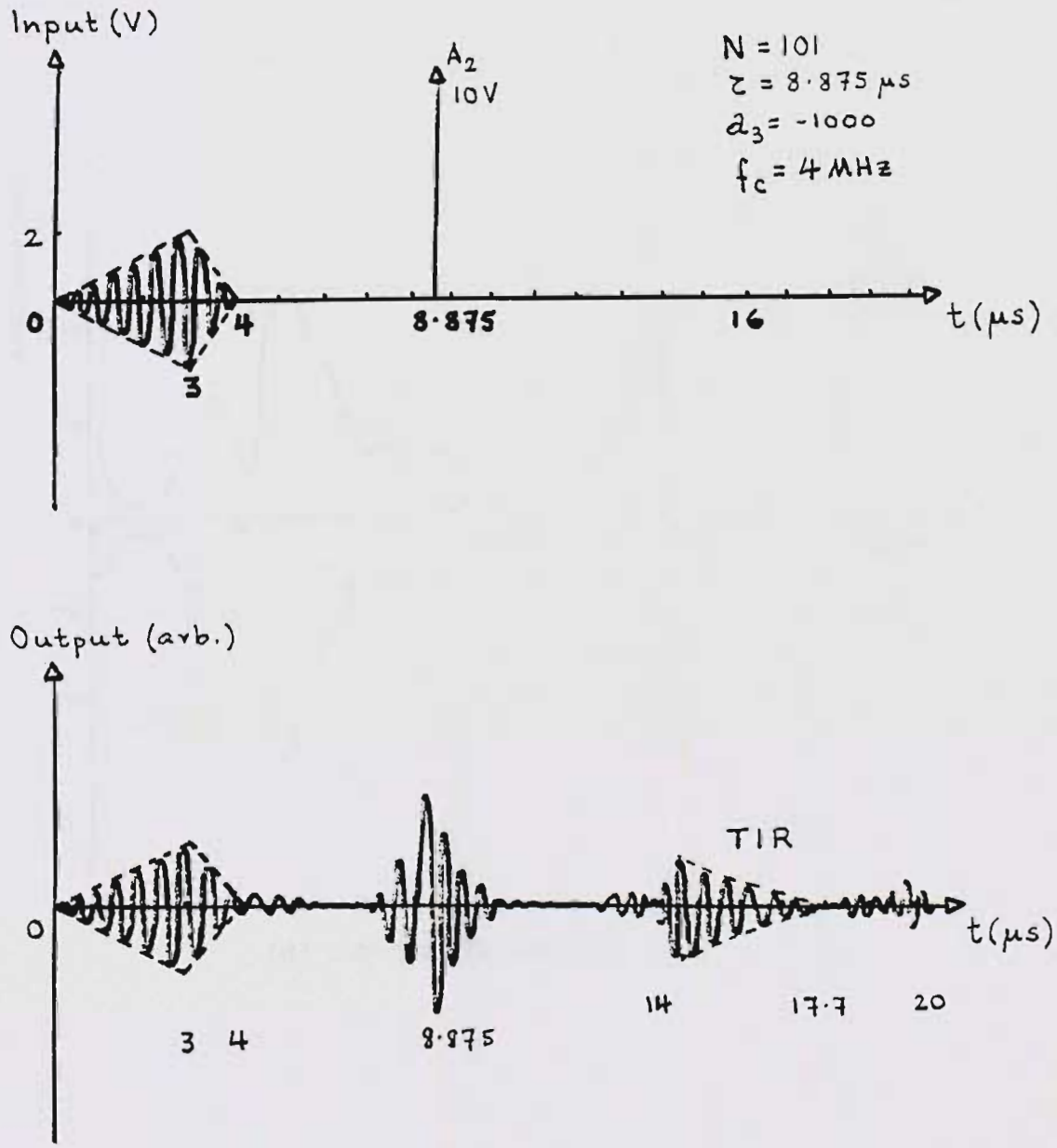

(c) Qualitative sketch for 4μs sawtooth.

Figure 2.23. (continued)

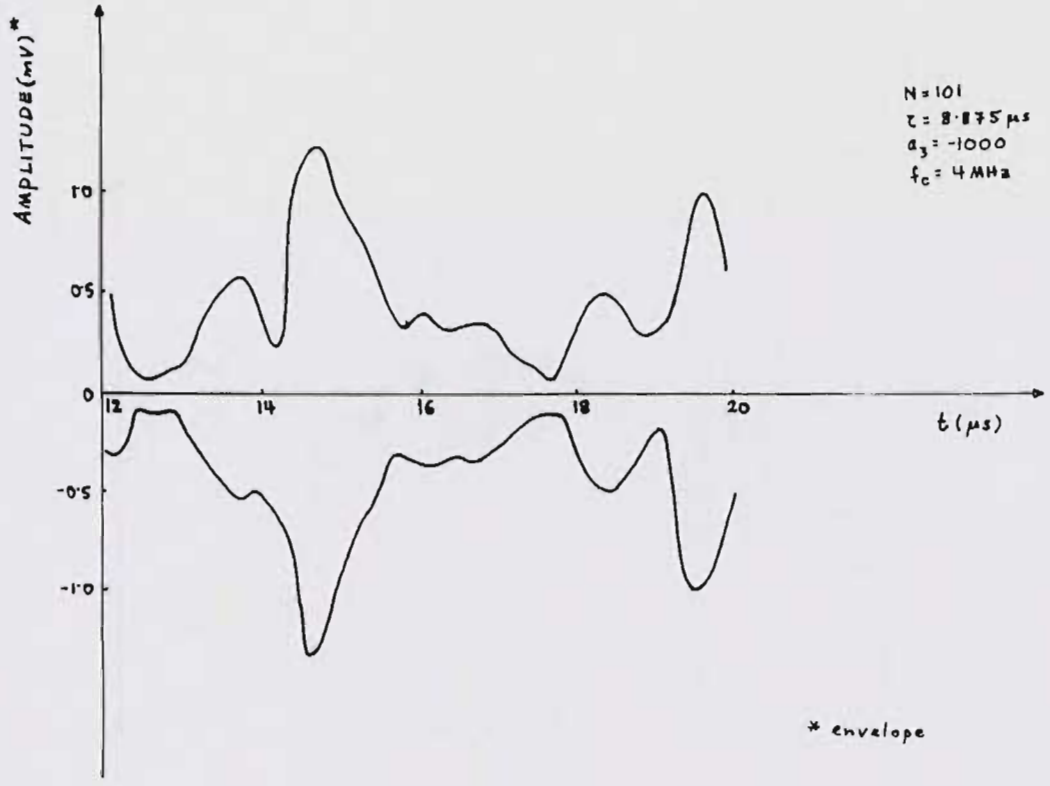

(d) Actual SPICE output.

Figure 2.23. (continued)

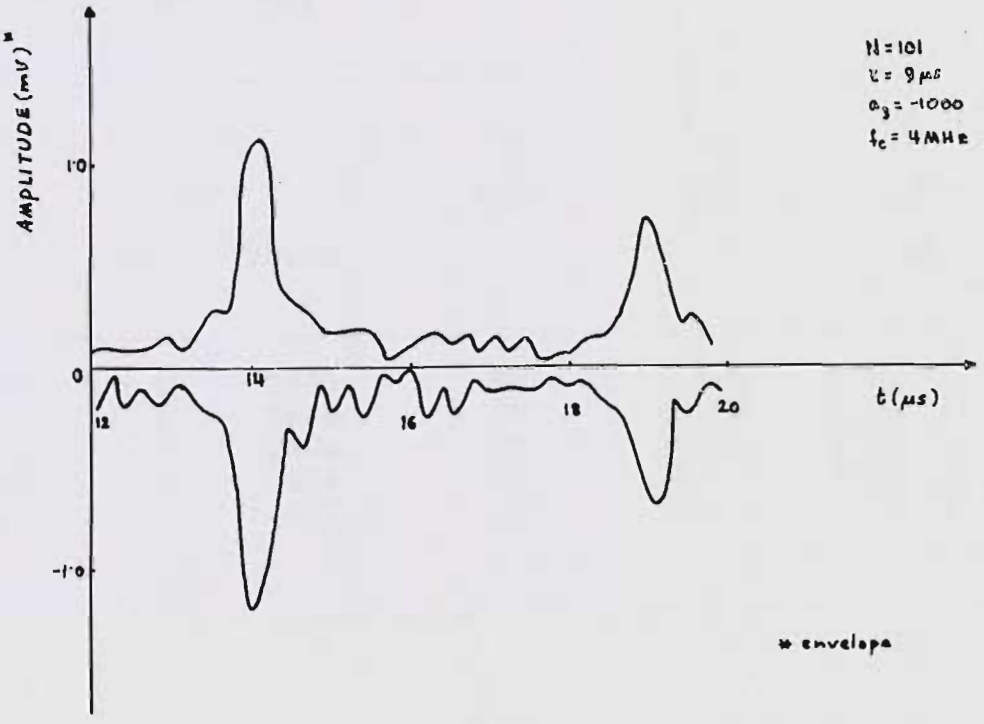

Figure 2.24. SPICE output for sampled 4μs r.f. sawtooth input, with τ=9μs.

Table 2.1

Summary of results for SPICE experiment with a nonlinear RLC circuit

(a) With step input

a_3 (V^{-2})	V_0 (V)		C_0 (pF)	C_{ls} (pF)	f_0 (MHz)	
	Th.	SPICE			Th. ls	Th. ss
10	0.1	.0803	58	53.65	1.84	1.77
15	0.1	.0826	58	51.62	1.88	1.77
20	0.1	.0850	58	49.3	1.92	1.77
25	0.1	.0884	58	47.12	1.96	1.77
27	0.1	.0927	58	46.4	1.98	1.77

a_3 (V^{-2})	f_0 (MHz) SPICE	
	ls	ss
10	1.82	1.76
15	1.87	1.76
20	1.87	1.76
25	1.94	1.76
27	1.95	1.82

Table 2.1 contd.

(b) With triangular input

t_r=.05μs, t_f=.05μs, t_d=.01μs.

V_{in} (V)	V_0 (mV)	a_3 (V^{-2})	$a_3\|V_0\|^2$	Comments
0.2	1.0	-10	-10^{-5}	Stable
0.2	0.5	-100	-25×10^{-6}	Stable
0.2	0.5	10	25×10^{-7}	Stable
0.2	1.0	1000	.001	Stable
0.2	1.0	10^5	0.1	Stable
0.2	.001	10^{15}	1000	Linear growth with neg. slope
2	10	100	.01	Stable
2	10	1000	.10	Stable
6	30	100	.10	Stable
8	50	100	.25	Unstable
10	100	-10	-0.1	Stable
10	100	100	1.0	Unstable
100	500	.01	25×10^{-4}	Stable
100	600	1	0.36	Unstable
100	200	10	0.4	Unstable

Table 2.2

Summary of results for SPICE experiment with N linear parallel RLC circuits

(a) N=21, Δf=25KHz, R=1M, C_0=58pF, f_c=2MHz
(b) N=21, Δf=75KHz, R=1M, C_0=58pF, f_c=2MHz

	LE width (μs)		LE time (μs)		2nd LE ampl. Ampl. at t=0	
	Th	SPICE	Th	SPICE	Th	SPICE
(a)	1st LE 1.9	1.925	40	40.05	0.5	0.528
	2nd LE		80	80.4		
(b)	1st LE 0.63	0.7	13.3	13.35	0.5	0.532
	2nd LE		26.7	26.9		

Table 2.3

Summary of results from SPICE nonlinear echo experiment

$a_3=950V^{-2}$, $f_c=2MHz$, $V_1:V_2=1:10$, $\Delta f_c=25KHz$, N=21

(a) Results for first two principal linear echoes with 2-pulse input ($\tau=14\mu s$).

	Time of LE (μs)		Width (μs)		Peak response (mV)	
	Th	SPICE	Th	SPICE	Th	SPICE
(i)	40	41.1	3.81	4.0	0.86	1.1
(ii)	54	54.1	3.81	3.8	8.60	10.0

	Peak/Min. resp		Echo Ampl (mV)		Echo ratio	
	Th	SPICE	Th	SPICE	Th	SPICE
(i)	21	22.3	0.61	1.0	10	8
(ii)	21	22.2	6.10	8.0		

Table 2.3 contd.

(b) Results for the nonlinear echo

(i) τ=14μs. (ii) τ=20μs.

	Time of NLE (μs)		NLE ampl. (mV)		NLE/Lin. resp.	
	Th	SPICE	Th	SPICE	Th	SPICE
(i)	28	27.5	3.5	5.7	∞	12.7
(ii)	40	39.5	4.2	7.5	7.95	16.6

CHAPTER III

DYNAMIC ECHOES WITH NONLINEAR COUPLING

In this chapter, we detail our theoretical studies and SPICE experiments with dynamic echoes under nonlinear coupling. At first, we felt intuitively that both the analysis as well as the execution of a nonlinear excitation experiment would be much simpler than the anharmonic nonlinearity experiments of Chapter II. As will be seen, our intuition was basically correct; however, it took quite a few experimental models for us to finally come up with the right combination of elements to achieve nonlinear coupling and, eventually, echoes.

III.1 Search for Nonlinear Coupling Configuration

A series of single nonlinear resonator stages were tried in an attempt to find the right configuration for nonlinear coupling echo generation. These are shown in Fig.3.1(a)-(e). The first circuit arrangement that was tried is shown in Fig.3.1(a). The nonlinear element here is appended in series with the input voltage source (in the

form of a dependent nonlinear source that depends cubically on the linear source). For an N element system, there is thus only one nonlinear element applied in common at the input. It was hoped that this would result in an effective nonlinear excitation of the system. It turned out from the SPICE experiments that this did not happen. In retrospect, this is quite understandable. Thus, for a two-pulse input, the dependent source merely applied the amplitude-cubed of the separate pulses to the system. The response that resulted was therefore linear, and only linear echoes were generated at the appropriate times.

A second circuit to be attempted is shown in Fig.3.1(b). It consisted of a linear series tuned circuit (L,C_0), to which a linear resistor R_0 and a nonlinear dependent source f(V) were connected in series. It was thought that this would result in an effective nonlinear resistor, thereby causing a nonlinear excitation of the tuned circuit. From SPICE experiments with a single circuit, and later, an ensemble of 21, it was found that the response was always linear and, of course, there were no echoes. The reason for this turned out to be rather simple. Near the resonant frequency, the RLC resonator becomes an open circuit. As a result, the voltage V on which the nonlinear source f(V) depends, goes to zero. The effect of

the nonlinearity is therefore nullified. The SPICE output for two delta pulses showed linear echoes at $t=1/\Delta f_c=T$ and $t=T+\tau$, where τ is the pulse separation, and the echo widths and amplitudes were approximately in agreement with theory. A typical output is shown in Fig.3.2.

Fig.3.1(c) shows a third circuit arrangement (henceforth called the nonlinear series coupling configuration). Here, each linear resonator at ω_0 is followed in series by a nonlinear dependent source f(V), and terminated by a linear resonator at ω_0 (to suppress the harmonics generated by f(V)). The source f(V) was chosen to be $V+a_3V^3$, where V is the linear resonator output, so that the final output would only contain terms proportional to a_3V^3. Theoretically, for N resonators, this would lead to the following three output terms in a 2-pulse experiment :

$$\text{Term 1} : A_1A_2^2(\sin((1/2)N\Delta\omega_c t)/\sin(\Delta\omega_c t/2))\cos\omega_c t. \quad (3.1a)$$

$$\text{Term 2} : A_1A_2^2(\sin(N\Delta\omega_c(t-2\tau)/2)/\sin(\Delta\omega_c(t-2\tau)/2))\times \times \cos\omega_c(t-2\tau). \quad (3.1b)$$

$$\text{Term 3} : A_2^3(\sin(N\Delta\omega_c(t-\tau)/2)/\sin(\Delta\omega_c(t-\tau)/2))\cos\omega_c(t-\tau). \quad (3.1c)$$

We may note that near $t=2\tau$, the amplitudes of (3.1b) and (3.1c) are $A_1A_2^2$ and A_2^3/N respectively. Now, since by choice $A_2>>A_1$, A_2^3/N is of the same order as $A_1A_2^2$ if $A_2 \sim NA_1$. Thus, for a certain choice of parameters, the spurious response humps of (3.1c) become comparable to the nonlinear echo term (3.1b). As a result the echo, if present, becomes indistinguishable.

A series of SPICE experiments were performed with the nonlinear series coupling configuration. The following set of parameters were used :

$$f(V)=V+a_3V^3. \qquad (3.2)$$

f_c=2MHz	Δf_c=25KHz
N=21	ΔT=0.11μs
τ=10μs	C_0=58pF
L_i variable, i=1,....,N	
$V_1:V_2$=1:20, 1:50	a_3=-10000

The SPICE outputs in this case did not yield any well-defined echoes at $t=2\tau$; however, near t=23μs, a noticeable response hump, not much larger than that in its neighborhood, was observed in most cases. A typical output is shown in Fig.3.3. Also, additional comparable humps were also observed near 36μs, 41μs, and 43μs. In terms of a nonlinear echo, however, these results are unsatisfactory.

It is instructive to mention here that, encouraged by the favorable indications of this circuit, we decided to try a SPICE experiment with 101 stages in the hope that a larger number of stages would enhance the amplitude of the nonlinear coupling echo, if present, and also position it nearer to $t=2\tau$. In trying to run this experiment from 15 to 25μs for $\tau=10\mu s$, we encountered both lack of available memory as well as very high computation time on SPICE. It was later found (see Chapter VI for details) that we could carry out the experiment in smaller time ranges (e.g. 2μs-steps starting at 15μs) without running into memory limitations. The results from this procedure turned out to be quite expensive, but it was found that indeed there was a significantly enhanced response hump near $t=20\mu s$ (instead of 23μs), although highly distorted in shape. Thus, it was concluded that a nonlinear coupling system would have to be somewhat similar to the above circuit, with some modifications.

A fourth configuration which was tried is shown in Fig.3.1(d). This configuration was later established as essentially a nonlinear damping system. We will discuss this, along with some mathematical derivations in Chapter IV. A series of experiments were conducted with this configuration with different values of N, a_3, Δf_c, τ, and

V_1:V_2. The results will be discussed in Chapter IV. It is sufficient to state here that none of the configurations yielded any significant nonlinear response- whether through nonlinear coupling or nonlinear damping. Comparison of the SPICE results with theoretical predictions showed that the linear component of the response was predominant in each case.

The fifth and final configuration (henceforth called the nonlinear output coupling configuration) used in the SPICE experiments is shown in Fig.3.1(e). This is a modification of the nonlinear series coupling configuration of Fig.3.1(c). The input stage of each resonator is now linear, and the linear output is designated V. The dependent nonlinear source f(V) is completely isolated from the input, and is chosen to be simply a_3V^3. The advantage of this design is that any coupling or feedback between the output stage and the input stage is now eliminated, except, of course, through f(V) itself. This simplifies the prediction of the behavior at the common output node "5", both mathematically and physically.

It is simple to show that for a 2-pulse input, the contribution at node "5" (in the absence of an output filter) due to an ensemble of N resonators is given by :

$$V_5 \sim \sum_{N,\omega_0} a_3((A_1/RC_0)e^{-t/T_d}\cos\omega_0 t + (A_2/RC_0)e^{-(t-\tau)/T_d}\cos\omega_0(t-\tau))^3, \qquad (3.3)$$

where ω_0=resonant frequency,

τ=pulse separation,

$T_d=2RC_0$,

A_1, A_2=pulse areas, and

a_3= cubic nonlinearity parameter.

Using some tedious mathematical manipulations, we can show that (3.3) reduces to :

$$V_5 \sim (3/4)PA_1^2A_2e^{-3(t-\tau/3)/T_d}F(t+\tau)\cos\omega_c(t+\tau)$$

$$+Pe^{-3t/T_d}((3/4)A_1^3+(3/2)e^{2\tau/T_d}A_1A_2^2)F(t)\cos\omega_c t$$

$$+(3/4)PA_1^2A_2e^{-3(t-\tau/3)/T_d}F(3(t-\tau/3))\cos3\omega_c(t-\tau/3)$$

$$+(3/4)PA_1A_2^2e^{-3(t-2\tau/3)/T_d}\times$$

$$\times F(3(t-2\tau/3))\cos3\omega_c(t-2\tau/3)$$

$$+ Pe^{-3t/T_d}((3/2)A_1^2A_2e^{\tau/T_d}+(3/4)A_2^3e^{3\tau/T_d})\times$$

$$\times F(t-\tau)\cos\omega_c(t-\tau)$$

$$+(1/4)PA_1^3 e^{-3t/T_d} F(3t)\cos 3\omega_c t$$

$$+(1/4)PA_2^3 e^{-3(t-\tau)/T_d} F(3(t-\tau))\cos 3\omega_c (t-\tau)$$

$$+(3/4)PA_1A_2^2 e^{-3(t-2\tau/3)/T_d} F(t-2\tau)\cos\omega_c (t-2\tau) \ , \qquad (3.4)$$

where $\Delta\omega_c$ is the resonator frequency separation, and ω_c the center frequency as defined by (2.23(b)). Also,

$$P=a_3/(R^3 C_0^3), \text{ and} \qquad (3.5a)$$

$$F(x)=(\sin(N/2)\Delta\omega_c x)/(\sin\Delta\omega_c x/2) \ . \qquad (3.5b)$$

Note that (3.4) is the exact form of the unloaded output at node "5". Of the eight terms in (3.4), we are primarily interested in the last one, which represents a nonlinear coupling echo at $t=2\tau$.

In order to isolate this term from the rest, we need to do the following :

(i) Eliminate the $3\omega_0$-components in (3.4).

(ii) Design the circuit such that the amplitudes of the remaining terms, except for the echo term, are very small near $t=2\tau$.

To accomplish the above, we introduce an output RLC filter as follows :

(a) The filter resonant frequency=ω_c.

(b) The filter bandwidth $B_f=1/RC_0 > N\Delta\omega_c$, so that it covers the spread of the resonators in the ensemble.

(c) We also choose $B_f << 3\omega_c$.

With the right choice of the filter parameters, one can then rewrite (3.4) as follows (ignoring any scaling factors for the moment) :

$$V_{5,u} \sim (3/4)PA_1^2A_2e^{-3(t-\tau/3)/T_d}F(t+\tau)\cos\omega_c(t+\tau)$$

$$+Pe^{-3t/T_d}((3/4)A_1^3+(3/2)e^{2\tau/T_d}A_1A_2^2)F(t)\cos\omega_c t$$

$$+Pe^{-3t/T_d}((3/2)A_1^2A_2e^{\tau/T_d}+(3/4)A_2^3e^{3\tau/T_d})F(t-\tau)\cos\omega_c(t-\tau)$$

$$+(3/4)PA_1A_2^2e^{-3(t-2\tau/3)/T_d}F(t-2\tau)\cos\omega_c(t-2\tau), \qquad (3.6)$$

where the subscript "u" stands for unscaled output.

Note that the $A_1^2A_2$ and A_1^3 terms in (3.6) can be neglected if we choose $A_2 >> A_1$.

Of the remaining terms, the undesirable ones are :

(a) The term proportional to $A_1A_2^2\cos\omega_c t$. Note that this term has repetitive maxima at t=0, T, 2T, ..., where $T=1/\Delta f_c$. But these are far separated from $t=2\tau$, the region of interest. In general, in the neighborhood of $t=2\tau$, one might expect this term to produce a component ~ $A_1A_2^2/N$. Note that this represents the maximum amplitude of a minor peak of the term under consideration (see Fig.2.10).

(b) The term proportional to $A_2^3\cos\omega_c(t-\tau)$. This term poses the greatest potential interference problem for the 2τ-echo. Although the maxima for this term are located at $t=\tau$, $T+\tau$, ..., one expects a component near $t=2\tau$ which is $\sim A_2^3/N$.

Now, since the actual echo term is proportional to $A_1A_2^2$, obviously for N sufficiently large, the component $A_1A_2^2/N$ of the term in (a) above near $t=2\tau$ will be small.

However, the term A_2^3/N in (b), which may be written as $A_2^2(A_2/N)$, may actually become comparable to the echo term $A_2^2A_1$ if one chooses $A_2/N\sim A_1$ or $A_2/A_1\sim N$. In order to eliminate this term, therefore, it is necessary to choose $N>>A_2/A_1$.

In summary, then, we need the following :

(i) $N\Delta\omega_c < B_f < 3\omega_c$, (3.7a)

(ii) $A_2>>A_1$, (3.7b)

(iii) $N>>A_2/A_1$, and (3.7c)

(iv) $T=1/\Delta f_c>>\tau$. (3.7d)

When the conditions specified by eq. 3.7(a)-(d) are satisfied, we should expect to see essentially the following response at node "5" :

$$V_{5,u}\sim(3/4)Pe^{-3(t-2\tau/3)/T_d}A_1A_2^2F(t-2\tau)\cos\omega_c(t-2\tau). \quad (3.8)$$

In the neighborhood of $t=2\tau$, this echo term then becomes:

$$V_{5,u}(2_t)\sim(3/4)Pe^{-4\tau/T_d}A_1A_2^2N. \quad (3.9)$$

Note that (3.9) is an explicit expression for the 2τ-nonlinear coupling echo as a function of τ. Note that it essentially represents a simple exponential decay with τ. This agrees with the expected amplitude vs. τ characteristics of a nonlinear coupling echo [6].

III.2 Implementation of Nonlinear Output Coupling Configuration

We have now finally arrived at a circuit configuration which appears to be suitable, at least theoretically, for the generation of dynamic nonlinear coupling echoes. We next

discuss the scaling factors that need to be incorporated in the theory due to the actual circuit model on SPICE, and the results of some of the preliminary experiments that were carried out before the rigorous theory was developed.

III.2.1 Scaling Factors

In view of the actual circuit model used on SPICE, one needs to scale (3.9) by introducing the effect of loading due to the output filter.

If the filter resistance is R_a, and the series resistance is R_b, then the open circuit impedance seen across R_a looking inward from the output is :

$$Z_{oc}=R_b \| R_b \| \ldots . \| R_b = R_b/N. \qquad (3.10)$$

Thus, the effective load impedance becomes :

$$R_L \sim R_a \| (R_b/N). \qquad (3.11)$$

Hence, the unscaled output at "5" now becomes modified by the loading factor :

$$K=R_L/(R_b+R_L). \qquad (3.12)$$

Thus, (3.9) is now modified as follows :

$$V_{5,s}(2\tau) \sim (3/4)PKNA_1A_2^2 e^{-4\tau/T_d} . \qquad (3.13)$$

(N.B. As a check, we may note that if the output filter were absent, then $R_a=\infty$; hence, from (3.11), $R_L \to R_b/N$. From (3.12), then, $K=1/(N+1) \to 1/N$ for large N. This is precisely the loading factor used in all previous filter-free N-resonator experiments (see eq.(2.76)).)

III.2.2 Preliminary Experiments with Nonlinear Output Coupling Configuration

Prior to developing the simplified theory of the generation of nonlinear coupling echoes by using the nonlinear output coupling model, we had conducted some experiments on SPICE using the same model, without any rigorous attention to the design requirements. These experiments indicated for the first time that this model had promise in terms of generating the type of echo we were looking for. We discuss briefly the results of some of these experiments in this section.

(a) With N=21, a_3=-1000, ensemble BW~500KHz, filter BW~1MHz, R_a=3K, C_0=C=58pF, R=1M, R_b=10M, τ=10μs.

Noticeable response humps were seen at t=19.7μs (0.4μV), t=40.9μs (0.4μV), and t=50.4μs (1.5μV) at node "5". The hump near 19.7μs had a duration of 3.2μs.

(b) Same as (a), but with R_a=1K, filter BW=3MHz.

In this case, two noticeable humps were seen near t=20μs (0.3μV), and t=23.3μs (0.3μV), each of about 1.35μs duration. However, because of the large filter bandwidth, there was significant harmonic distortion.

(c) Same as (a), but with the output filter replaced by a 100M termination.

In this case, the output showed several comparable response humps, and harmonic distortion was evident. Thus, for a well defined echo near 2τ, one needs an output filter to reduce distortion and undesirable response humps.

(d) Same as (a), but with R_a=5K.

In this case, a significantly enhanced 2τ-echo was seen near t=20μs. It had an amplitude of 1.136μV (compared to 0.35μV for the nearest neighbor), and a duration of 2.6μs. An experiment with R_a=10K, however, resulted in an echo which was virtually lost in the background noise.

The above observations implied that for a reasonable filter bandwidth (covering at least the spread of the resonators, but much smaller than $3\omega_0$), and a sufficiently large N, all the undesirable response components are attenuated, thereby enhancing the nonlinear coupling echo.

III.2.3 Dynamic Nonlinear Echo Experiments with Nonlinear Output Coupling Configuration

Based on the design constraints defined by eq.3.13(a)-(d), we next carried out a set of SPICE experiments with essentially the following parameters :

$V_1:V_2=1:10$	$\tau=10\mu s$
$a_3=-1000$	R=1M
$C_0=C=58pF$	$R_b=10M$
$R_a=5K$	N=63
$\Delta f_c=25KHz$	$f_c=2MHz$
Filter BW~600KHz	

With the above set of parameters, and slight variations of them, SPICE experiments yielded well-defined nonlinear coupling echoes near $t=2\tau$ following 2-pulse excitations of pulse separation τ. The theoretical and SPICE results were reasonably close, especially in view of the restrictions

involved in the simplified theory. Table III.1 summarizes the theoretical and SPICE results for the echo duration, and the amplitudes near $t=2\tau$, T, and $T+\tau$. It may be seen from the Table that the various quantities are in reasonable agreement whenever the parameters chosen in the experiment closely satisfy the conditions 3.13(a)-(d), and discrepancies occur whenever any of the conditions is violated (for example, if N is too small, or if the filter bandwidth is too large or too small.). In Fig.3.4, a typical nonlinear coupling echo from SPICE is shown.

Echo vs. τ Characteristics:

Theoretically, the echo amplitude decays as $\exp(-4\tau/T_d)$. However, in the actual experiments, due to the spread in the Q's of the resonators, the overall decay was not a simple exponential. As can be seen from Fig.3.5, the experimental curve decays somewhat faster than the theoretical curve; however, they are in reasonable agreement. We may also note that at t=0, the echo amplitude is expected to be a maximum. This is intuitively understandable, because by the time the "second" pulse is applied (also at t=0), the vibrations of the resonators set up by the first pulse have not decayed at all, thus resulting in a strong 2-pulse $A_2^2A_1$ coupling. This

characteristic, which is quite different from that of a nonlinear anharmonic echo, is well known in the literature [6] .

Echo vs. A_1 Characteristics:

For this, we kept τ, A_2, and a_3 fixed, and varied A_1 (i.e. V_1). The SPICE results were compared with theory. Fig.3.6 shows a plot of the echo amplitude vs. V_1. We find from the plot that at high levels, there is saturation. For small values of V_1, the amplitude is reasonably linear. However, for large A_2/A_1 ratios, the amplitude deviates from expectation (with additional comparable amplitudes beginning to appear near t=23μs.). This is quite understandable, since larger A_2/A_1 ratios lead to greater interference of the echo with noise.

Echo vs. A_2 Characteristics:

For this, we kept τ, A_1, and a_3 fixed, and varied A_2 (i.e. V_2). Fig.3.7 shows a plot of the echo amplitude vs. V_2. Here, once again, for large values of A_2/A_1, the nonlinear coupling echo starts to deviate from expectation. This may once again be attributed to greater interference at larger pulse ratios. However, the echo vs. V_2 curve is remarkably parabolic all the way upto V_2=25V, even though

significant noise amplitudes begin to appear at larger V_2 values. Another factor to take note of is that, in the nonlinear coupling experiments, the effect of high-level splitting is far less visible than in the case of nonlinear anharmonic echo experiments.

III.3 Time Inverted Recall Experiments in the Nonlinear Coupling Case

We now discuss the experiments using nonlinear coupling to generate time inverted recall (TIR) of an arbitrary input signal. We may recall that in Chapter II, TIR experiments with finite duration r.f. sawtooth inputs were moderately successful, as long as the input signal remained sufficiently small in both amplitude and duration. For larger amplitudes and/or durations, the recalled TIR signal was found to undergo unexplained blanking and reinforcing in regions outside the domain of the TIR signal, and was also distorted. This situation was found to persist even if the recall pulse were slightly staggered (although a slight improvement could be seen) relative to the input signal, or if a sampled version of the analog r.f. input were applied.

The TIR experiments with nonlinear coupling were conducted with appropriately sampled versions of the actual

analog r.f. input signals. It was hoped that this might yield a "cleaner" TIR response, since the spectrum of the sampled signal would have well-defined separation between the fundamental and the higher order sidebands, so that the latter could be filtered out more readily. From the actual SPICE experiments, this was indeed found to be true. Two different r.f. envelopes were used: a square pulse and a sawtooth. We discuss the theory and the experiments for these cases next.

III.3.1 Time Inverted Recall of R.F. Square Wave Input

In Fig.3.8(a) and (b) we show the actual input and the sampled version respectively. Note that the sampling pulses are applied every one-half carrier cycle. In Appendix H, the mathematical details of the resulting TIR signal from the above input followed by a recall pulse at $t=\tau$ are worked out. It is shown that the recalled TIR signal is given by :

$$V_0^{TIR}(t) \sim \sum_{i=0}^{2T/T_c} (-1)^i (3/4) P A_1 A_2^2 e^{-3(t-iT_c/6-2\tau/3)/T_d} \times \times F(t-2\tau+iT_c/2)\cos\omega_c(t-2\tau+iT_c/2), \quad (3.14)$$

where P and F(x) are defined in 3.5(a) and (b). Also, T is the signal duration, T_c the carrier period, and τ the pulse separation.

In Fig.3.9 we show a plot of eq.(3.14) in the time range $t=2\tau-T$ to $t=2\tau$ (with a few microseconds before and after). From the plot we find that there is no significant decay of the TIR amplitude following the initial rise. This, however, is not the case with the actual SPICE output.

A SPICE experiment was first conducted with an analog r.f. square pulse with the following parameters (note that this and all the subsequent TIR experiments were done with a 5K output filter) :

N=63; pulse duration=4μs; amplitude=2V;
R.F.=2MHz; recall pulse=10V; τ=10μs.

The SPICE output was plotted from t=14μs to t=24.5μs. From the plot shown in Fig.3.10, we can see that although the response has a peak at around 16μs, it decays rapidly thereafter, and the envelope does not resemble a square wave at all. Thus, the recalled TIR signal is highly distorted, as was the case with the 4μs r.f. sawtooth inputs in the anharmonic case.

A second SPICE experiment was done with essentially the same parameters, but the analog r.f. square pulse was

replaced by a sampled r.f. square pulse with plus-minus sampling, and a sampling frequency of 4MHz. As can be seen from Fig.3.11, the envelope of the SPICE response in the same time range now looks a lot closer to a square pulse, although there is a slight droop in the envelope around 19μs. Thus, the use of a sampled r.f. input has indeed improved the shape of the recalled TIR signal, and made it look closer to the theoretical TIR signal of Fig.3.9.

III.3.2 Time Inverted Recall of R.F. Sawtooth Input

The input (analog and sampled) for this case is shown in Fig.3.12(a) and (b). It is clear that in this case the amplitude A_1, assumed constant for the r.f. square pulse input, is a function of time (or, in the sampled domain, a function of the position of the i-th sample.). In a few simple steps (see Appendix H) we can show that the TIR response is now given by :

$$V_O^{TIR}(t) \sim \sum_{i=0}^{2T/T_c} (-1)^i \, i(3/4)PQA_2^2 \, e^{-3(t-iT_c/6-2\tau/3)/T_d} \times \\ \times F(t-2\tau+iT_c/2)\cos\omega_c(t-2\tau+iT_c/2), \qquad (3.15)$$

where P and F(x) are defined by 3.5(a) and (b), and

$$Q=BV_p(T_c/2T),$$

$B=\Delta T/2$, (ΔT=pulse duration)

V_p=peak sawtooth amplitude,

T_c=carrier period, and

T=signal duration.

An analytical plot of (3.15) over the range $t=2\tau-T$ to $t=2\tau$ is shown in Fig.3.13. We may note the reversal in the echo slope as expected. However, there is no significant droop in the falling slope of the sawtooth, which, once again, was the case with the actual SPICE experiment.

The first SPICE experiment to be performed in this case consisted of a 3μs r.f. analog sawtooth input with the following parameters:

R.F.=2MHz; τ=10μs; N=63;

Sawtooth peak=2V at t=3μs; duration=3μs;

Recall pulse=10V; τ=10μs.

From Fig.3.14, we find that the actual SPICE envelope in this case has reproduced the ideal TIR shape reasonably well, although there still exists a slight decay in the trailing edge of the TIR signal.

A second SPICE experiment was performed with a 2-slope r.f. sawtooth input with the following parameters :

R.F.=2MHz; τ=10μs; N=63;

Sawtooth peak=2V at t=3μs; duration=4μs;

Recall pulse=10V; τ=10μs.

In constructing the r.f. signal on SPICE, the piecewise linear model was used, first by taking 4 points every half carrier cycle, and later by taking 8 points per half carrier cycle. The SPICE envelopes in the range 14μs to 24μs in the two cases are shown in Fig.3.15(a) and (b). We find from the two plots that the envelopes have a somewhat distorted TIR shape, although the extent of the distortion is not as severe as was encountered in the corresponding anharmonic experiments. We also find that the amplitude of the noise is reduced by a factor 8, while the signal amplitude is only reduced by a factor 2.5 when the input on SPICE is constructed with greater resolution (compare Fig.3.15(a) with 3.15(b)). This indicates a net improvement in the SNR by a factor 3.2.

The last time inverted recall experiment in this series consisted of a sampled r.f. sawtooth input with the following parameters:

N=63; r.f.=2MHz; sampling frequency=4MHz;

Sawtooth peak=2V at t=4μs; duration=4μs;

Recall pulse=10V; τ=10μs.

The SPICE envelope for this case is shown in Fig.3.16. It is evident that the use of the sampled r.f. input has once again improved the TIR shape of the recalled signal, and the previously noticed decay along the trailing edge of the recalled sawtooth has been significantly reduced. The overall signal to noise ratio has also increased noticeably.

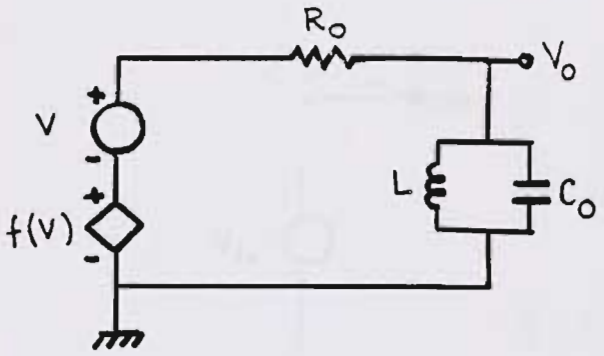

(a) First nonlinear resistor circuit.

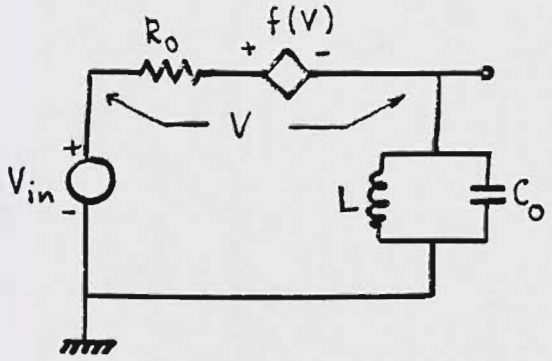

(b) Second nonlinear resistor circuit.

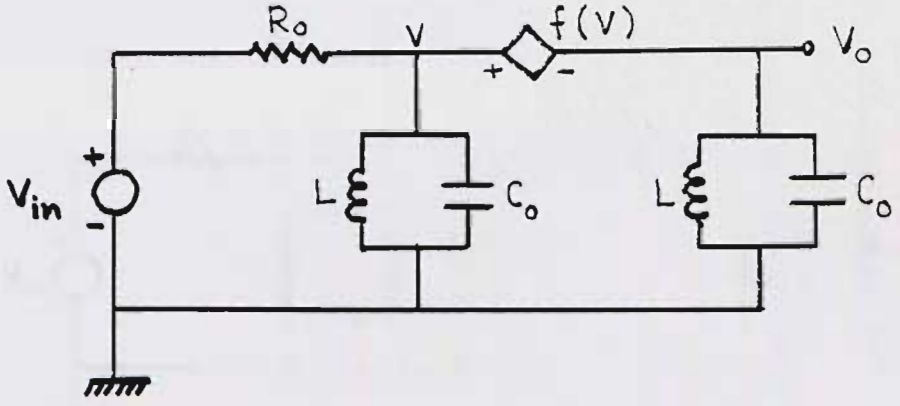

(c) Nonlinear series coupling configuration.

Figure 3.1. Nonlinear circuits attempted in the search for nonlinear coupling configuration.

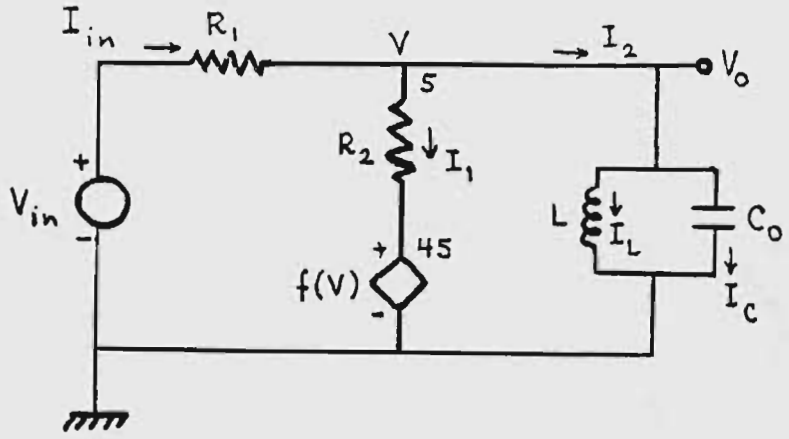

(d) Nonlinear damping configuration.

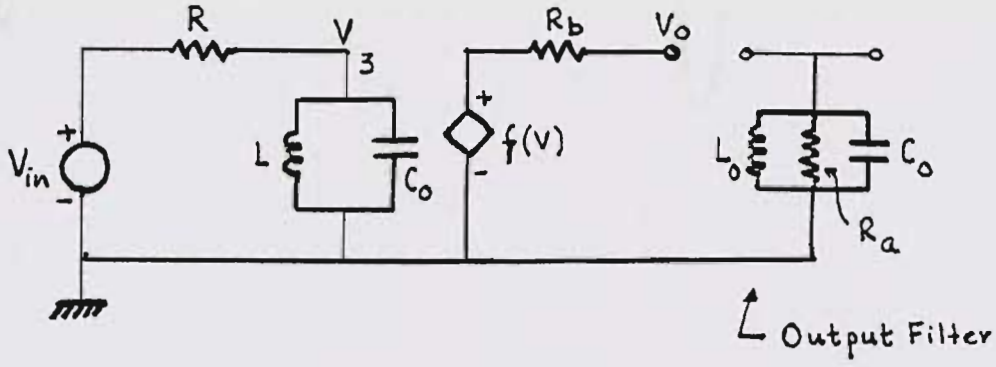

(e) Nonlinear output coupling configuration.

Figure 3.1. (continued)

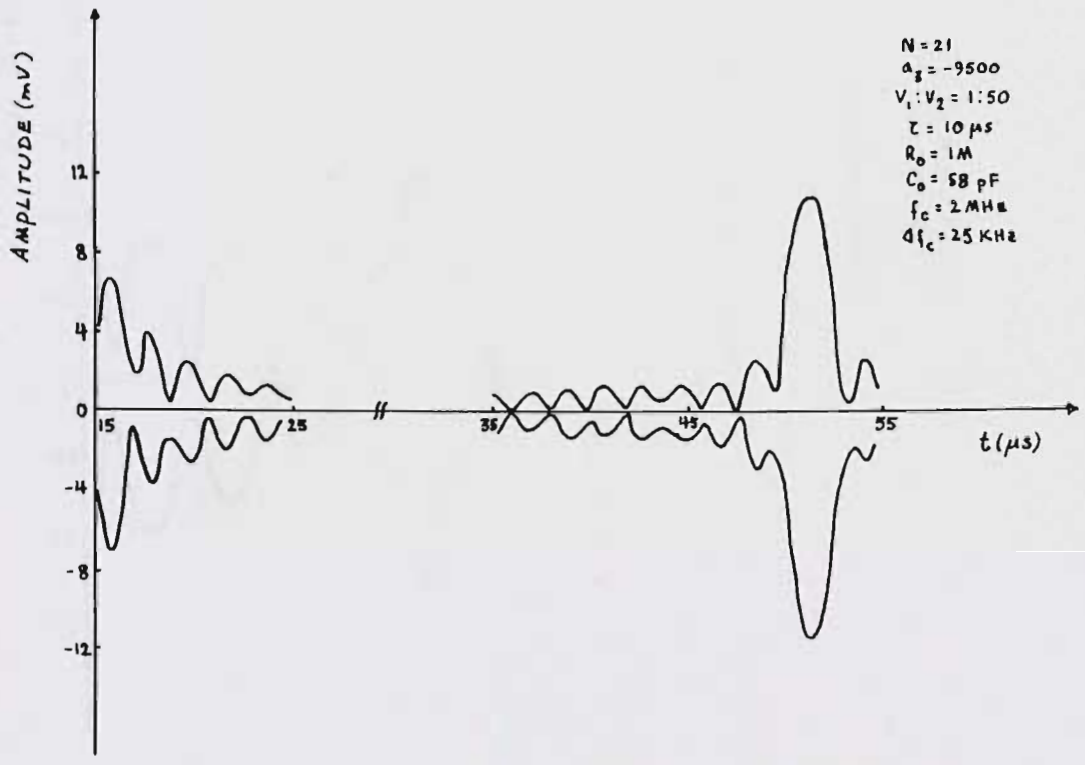

Figure 3.2. Typical SPICE output for the circuit in Fig.3.1(b), with N=21 (only envelope is shown).

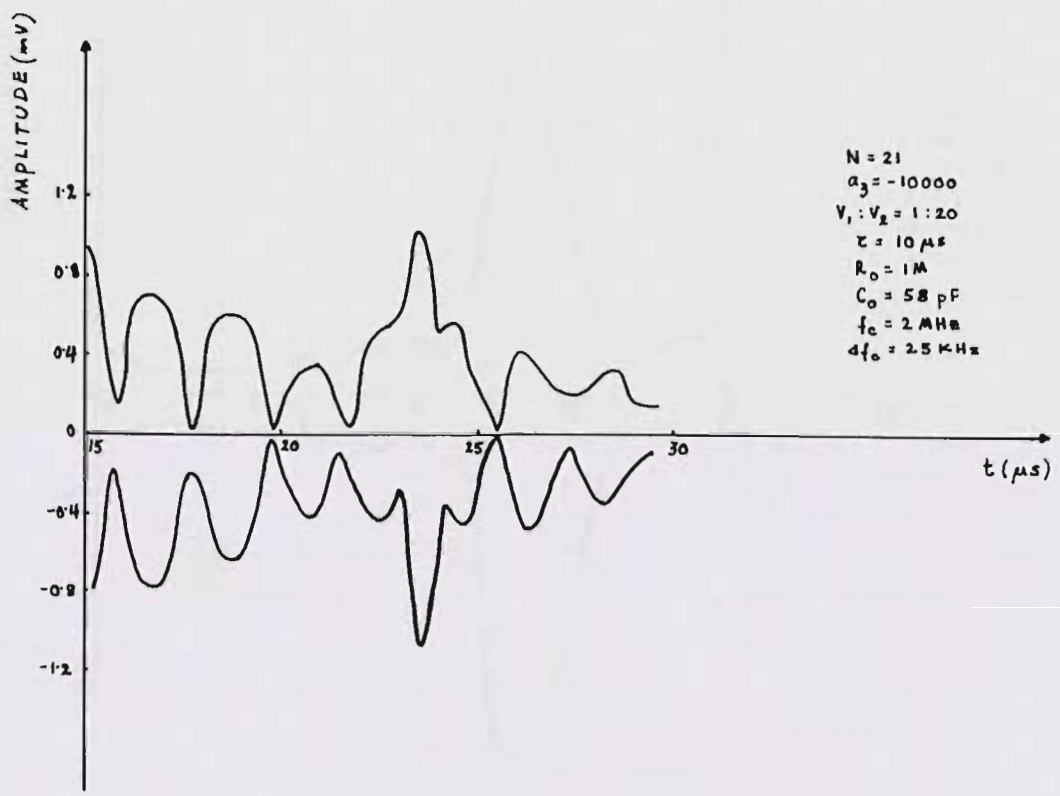

Figure 3.3. Typical SPICE output for the circuit in Fig.3.1(c), with N=21 (only envelope is shown).

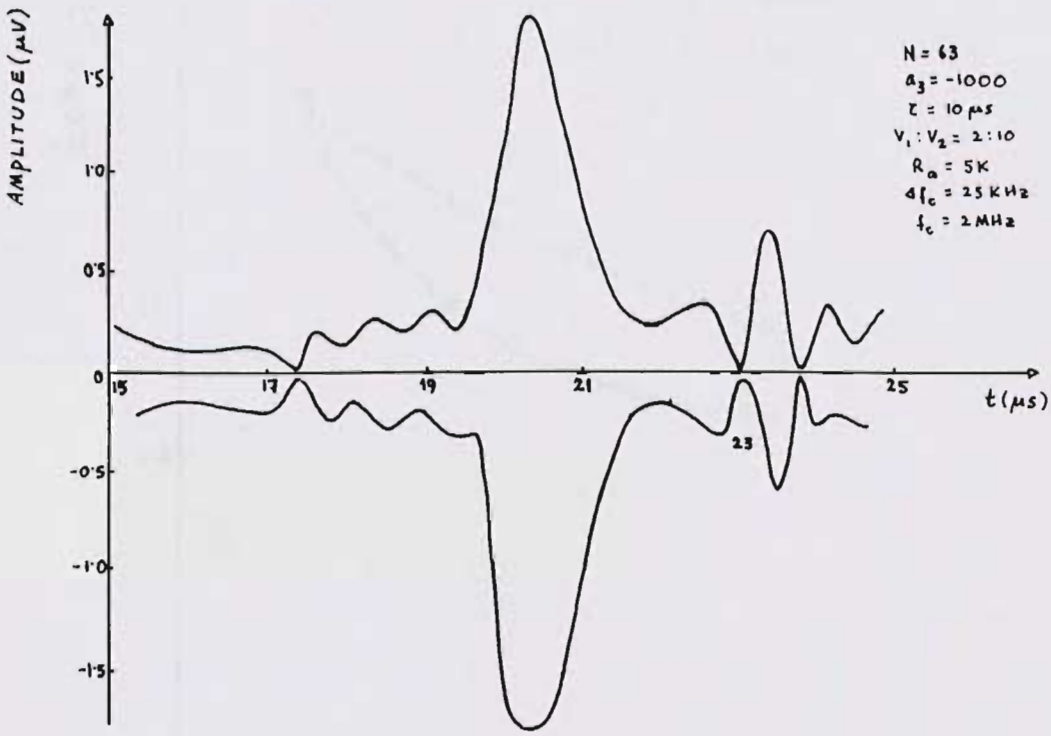

Figure 3.4. Typical nonlinear coupling echo from SPICE (only envelope is shown).

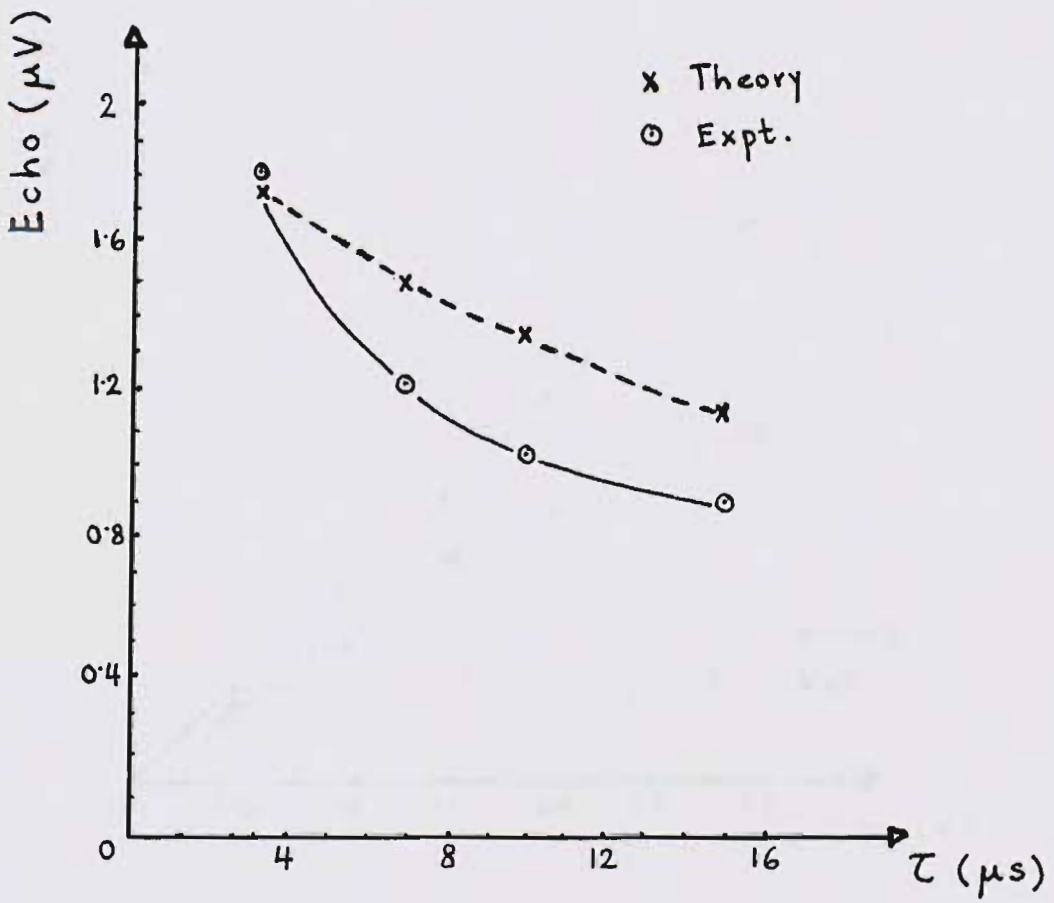

Figure 3.5. Nonlinear coupling echo vs. τ.

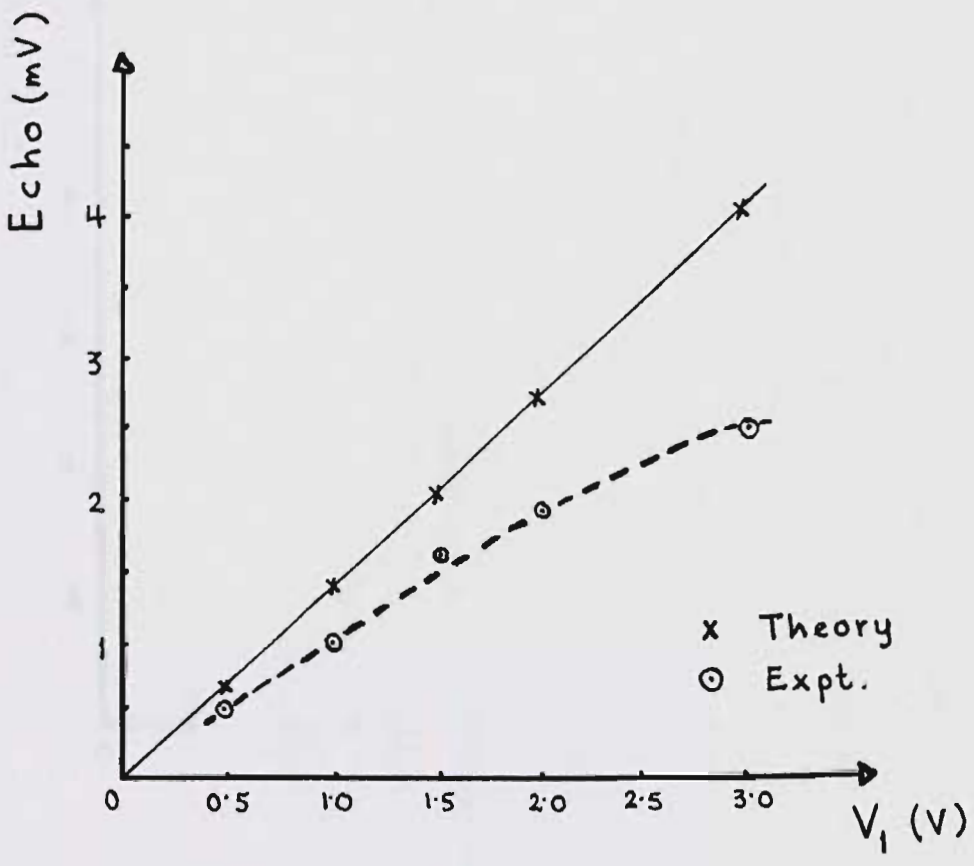

Figure 3.6. Nonlinear coupling echo vs. A_1.

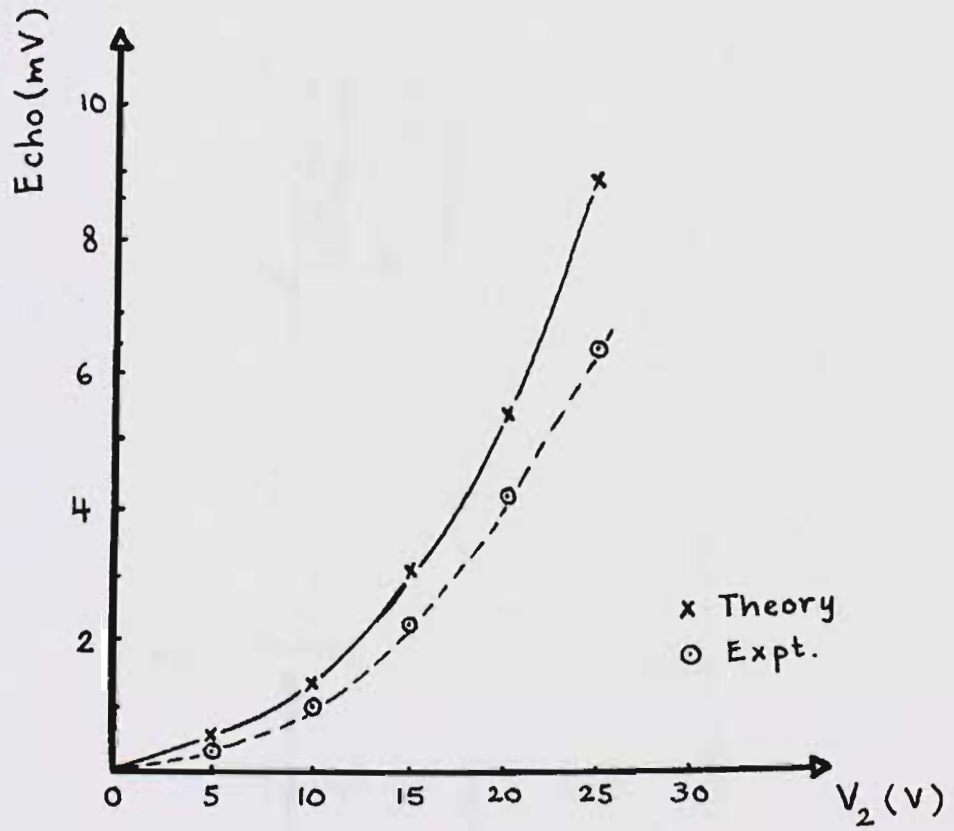

Figure 3.7. Nonlinear coupling echo vs. A_2.

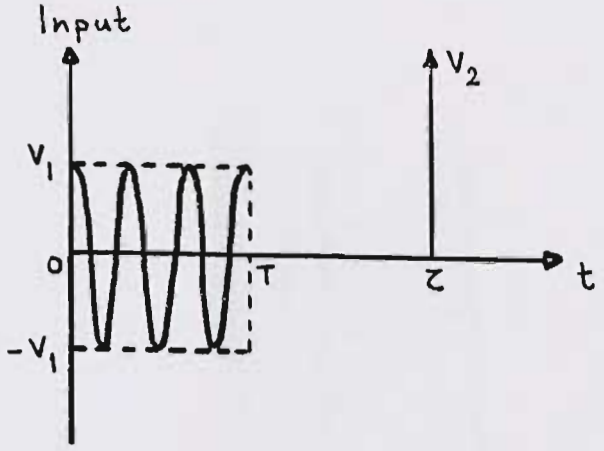

(a) Analog.

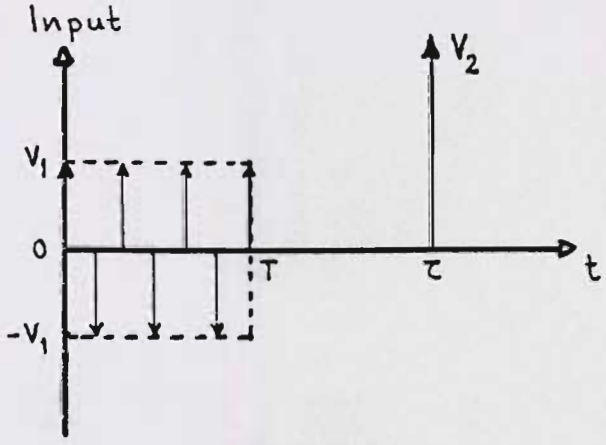

(b) Sampled.

Figure 3.8. R.F. square wave inputs, analog and sampled.

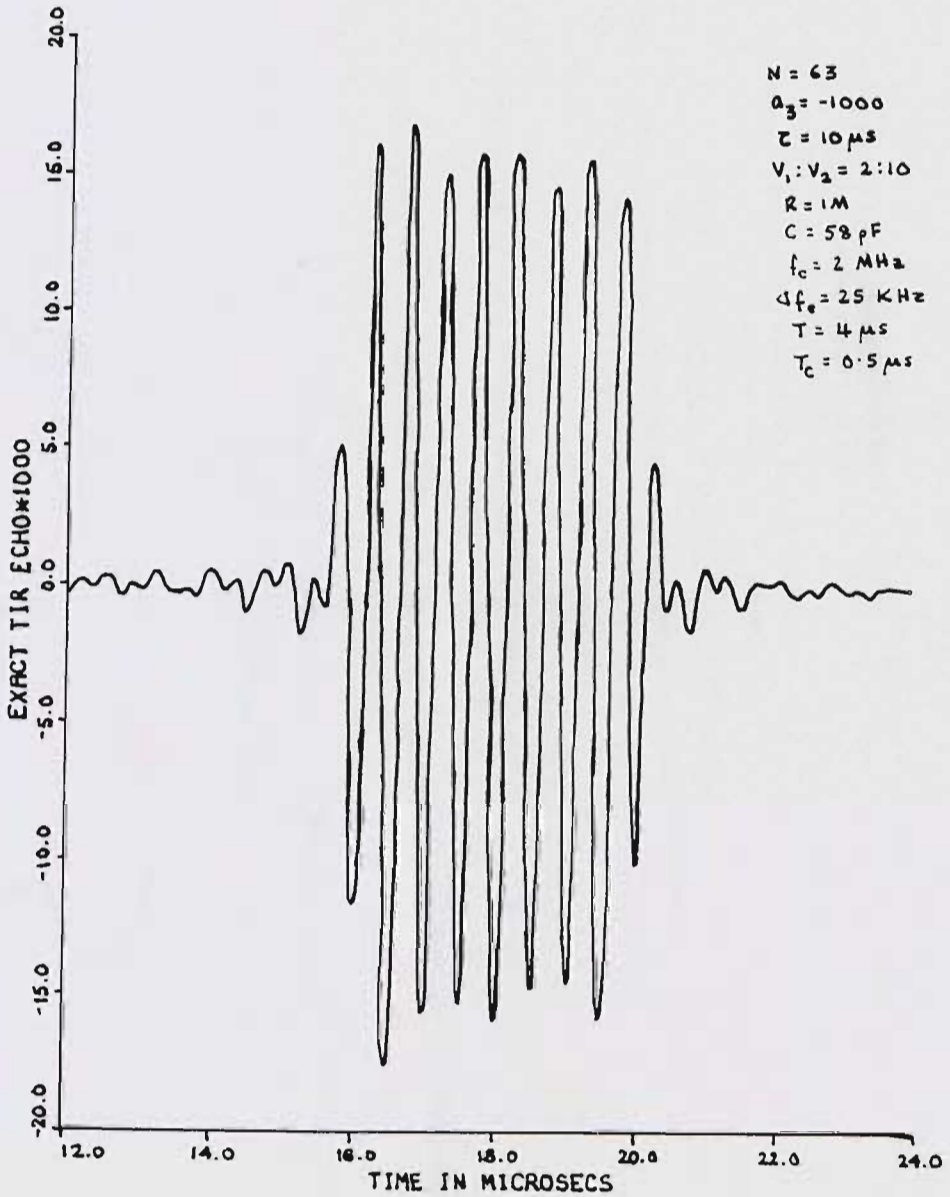

Figure 3.9. Analytical plot of TIR echo of r.f. square wave input.

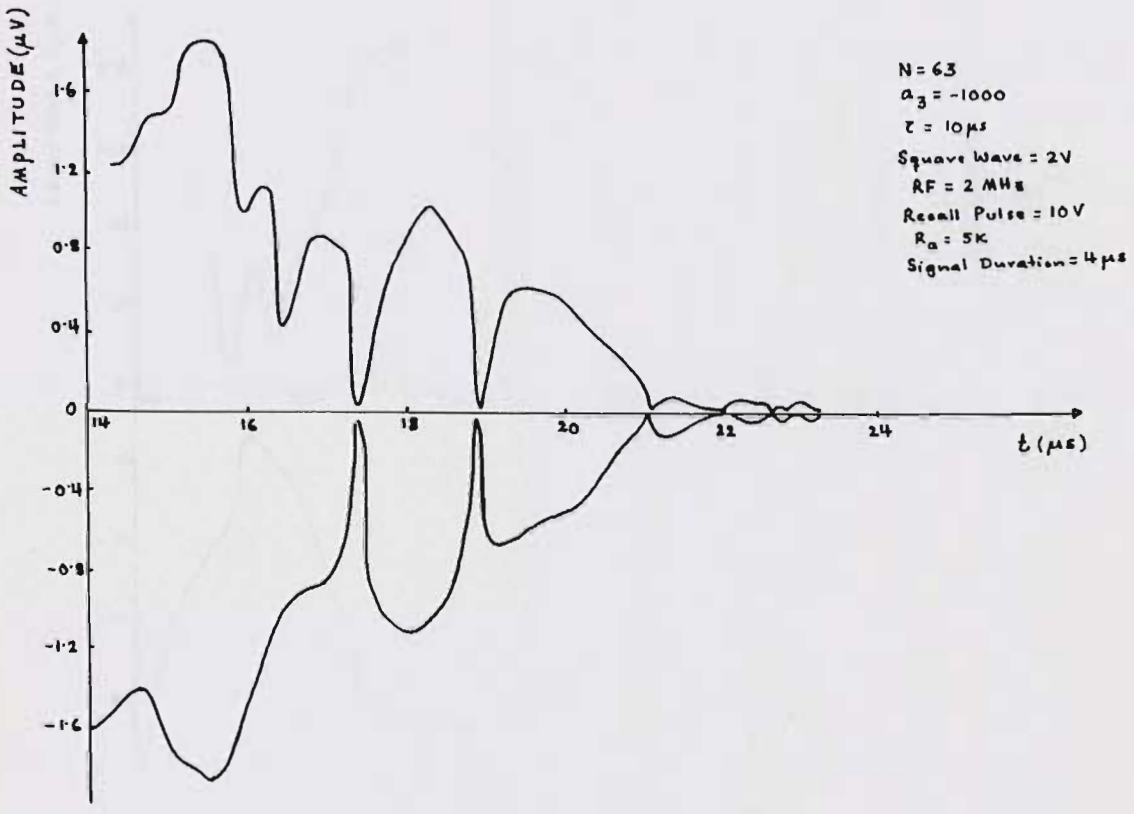

Figure 3.10. SPICE output for TIR echo of analog r.f. square wave input (only envelope is shown).

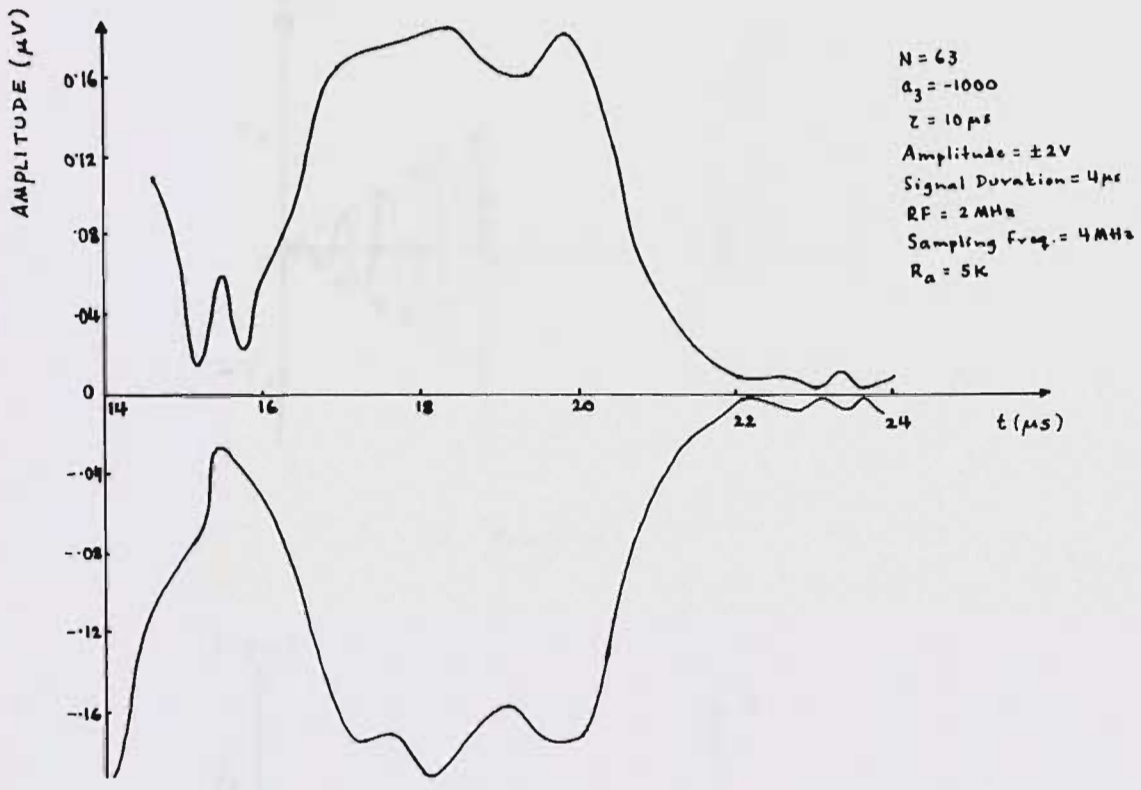

Figure 3.11. SPICE output for TIR echo of sampled r.f. square wave input (only envelope is shown).

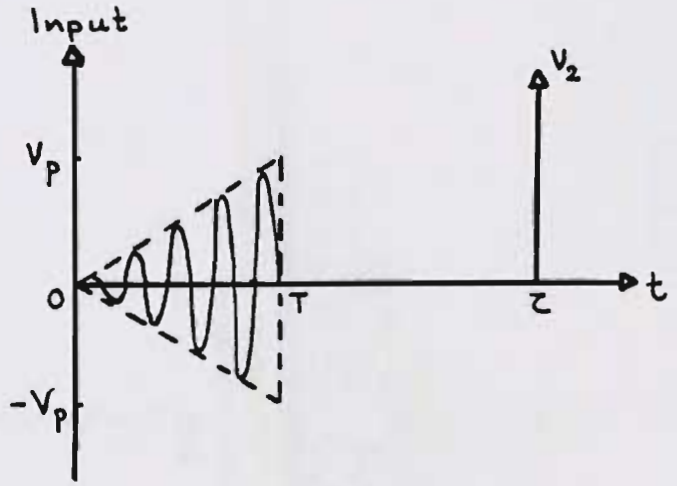

(a) Analog.

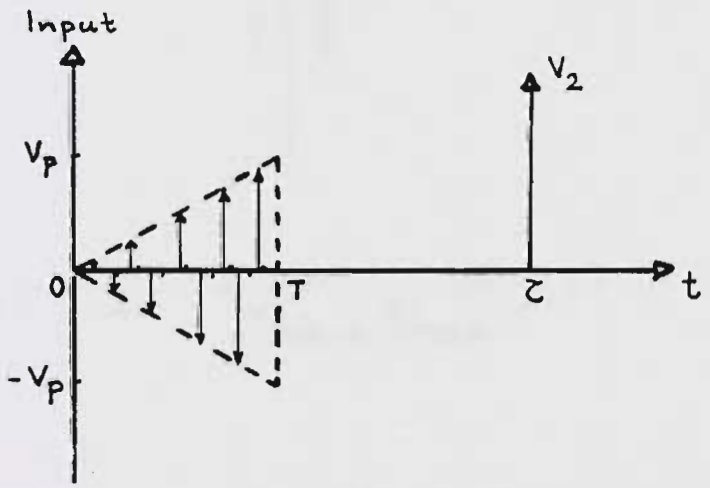

(b) Sampled.

Figure 3.12. R.F. sawtooth inputs, analog and sampled.

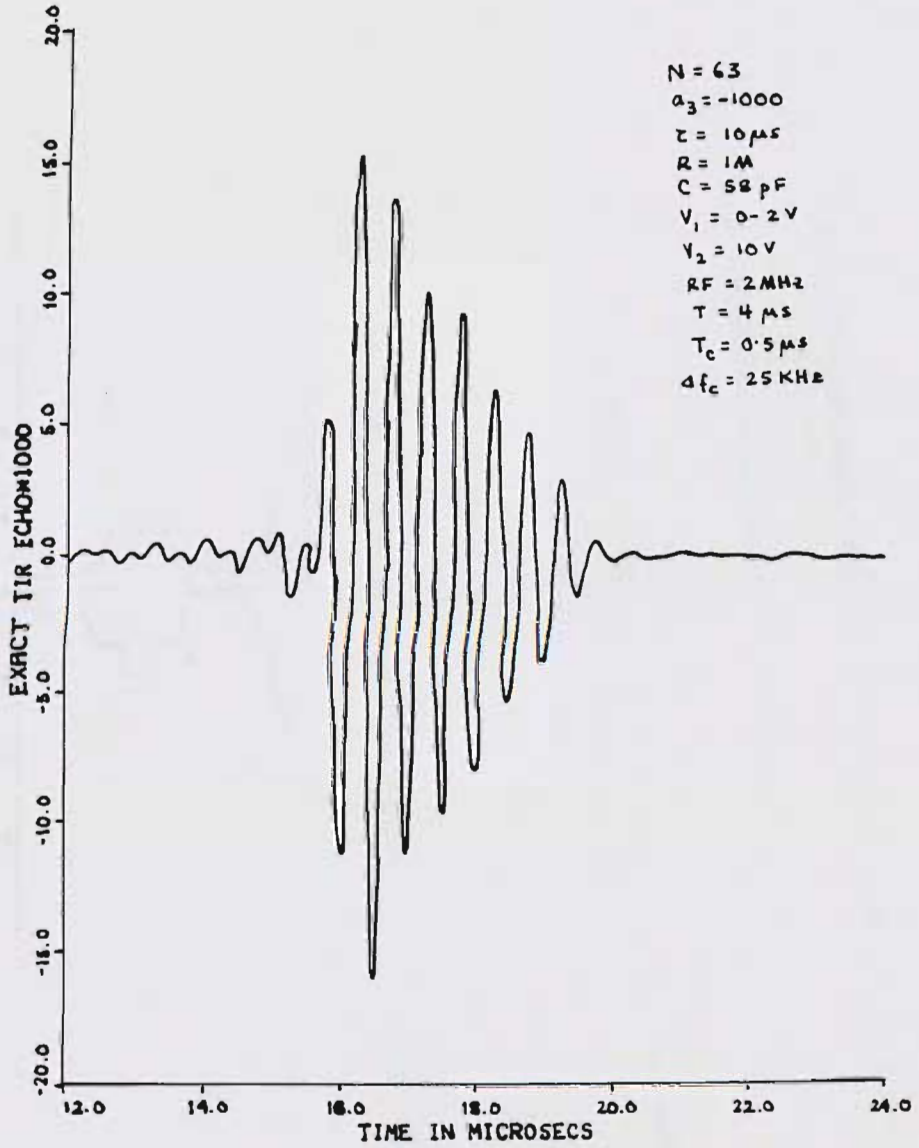

Figure 3.13. Analytical plot of TIR echo of r.f. sawtooth input.

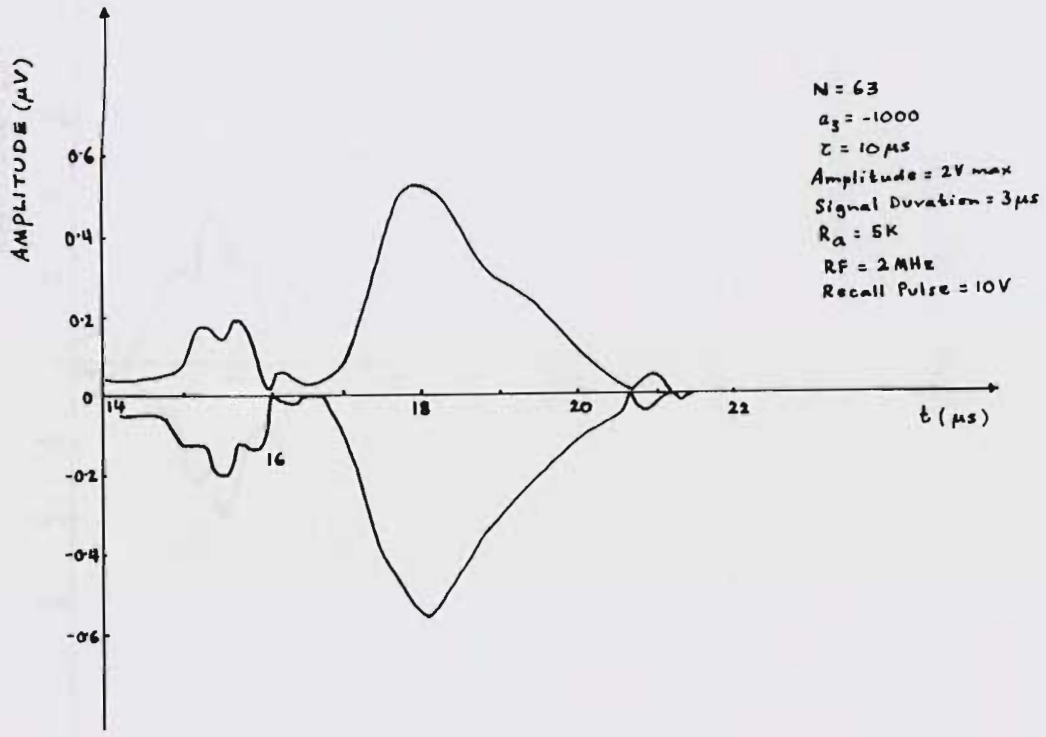

Figure 3.14. SPICE output for TIR echo of analog r.f. sawtooth input (only envelope is shown).

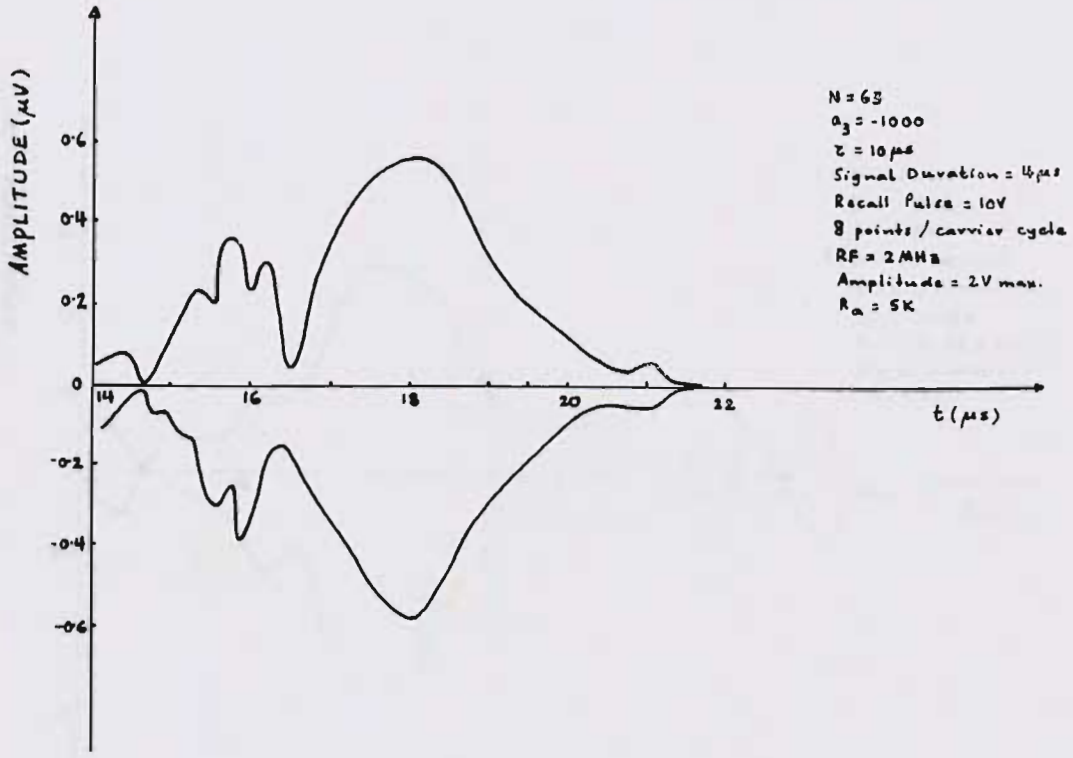

(a) 8 points per carrier cycle construction (only envelope is shown).

Figure 3.15. SPICE outputs for TIR echo of 2-slope r.f. sawtooth input.

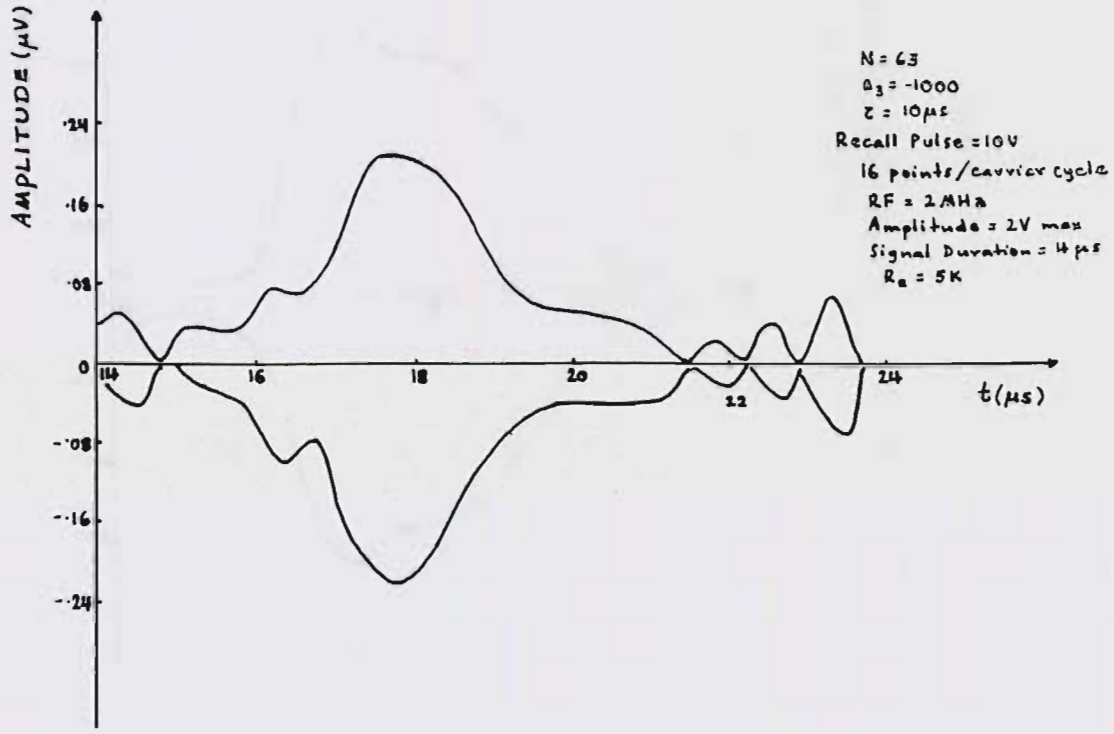

(b) 16 points per carrier cycle construction (only envelope is shown).

Figure 3.15. (continued)

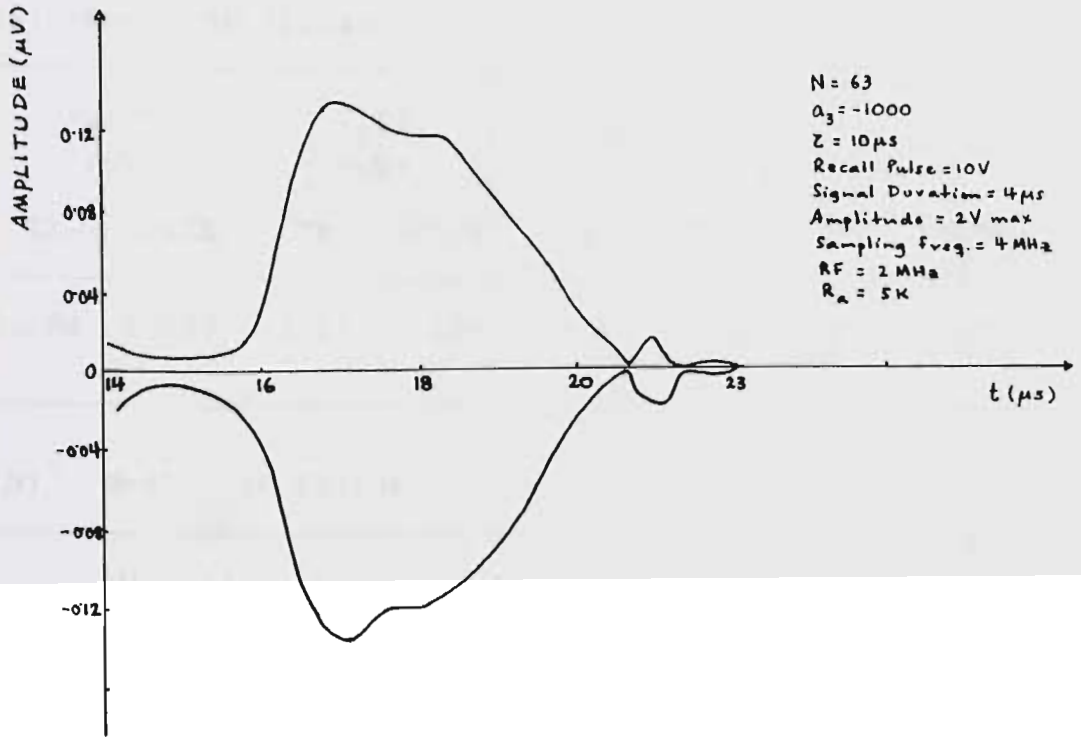

Figure 3.16. SPICE output for TIR echo of sampled r.f. sawtooth input (only envelope is shown).

Table 3.1

Summary of results for nonlinear coupling echo

$R_L = R_a \| (R_b/N) \sim 4.85K\Omega$; hence, $K \sim 4.85 \times 10^{-4}$.

(a) N=63, 5K filter

$V_5(2\tau)$ (μV)		$V_5(T)$ (μV)		$V_5(T+\tau)$ (μV)		T_W (μs)	
Th	SPICE	Th	SPICE	Th	SPICE	Th	SPICE
1.384	1.037	1.24	1.138	5.2	4.65	.635	0.8

(b) N=43, 5K filter

$V_5(2\tau)$ (μV)		T_W (μs)	
Th	SPICE	Th	SPICE
0.97	1.136	0.93	.925

(c) N=21, 3K filter

$V_5(2\tau)$ (μV)		T_W (μs)	
Th	SPICE	Th	SPICE
.285	.393	1.9	1.6

CHAPTER IV

DYNAMIC ECHOES WITH NONLINEAR DAMPING

In this chapter, we discuss the case of dynamic nonlinear echoes where the nonlinearity is associated with the damping or loss mechanism of the system. In our SPICE experiments, we arrived at a circuit model for nonlinear damping while investigating nonlinear coupling echoes. As mentioned in Chapter III, the circuit configuration of Fig.3.1(d) represents a nonlinear damping system. We first attempt to show why this is the case. Thereafter, we describe some of the SPICE experiments with an ensemble of such circuits, none of which, unfortunately, yielded any nonlinear echo. Finally, we argue that nonlinear damping echoes could not be generated in our SPICE experiments because the chosen experimental parameters did not satisfy all the conditions stipulated by theory.

IV.1 Analytical Investigation of Nonlinear Damping in an RLC Resonator

From the circuit configuration of Fig.3.1(d), we can write the following :

$$V_0=LdI_L/dt, \tag{4.1a}$$

$$I_C=CdV_0/dt, \tag{4.1b}$$

$$V_0=I_1R_2+f(V_0), \tag{4.1c}$$

$$V_{in}=R_1I_{in}+V_0, \tag{4.1d}$$

$$I_{in}=I_1+I_2=I_1+I_L+I_C, \text{ and,} \tag{4.1e}$$

$$\text{let} \quad f(V_0)=a_3V_0^3. \tag{4.1f}$$

Eliminating I_{in} from (4.1d) and (4.1e), and taking the derivative, we obtain :

$$(1/R_1)(dV_{in}/dt-dV_0/dt)=dI_1/dt+dI_L/dt+dI_C/dt, \tag{4.2}$$

which, upon using (4.1a-c) and (4.1f) leads to :

$$(1/R_1)dV_{in}/dt-(1/R_1)dV_0/dt=(1/R_2)dV_0/dt$$

$$-(3a_3/R_2)V_0^2dV_0/dt+V_0/L+Cd^2V_0/dt^2. \tag{4.3}$$

If we let $R_1=R_2=R$ in (4.3), we get :

$$dV_{in}/dt=RV_0/L+(2-3a_3V_0^2)dV_0/dt+RCd^2V_0/dt^2. \tag{4.4}$$

Eq.(4.4) is the nonlinear differential equation which describes the circuit of Fig.3.1(d). We can easily show that by letting $a_3=0$ in (4.4), the linear pulse response of the circuit may be written as :

$$V_0(t) \sim (A/RC)e^{-t/RC}\cos\omega_0 t, \qquad (4.5)$$

where A is the pulse area,

$\omega_0^2 = 1/LC$, and we assume that

$Q_0 = \omega_0 CR >> 1$.

Now, we may rewrite (4.4) as follows :

$$dV_{in}/dt = (V_0 + (L/R)(2-3a_3V_0^2)dV_0/dt + LCd^2V_0/dt^2)(R/L) . \qquad (4.6)$$

The nonlinear term in (4.6) can be written as :

$$(L/R)(2-3a_3V_0^2)dV_0/dt = (2L/R)dV_0/dt - 3a_3(L/R)V_0^2\,dV_0/dt . \qquad (4.7)$$

If we assume in (4.7) that $V_0 = V_m\cos(\omega_0 t+\phi)$, then, after some algebra, we can show that the LHS of (4.7) becomes :

$$LHS = -(2\omega_0 L/R)V_m(1-(3/4)a_3V_m^2)\sin(\omega_0 t+\phi)$$

$$+(3/4)a_3(\omega_0 L/R)V_m^3(\sin 3(\omega_0 t+\phi) - \sin(\omega_0 t+\phi)) . \qquad (4.8)$$

Ignoring the "$3\omega_0$" term in (4.8), we get :

$$LHS = -(2\omega_0 L/R)V_m(1-(3/8)a_3V_m^2)\sin(\omega_0 t+\phi) \qquad (4.9)$$

$$= -(2\omega_0 L/R_{ls})V_m\sin(\omega_0 t+\phi) , \qquad (4.10)$$

where $R_{ls}=R/(1-(3/8)a_3V_m^2)$ (4.11)

is a large signal nonlinear resistance, and V_m is the output amplitude. $V_m=A/RC$.

Since the linear solution of (4.4) to a delta function input $A\delta(t)$ is given by (4.5), we may write, to a first approximation, the nonlinear solution as :

$$V_{0,nl}\sim(A/RC)e^{-t/R_{ls}C}\cos\omega_0 t. \quad (4.12)$$

In general, the nonlinearity will cause a change in the coupling as well as the damping of the resonator response.

The physical interpretation of (4.12) is that, in response to a delta function input, the linear capacitor C will charge up to a maximum regardless of the nonlinearity, and then discharge with an amplitude-dependent damping factor. Thus, it seems reasonable to assume that the effect of the nonlinearity on the coupling to the resonator will be small compared to its effect on the damping of the response.

Assuming nonlinear damping to be predominant, we can then derive the following :

Case A : Large-signal damping factor

Near t=0, if we measure the response amplitudes V_1

and V_2 at times t_1 and t_2 respectively, such that $t_2-t_1<<RC$, then the large signal damping factor α will be given by :

$$\alpha=1/R_{ls}C \qquad (4.12a)$$

$$\sim(\ln(V_1/V_2)/(t_2-t_1)). \qquad (4.12b)$$

Case B : Small-signal damping factor

For $t>>RC$, if we measure (V_1, V_2) at (t_1, t_2) such that $t_2-t_1<<RC$, the small signal damping factor β is given by :

$$\beta=1/RC \qquad (4.13a)$$

$$\sim(\ln(V_1/V_2)/(t_2-t_1)). \qquad (4.13b)$$

Experimental Results from SPICE

A series of SPICE experiments were performed with the following parameters :

L=0.1242mH, C=58pF, R=2M, V_{in}=10V (triangular pulse), Triangle base width=0.11μs.

The results for the above set of parameters are summarized in Table 4.1. The value of a_3 was varied from -100 to -100000, and the corresponding response amplitudes

and the large and small signal damping factors were measured from SPICE, and compared with theory. A typical SPICE output is shown in Fig.4.1. It is clear from the table that the large-signal damping factors agree fairly well with theory. On the other hand, the small-signal damping factors do not seem to agree well. This may be attributed to the fact that these were measured near 15μs, instead of t~116μs, in order to minimize computation costs. Hence, one cannot expect the measured damping factors to be truly small-signal, since one needs to be at least 2RC (=116μs) away to measure them accurately. The purpose of the measurements at t=15μs was to observe the trends of the damping factors. It is encouraging to note that the damping factor at t=15μs is smaller than that at t=0 in each case. Overall, the above experiments indicate that the assumption that the nonlinear damping effect is stronger than that due to nonlinear coupling in this circuit is reasonable.

IV.2 Effect of Nonlinear Damping on an Ensemble of Resonators

Consider an ensemble of N discrete nonlinear resonators of the kind described in section IV.1. If we assume that for an individual resonator, the effect of nonlinear coupling is small (as was proven in the preceding section), then the pulse response of the resonator may be written as :

$$V_{0,nl} \sim (A/RC) e^{-t/R_{ls}C} \cos\omega_0 t, \qquad (4.14)$$

where R_{ls} and ω_0 have been defined earlier.

Using (4.11), we can express (4.14) as follows :

$$V_{0,nl} \sim (A/RC) e^{-t/RC} \, e^{(3/8)a_3 V_m^2 t/RC} \cos\omega_0 t, \qquad (4.15)$$

which for the ith resonator in the ensemble may be written as :

$$V_{0,nl}^{i} \sim (A/RC) e^{-t/RC} \, e^{-\gamma V_{m,i}^2 t} \cos\omega_{0,i} t, \qquad (4.16)$$

where $\gamma = -(3/8)a_3/RC.$ (4.17)

To arrive at (4.16), we have assumed that :

$$|(3/8)a_3 V_m^2| << 1. \qquad (4.18)$$

Now, the effective amplitude across the ith resonator following two delta-pulses applied at t=0 and t=τ will be given by :

$$V_{m,i}^2 \sim A_1'^2 + A_2'^2 + 2A_1' A_2' \cos\omega_{0,i}\tau, \qquad (4.19)$$

where $A_1' \sim (A_1/RC) e^{-t/RC},$ (4.20a)

$A_2' \sim (A_2/RC) e^{-(t-\tau)/RC},$ and (4.20b)

A_1 and A_2 are the pulse areas respectively.

Using (4.18) through (4.20), and the additional assumptions that

$$A_2 >> A_1, \text{ and} \tag{4.21a}$$

$$|2\gamma(t-\tau)A_1' A_2'| << 1, \tag{4.21b}$$

we can show after some algebra that the nonlinear response is given by (see Appendix I for details):

$$V_{0,nl}^{i} \sim P(t)\cos\omega_{0,i}(t-\tau) - (1/2)Q(t)(\cos\omega_{0,i}t + \cos\omega_{0,i}(t-2\tau)), \tag{4.22}$$

$$\text{where } P(t) = (A_2/RC)e^{-((1/RC)+\gamma(A_1'^2 + A_2'^2))(t-\tau)}, \tag{4.23a}$$

$$\text{and} \quad Q(t) = 2\gamma A_1' A_2'(t-\tau)P(t). \tag{4.23b}$$

Now, suppose that the resonator ensemble consists of N independent resonators separated by $\Delta\omega_c$, and centered at ω_c. Then,

$$\omega_i = \omega_c - ((N+1)/2)\Delta\omega_c + i\Delta\omega_c. \tag{4.24}$$

Using (4.24), and ignoring coupling effects, we obtain the macroscopic two-pulse response as :

$$V_{0,nl} \sim P(t)\sum_i \cos\omega_{0,i}(t-\tau) - (1/2)Q(t)\sum_i \cos\omega_{0,i}t$$

$$-(1/2)Q(t)\sum_i \cos\omega_{0,i}(t-2\tau). \qquad (4.25)$$

Using the result:

$$\sum_{i=1}^{N} \cos\omega_i t = F(t)\cos\omega_c t, \qquad (4.26)$$

where F(x) is defined by (3.5b), we can show that (4.25) reduces to :

$$V_{0,nl} \sim P(t)F(t-\tau)\cos\omega_c(t-\tau) - (1/2)Q(t)F(t)\cos\omega_c t$$

$$-(1/2)Q(t)F(t-2\tau)\cos\omega_c(t-2\tau). \qquad (4.27)$$

Of the three periodic terms in (4.27), the last one represents a nonlinear damping echo centered at $t=2\tau$. Note that the amplitude of the nonlinear damping echo is given by $NQ(t)$ at $t=2\tau$.

However, $P(t) >> Q(t)$ (see (4.21b) and (4.23b)). (4.28a)

Hence, $NP(t) >> NQ(t)$. (4.28b)

Therefore, in order that the nonlinear damping echo be identifiable above the tails of the terms involving P(t) near $t=2\tau$, we should have:

$$NP(t)/N << NQ(t), \text{ at } t=2\tau,$$

Or, $N>>P(t)/Q(t)$. (4.29a)

And, $\tau>>T_w$, where (4.29b)

$T_w=1/N\Delta f_c$ (4.29c)

is the duration of each F(x) term in (4.27).

Hence, only if the conditions (4.18), (4.21a), (4.21b), (4.29a) and (4.29b) are satisfied, we can expect to see a nonlinear damping echo near $t=2\tau$.

IV.3 Summary of SPICE Results for the Nonlinear Damping System

In this section, we discuss the results obtained from some of the SPICE experiments that were performed using an ensemble of nonlinear damping resonators. Most of these were done prior to developing the rigorous theory, and none resulted in nonlinear echoes.

The essential results from this set of experiments are given in Table 4.2. From the table, we find that although the linear response components agree reasonably well in all cases, the nonlinear response components are either negligible, or do not manifest themselves on SPICE. Also, for the 2-pulse cases, no discernable nonlinear echo is seen

near $t=2\tau$ in any case. A typical SPICE output is shown in Fig.4.2. In section IV.4, we attempt to show that the absence of the nonlinear damping echo is due to the violation of at least one of the criteria necessary for its existence, as established earlier.

To conclude our report of this series of experiments, we need to mention a few experiments with a single nonlinear damping circuit with a single pulse input that were carried out to verify if the dependent source f(V) did indeed vary as a_3V^3. The results are presented in Table 4.3. When a_3 is kept fixed at -1000, and the pulse amplitude is varied from 1V to 1000V, we find that the output at node '45' as obtained from SPICE agrees remarkably well with theory (see Table 4.3(a)). The same is true for the node when the pulse amplitude is kept fixed at 10V, and a_3 is varied from -100 to -100000 (see Table 4.3(b)). Thus, the dependent source does vary as a_3V^3.

IV.4 Test of Inequalities in Nonlinear Damping Experiments

In conclusion of this chapter, we now check the parameters used in the unsuccessful nonlinear damping experiments to see if they satisfy the conditions stipulated

by theory. To do so, we first state the conditions to be tested, viz.,

$$|(3/8)a_3V_m^2|<<1. \tag{4.18}$$

$$A_2>>A_1. \tag{4.21a}$$

$$|2\gamma' A_1' A_2'|<<1, \quad \gamma'=\gamma(t-\tau). \tag{4.21b}$$

$$P(t)<<NQ(t). \tag{4.29a}$$

$$\tau>>T_W. \tag{4.29b}$$

The parameters above have been defined in the equations earlier in the chapter.

Typical set of circuit values:

$R=2M$, $C=58pF$, $a_3=-950V^{-2}$, $\tau=10\mu s$,
$N=21$, $\Delta T=0.11\mu s$, $\Delta f_c=25KHz$, $V_1:V_2=1:20$.

We can show that $V_m\sim 9.48mV$.

Thus, $|(3/8)a_3V_m^2|\sim 0.032<<1$,

which satisfies (4.18).

Assuming $t\sim 2\tau$ in the neighborhood of observation, we find :

$$|\gamma'|\sim|\gamma\tau|\sim 30.7.$$

Since RC=116μs>>τ, the exponential terms in the inequalities are approximately 1.

We then have,

$A_1' \sim 0.474mV$, and $A_2' \sim 9.48mV$.

This leads to:

$|2\gamma' A_1' A_2'| \sim 276\ 10^{-6} << 1$,

which satisfies condition (4.21b).

Also, $T_W = 1/N\Delta f_c \sim 1.9\mu s$.

Hence, $\tau = 10\mu s >> T_W$, which satisfies (4.29c).

Since by choice $V_2:V_1 = 20:1$, (4.21a) is satisfied.

We can also show that:

$P(t) \sim A_2' \sim 9.48mV$, and,

$Q(t) \sim 2.617\mu V = NQ(t) \sim 54.96\mu V$.

Thus, $P(t) = 9.48mV >> NQ(t)$, which severely violates condition (4.29a). This violation is the probable cause behind the failure of the SPICE nonlinear damping echo experiments.

As a note of interest, we may evaluate the minimum N needed to satisfy (4.29a).

From (4.29a), we need,

N>>P(t)/Q(t). For the present case, this leads to :

N>>9.48mV/2.62μV~3622!

Clearly, the above is far greater than our SPICE capability.

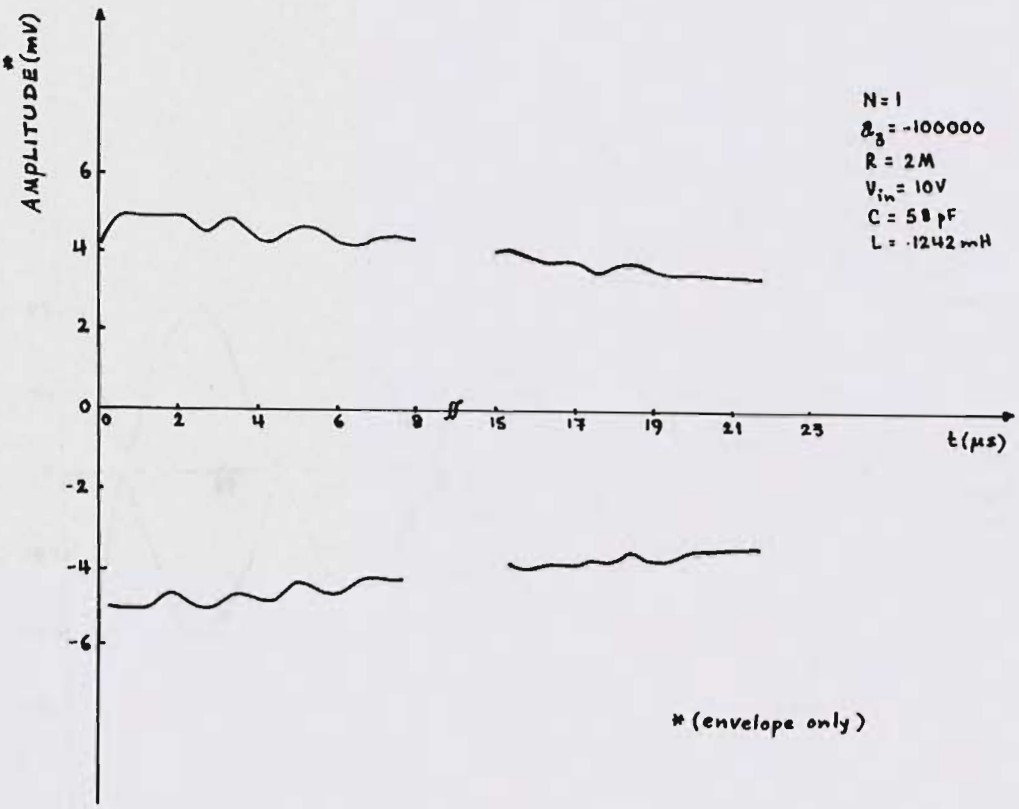

Figure 4.1. Typical SPICE output from a single nonlinear damping circuit.

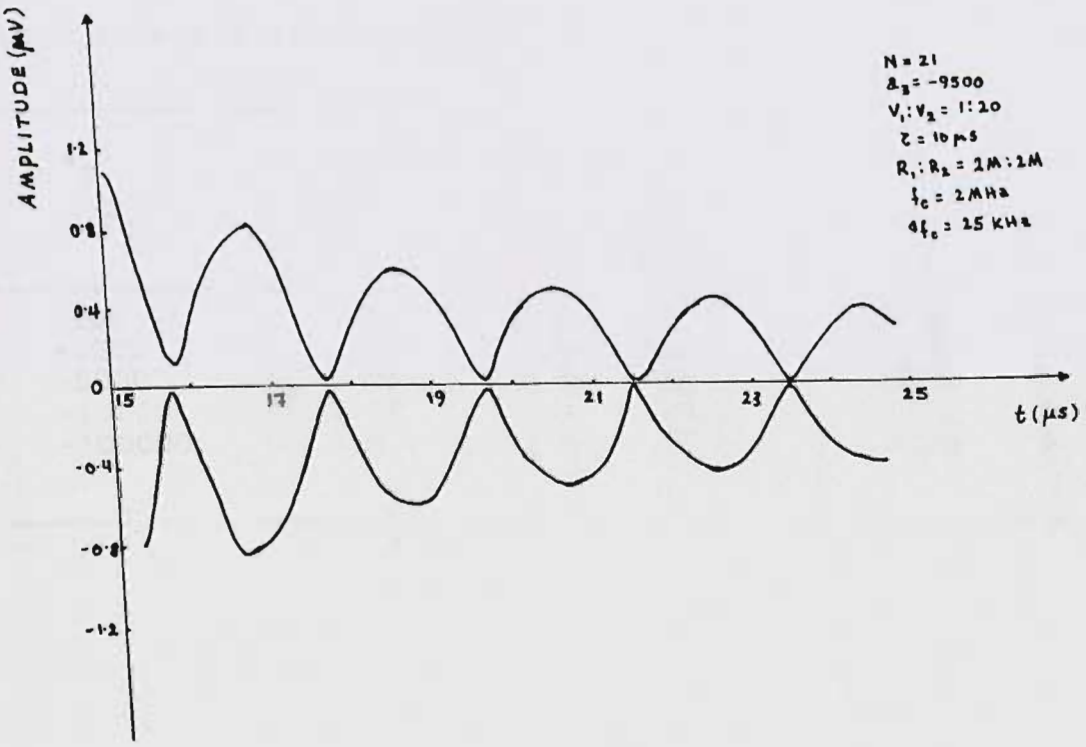

Figure 4.2. Typical SPICE output from N nonlinear damping circuits to 2-pulse input (only envelope is shown).

Table 4.1

Measurement of large and small-signal damping constants from nonlinear damping circuit

With the parameters specified in section IV.1, we have:

V_m(theory)~4.7mV; from SPICE, V_m~4.93mV.

Also, β (small signal)=1/RC~$8.62\times10^3 sec^{-1}$.

a_3 (V^{-2})	R_{ls}/R	α(near t=0) ($\times10^3 sec^{-1}$) Th	SPICE	β (near t=15μs) ($\times10^3 sec^{-1}$) Th	SPICE
-100	1.0	8.62	9.7	8.62	8.43
-1000	1.01	8.69	9.71	8.62	9.1
-5000	1.04	8.96	10.1	8.62	9.1
-10000	1.08	9.3	10.3	8.62	9.1
-100000	1.8	15.5	17.3	8.62	9.0

Table 4.2

Summary of SPICE results for the nonlinear damping system

Lin. Resp. (mV) Th	SPICE	At (μs)	Nonlin. Resp. (mV) Th	SPICE	At (μs)	Combined Resp. (mV) Th	SPICE	At (μs)
(i) N=21; a_3=-95000; V_1:V_2=1:10; R_1:R_2=2M:2M; τ=10μs; Obs. range=15-45μs.								
0.23	-	15	.24	-	15	.465	.51	15
(ii) N=21; a_3=0; V_1:V_2=1:0; R_1:R_2=2M:200M; τ=10μs; Obs. range=15-45μs.								
0.023	.025	15	0	0	15	.023	.025	15
0.47	.48	40	0	0	40	.47	.48	40
(iii)N=21; a_3=-950; V_1:V_2=1:20; R_1:R_2=2M:2M; τ=10μs; Obs. range=15-25μs.								
0.451	-	15	.038	-	15	.489	.546	20
(iv) N=1; a_3=-1000; V_1:V_2=10:0; R_1:R_2=.4M:.4M; Obs. range=0-15μs.								
23.5	-	10	6	-	10	29.5	24	10
(v) N=1; a_3=-950; V_1:V_2=10:0; R_1:R_2=2M:2M; Obs. range=0-15μs.								
4.7	-	10	neg.	-	10	4.7	4.93	10
(note: here, because of a large time constant output filter, the output grew from zero with a time constant of about 2RC=1.16ms.)								
(vi) N=21; a_3=-950; V_1:V_2=1:20; R_1:R_2; Δf_c=5KHz; τ=25μs; Obs. range=0-60μs.								
9.47	-	25	0.4	-	25	9.87	9.84	25

Table 4.3

Test results for dependent nonlinear source in the nonlinear damping circuit

(a) With a_3=-1000.

V_{in}(V)	V_{45}(mV)	SPICE out (mV)
1	1.06×10^{-4}	2.14×10^{-4}
10	0.103	0.118
50	13.25	14.91
100	106.0	118.0
200	848.0	900.0
1000	106×10^{3}	78×10^{3}

(b) With V_{in}=10V.

a_3	V_{45}(mV)	SPICE out (mV)
-100	.0103	.012
-1000	.103	.118
-10000	1.03	1.195
-10^{5}	10.3	11.76

CHAPTER V

GENERATION OF MEMORY ECHOES BY ELECTRONIC HOLOGRAPHY

As discussed in the introduction, the discovery of very long and virtually indestructible memories in stimulated or three-pulse echo experiments with piezoelectric powders was perhaps the most intriguing aspect of nonlinear echo phenomena. Prior to that, in echo experiments with piezoelectric crystals, it had already been reported that the three-pulse echo showed "anomalous persistence" [3]. However, the storage or recall times of these echoes, although still very large compared to the lifetimes of acoustic phonons, electronic traps, or acoustic holograms, were still relatively finite (of the order of several hours typically). In powders, however, experiments revealed memory echoes that lasted for weeks [23]. Moreover, it was demonstrated that the memory echo could not be destroyed by disrupting the orientation of the powder grains [24]. Korpel's theory based on phase conjugation and electronic holography via nonlinear parametric interactions in resonator ensembles gave a theoretical explanation for the generation and long-term storage properties of the memory

echo. The theory actually went beyond a simple pulse-echo model to include any finite, arbitrary input, and thereby led to more general signal processing and storage possibilities.

In this chapter, we discuss the basic long-term storage model due to Korpel, and apply the theory specifically to pulse inputs, and later, to more general inputs for time-inverted and non-time-inverted recall. We also discuss concurrently how simply the model is implemented on SPICE in each case, by tailoring the nonlinear parameter of each resonator in accordance with the energy in the corresponding spectral component of the input. SPICE results are then presented and discussed. Finally, to demonstrate a signal processing application, a SPICE experiment involving a static-echo correlator is carried out.

V.1 Basic Long-Term Storage Model

Following the treatment in [6], if the general input signal is given by:

$$e(t)=e_1(t)+e_2(t-\tau), \tag{5.1}$$

then the spectrum of the input signal for $t>\tau$ is given by:

$$\phi(\omega)=\phi_1(\omega)+\phi_2(\omega)e^{-j\omega\tau}. \tag{5.2}$$

Now, let $e_r(t)=\delta(t-T)$ (5.3)

be the recall pulse applied at t=T, so that it has the spectrum

$$\phi_r(\omega)=e^{-j\omega T}. \quad (5.4)$$

Then, according to the model suggested by Korpel, application of the input e(t) (also called "write-in"), through the nonlinearity of the system, alters the coupling to each individual resonator or eigenmode of the system by an amount ΔK given by :

$$\Delta K \propto |\phi(\omega)|^2. \quad (5.5)$$

Hence, following the application of the "recall" pulse, the spectrum of the recalled signal is given by :

$$\phi''(\omega) \propto |\phi(\omega)|^2 \phi_r(\omega). \quad (5.6)$$

Using (5.2) and (5.4) in (5.6), we obtain :

$$\phi'' \propto |\phi_1|^2 e^{-j\omega T} + |\phi_2|^2 e^{-j\omega T} + \phi_2^* \phi_1 e^{-j\omega(T-\tau)} + \phi_2 \phi_1^* e^{-j\omega(T+\tau)}. \quad (5.7)$$

In general, the spectrum in (5.6) leads to a recalled time domain signal given by the triple product

$$e''(t) \propto e(t) \circledast e(t) * e_r(t), \quad (5.8)$$

where ⊛ denotes correlation and * denotes convolution.

V.2 Memory Echo for 2-pulse Write-In

Let the write-in signal consist of two delta pulses such that

$$e(t)=A_1\delta(t)+A_2\delta(t-\tau), \tag{5.9a}$$

where A_1 and A_2 are the pulse areas.

Then, $\phi(\omega)=A_1+A_2e^{-j\omega\tau}$. (5.9b)

Let the static recall pulse (of area A_3) be given by

$$e_r(t)=A_3\delta(t-T), \text{ so that} \tag{5.10a}$$

$$\phi_r(\omega)=A_3e^{-j\omega T}. \tag{5.10b}$$

Next, let us consider a single linear RLC resonator with a resonant frequency ω_0. Then, the linear response to a static recall pulse $e_r(t)$ will be given by :

$$V(t)=(A_3/RC)e^{-(t-\tau)/2RC}\cos\omega_0(t-T), \quad t>T. \tag{5.11}$$

Now, suppose that following the "write-in" process, the coupling to the resonator is altered according to the following prescription :

$$\Delta K=a_1(\omega_0)=K_1|\phi(\omega_0)|^2, \tag{5.12}$$

where K_1 is a constant of proportionality, a_1 is a coupling parameter (to be used on SPICE later), and, from (5.9b),

$$|\phi(\omega_0)|^2=A_1^2+A_2^2+2A_1A_2\cos\omega_0\tau. \qquad (5.13)$$

Suppose in our SPICE experiment, we introduce a dependent voltage source which is given by :

$$f(V)=a_1V(t)\ , \qquad (5.14)$$

where a_1 is given by (5.12), and is dimensionless.

Using (5.11) and (5.12) in (5.14), we can show that the output across the source f(V) will be given by :

$$V_{0,i}(t)\sim(K_1(A_1^2+A_2^2)A_3/RC)e^{-(t-T)/2RC}\cos\omega_{0,i}(t-T)$$
$$+(K_1A_1A_2A_3/RC)e^{-(t-T)/2RC}\cos\omega_{0,i}(t-(T-\tau))$$
$$+(K_1A_1A_2A_3/RC)e^{-(t-T)/2RC}\cos\omega_{0,i}(t-(T+\tau)),\quad t>T. \qquad (5.15)$$

Note that the subscript "i" refers to the ith resonator in an ensemble of resonators to be used later.

In deriving (5.15), we have assumed that following two input pulses applied at t=0 and t=τ, the coupling to each

resonator is changed by the amount presribed by (5.12). Once this change has taken place, one can assume that the system then preserves permanently the information of the applied write-in through these selectively altered coupling parameters. Hence, we may apply the third or "recall" pulse at any time t=T thereafter. Thus, once we assume a form of a_1 as in (5.12), we may set T=0 in an actual SPICE experiment.

Now, if we sum (5.15) over N linear resonators, the macroscopic response will be given by :

$$V_0(t)=\sum_{i=1}^{N} V_{0,i}(t)$$

$$\sim(KK_1(A_1^2+A_2^2)A_3/RC)e^{-(t-T)/2RC}F(t-T)\cos\omega_c(t-T)$$

$$+(KK_1A_1A_2A_3/RC)e^{-(t-T)/2RC}F(t-(T-\tau))\cos\omega_c(t-(T-\tau))$$

$$+(KK_1A_1A_2A_3/RC)e^{-(t-T)/2RC}F(t-(T+\tau))\cos\omega_c(t-(T+\tau)), \qquad (5.16)$$

where the function F(x) is defined by (3.5b), and K is the scaling factor discussed earlier.

Note that the three terms in (5.16) represent $\sin N\theta/\sin\theta$ type responses centered at $t=T$, $T-\tau$, and $T+\tau$ respectively. Of these, the last one is the memory or static echo term.

From the above, we may conclude that if we take an ensemble of linear RLC resonators whose coupling parameters have been altered in accordance with (5.12) (this is reminiscent of the process of "preparing" a hologram by using an object field and a reference; in this case, we use two write-in pulses), then by applying a "recall" pulse any time $t=T$ later (which is similar to "reading" a hologram), we can obtain a holographic readout of the stored information in the form of a memory echo.

If we make N sufficiently large, and choose A_2, $A_3 >> A_1$, then we can ensure that the response humps in (5.16) will be narrow enough so that the memory echo will not be swamped by the tails of the undesirable responses. Also, we must make $1/\Delta f_c$ large enough so that the terms in (5.16) repeat over a long interval.

Thus, we need :

$$N >> 1, \tag{5.17a}$$

$$1/N\Delta f_c << \tau, \tag{5.17b}$$

$$1/\Delta f_c >> \tau . \qquad (5.17c)$$

If eq.(5.17a-c) are satisfied, we should expect to see a memory echo near $t=T+\tau$, which, for $T=0$, will be given by :

$$V_0(t) \sim (KK_1A_1A_2A_3/RC)e^{-t/2RC} F(t-\tau)\cos\omega_c(t-\tau). \qquad (5.18)$$

V.3 Non-Time-Inverted and Time-Inverted Memory Echo

It turns out that using the basic long-term storage model, it is possible to predict non-time-inverted and time-inverted memory echoes of arbitrary input write-in signals.

Thus, if we ignore the effect of the first three terms in (5.7) in the time range $t>T$, then, near $t=T+\tau$, the fourth term represents the potentially useful correlation :

$$\phi''(\omega) \sim \phi_2\phi_1^* e^{-j\omega(T+\tau)}, \text{ and,} \qquad (5.19a)$$

$$E''(t) \sim e_2(t-(T+\tau)) \circledast e_1(t-(T+\tau)). \qquad (5.19b)$$

If, now, in (5.19b), we choose

$e_1(t)=\delta(t)$, then we obtain

$$E''(t) \sim e_2(t-(T+\tau)), \qquad (5.20)$$

which is a non-time-inverted replica of e_2 centered at $t=T+\tau$.

On the other hand, if we choose

$e_2(t)=\delta(t)$, then from (5.19a) we obtain

$$E''(t)\sim e_1((T+\tau)-t), \qquad (5.21)$$

which is a time-inverted replica of the signal e_1 centered $t=T+\tau$.

We may note that in deriving the results for pulse as well as arbitrary input write-in signals, we have placed no restrictions on the time of application T of the recall pulse. Thus, the basic long-term storage model predicts memory echoes which have essentially infinite recall times.

V.4 SPICE Implementation of 3-Pulse Memory Echo

From our discussion in the preceding section, we can now design an N-element SPICE experiment to generate pulse memory echoes. For this, we have to first compute the spectral amplitudes of the "write-in", which would consist of two pulses separated by τ in this case. Thereafter, we have to assign the values of a_1 for each resonator (note

that the resonators are linear). Finally, we have to apply a "recall" pulse at t=T=0 for simplicity.

Typical Design Set

Let us choose the following :

$V_1:V_2:V_3=1:10:10$ ΔT=pulse duration=0.11μs

$\tau=10\mu s$ $f_c=2MHz$

$\Delta f_c=25KHz$ $a_1=-1000$ at $f_0=f_c$

N=63

From the above, using (5.12), we can solve for the constant K_1. We then have,

$$K_1\sim -2.7548\times 10^{15}\ V^{-2}sec^{-2}.$$

Using (5.17), and the values above, we can show that the parameter a_1 will be given by :

$$a_1(\omega_0)\sim K_1(A_2^2+2A_1A_2\cos i\Delta\omega_c\tau),\quad i=1,\ldots,N \qquad (5.22)$$

where we have assumed that $A_1^2<<A_2^2$.

With the above, we then obtain the values of a_1 as tabulated in Table 5.1.

A SPICE memory echo experiment with N=63 was then conducted for the above set of values. A recall pulse was

applied at t=0, and the experimental values were plotted from t=7μs to t=15μs. The circuit components were chosen as follows :

$C=58pF \quad L_i$ variable, $i=1,..,63$

$R=0.5M\Omega \quad R_1=10M\Omega$.

Fig.5.1 shows one of the 63 linear resonators used in the experiment.

The output at node "5" from SPICE showed a remarkably well defined memory echo pulse centered at t=10μs, as expected (since the echo should appear at $t=T+\tau=\tau=10\mu s$). The output from 7μs to 15μs is shown in Fig.5.2. Note that the width of the echo is approximately 0.8μs, which is close to the theoretical value of ~40/63~0.7μs. If we compute the amplitude of the memory echo using (5.18), we obtain :

$$Amp \sim K_1 A_1 A_2 A_3 / RC \sim 1.2V.$$

Because of the 5K output filter used in the experiment, the above amplitude would be modified as follows:

$$Amp\ (corrected) \sim 5K/(5K+10M\|10M\|..\|10M)Amp \sim 1.2/40=3\times10^{-2}V.$$

From SPICE, the memory echo amplitude is obtained as approximately $2.2\times10^{-2}V$, which is close to the theoretical value, considering the approximations made in the calculations.

V.5 Implementation of Non-Time-Inverted Recall Using Memory Echo

For an arbitrary input "write-in", we have to first evaluate the spectral amplitudes. In order to achieve non-time-inverted recall, let us choose an input "write-in" sequence as given by Fig.5.3. In the figure, e_1 is a delta pulse of area A_1, and e_2 is a sampled R.F. sawtooth of duration T_s, applied at $t=\tau-T_s$. The sampling pulses appear every $T_c/2$ seconds, where T_c is the R.F. carrier period.

From Fig.5.3, we can write the following :

Analog Envelope $e_2(t)=(A_2/T_s)(t-\tau+T_s)$. (5.23)

Sampled Signal

$$e_s(t)=\sum_{i=0}^{2T_s/T_c}(iA_2T_c/2T_s)(-1)^i\delta(t-(\tau-T_s+iT_c/2)). \tag{5.24}$$

Hence, the total "write-in" signal becomes:

$$V_{in}(t)=A_1\delta(t)+e_s(t). \tag{5.25}$$

The spectrum of (5.25) is given by:

$$V_{in}(\omega)=A_1+\sum_{i=0}^{2T_s/T_c}(A_2T_c/2T_s)i(-1)^i e^{-j\omega(\tau-T_s+iT_c/2)}. \tag{5.26}$$

We now need to evaluate $a_1(\omega_0)$ for each resonator using (5.26). This is easily accomplished by computing $|V_{in}(\omega_0)|^2$ on the computer.

It is interesting to note here that in the computation of the a_1 values, the factor $(-1)^i$ in (5.26) had initially been inadvertantly left out. When the resulting a_1 values were used in the SPICE program, the expected non-time-inverted signal was not seen. This observation is easily explained by the fact that the above error led to a unipolar, sampled input sequence centered at $2\omega_c$, which was rejected by the linear resonator ensemble centered at ω_c.

When the $(-1)^i$ factor was restored in (5.26), the $|V_{in}(\omega_0)|^2$ and normalized a_1 (normalized to a_1=-1000 at ω_c) values given in Table 5.2 were generated. It was found that for N resonators in the ensemble (where N is odd),

$$|a_1|_k=|a_1|_{(N+1)-k}\ , \qquad (5.27)$$

which indicates a symmetrical spectrum.

With the above values of a_1, a SPICE experiment with 63 resonators was conducted. A single recall pulse (10V) was applied at t=T=0, and the experiment was run from 4μs to 14μs. The circuit parameters were identical to the experiment in section V.4. The resulting SPICE output in the

same time range is shown in Fig.5.4. From the output plot, we see that a non-time-inverted memory echo of e_2 has indeed been generated. The echo extends from $t=T+(\tau-T_s)=0+(10-4)=6\mu s$, to $t=T+\tau=0+10=10\mu s$, as expected. More interestingly, we find that the envelope of the echo is a fairly well-defined sawtooth which is much cleaner than was obtained in any of the previously attempted dynamic TIR experiments (anharmonic or nonlinear coupling).

V.6 Implementation of Time-Inverted Recall Using Memory Echo

For time-inverted recall, we choose the input "write-in" sequence shown in Fig.5.5. Here, the signal e_1 is a sampled R.F. sawtooth of duration T_s, and e_2 is a pulse of area A_2 applied at $t=\tau$.

In this case, we can write,

Analog Envelope $\quad e_1(t)=(A_1/T_s)t. \qquad (5.28)$

Sampled Signal

$$e_s(t)=\sum_{i=0}^{2T_s/T_c}(iA_1T_c/2T_s)(-1)^i\,\delta(t-iT_c/2). \qquad (5.29)$$

Hence, the total signal becomes :

$$V_{in}(t) = e_s(t) + A_2\delta(t-\tau). \qquad (5.30)$$

The spectrum of the above signal is given by :

$$V_{in}(\omega) = \sum_{i=0}^{2T_s/T_c} (i(-1)^i A_1 T_c/2T_s) e^{-ji\omega T_c/2} + A_2 e^{-j\omega\tau}, \qquad (5.31)$$

where T_c is the carrier period defined earlier.

The numerically computed values of $|V_{in}(\omega_0)|^2$ and the normalized values of a_1 for N=63 resonators are given in Table 5.3. Once again, the spectrum is found to be symmetrical.

A SPICE memory TIR experiment with the above a_1 values was conducted with 63 resonators, using a 10V static recall pulse applied at t=T=0, and the experiment was run from 4μs to 14μs. The circuit parameters were identical to those used in the preceding sections. Fig.5.6 shows a plot of the SPICE output in the same time range in this case. From the plot, we find that a time-inverted replica of e_1 has been generated as expected, extending from $t=T+\tau-T_s=0+10-4=6\mu s$ to $t=T+\tau=10\mu s$. The recall signal, once again, has superior clarity as compared with those obtained in dynamic TIR experiments.

The above experiments demonstrate the validity and scope of the Korpel and Longuet-Higgins model of long-term storage and recall of arbitrary signals based on the principles of electronic holography, and show that , theoretically at least, there is no limit on the recall time t=T of the recalled signal.

V.7 Implementation of a Static Echo Correlator

In order to demonstrate the signal processing capability of the long-term memory echo based on electronic holography principles, we decided to generate the time-correlation function of an arbitrary input "write-in", by using the concept of electronic holography and long-term storage as discussed in this chapter.

If we start from (5.7), and ignore the effect of the first three terms, then, for a static recall pulse applied at t=T, the resulting recalled signal is shown to be a correlation of the components $e_1(t)$ and $e_2(t-\tau)$ of the applied input "write-in", as given by (5.19a) and (5.19b). Note that the correlation is centered at $t=T+\tau$, where τ is the center-to-center separation of the two time-limited components e_1 and e_2 of the input "write-in".

Thus, for our SPICE experiment, we would have to follow the steps below :

(i) Define the input "write-in" as the combination of two arbitrary, finite duration signals e_1 and e_2, separated center- to-center by τ.

(ii) Using the methods outlined in the preceding sections, numerically evaluate the spectral components of the input corresponding to the resonant frequencies of the resonator ensemble.

(iii) From (ii), calculate the normalized values of the parameter a_1 of the ensemble, choosing a_1 to be -1000 at the center frequency of the ensemble.

(iv) Incorporate the above a_1 values in the linear resonator ensemble to be used on SPICE.

(v) Apply a static recall pulse of area A_3 to the linear ensemble at t=T=0.

With the above prescription, a SPICE experiment was conducted with essentially the same circuit parameters as in the preceding sections. The input "write-in" was chosen as two R.F. square pulses (R.F.=2MHz), the first extending from 0 to 4μs, and the second from 8 to 12μs. Both pulses had a

2V amplitude. The input is shown in Fig.5.7. The corresponding a_1 values are listed in Table 5.4.

When a 10V recall pulse was applied to the resulting linear ensemble at t=T=0, the SPICE output of Fig.5.8 was obtained in the time range 3.5 to 16μs. As can be readily verified, the plot shows the correlation of the two inputs e_1 and e_2 which extends from t=4μs (which is where the correlation begins) to t=12μs (where the correlation ends). We may note that the correlation is centered at t=8μs, which is indeed the center-to-center separation of the input "write-in" components (=10-2=8μs). The isosceles triangle shape of the correlation can also be readily verified.

We can conclude from the experiments in this chapter that the long-term storage model does indeed show the existence of 3-pulse memory echoes in resonator ensembles, as well as the possibilty of non-time-inverted and time-inverted recall of arbitrary inputs with no restriction on the recall time. This would then verify the extremely long-term persistence of the static memory as reported in the literature. Furthermore, the experiment in section V.7 shows that the same principle can be utilized for other signal processing applications such as correlation and convolution.

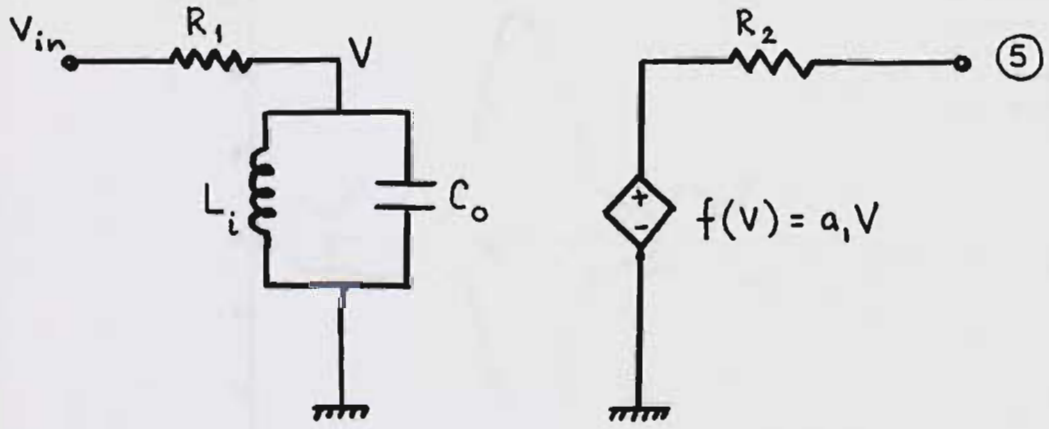

Figure 5.1. One of 63 linear resonators used to simulate memory echo.

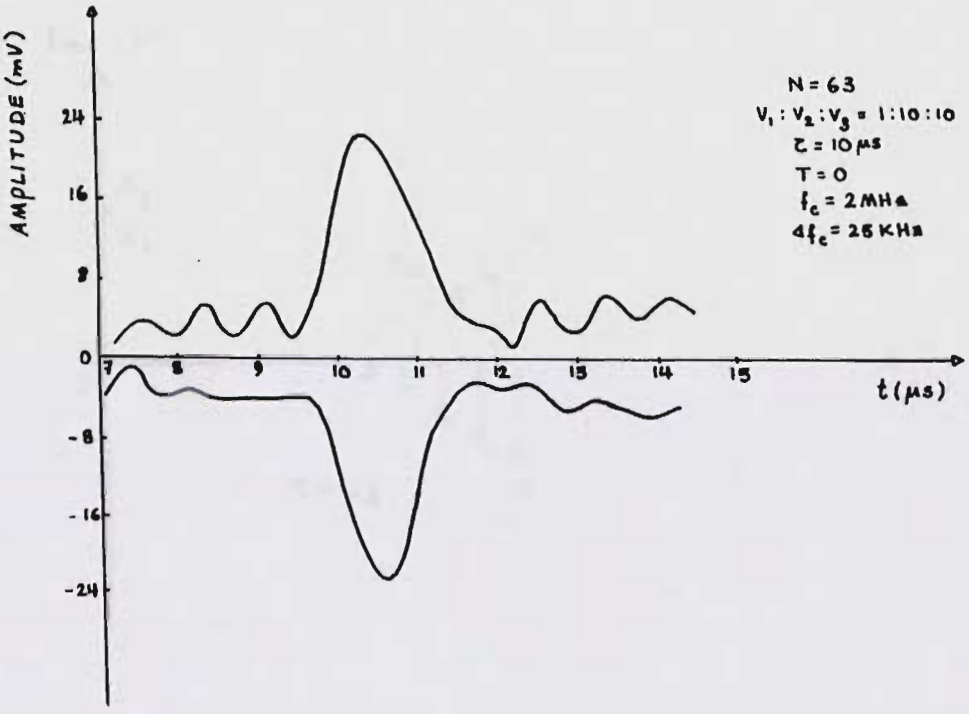

Figure 5.2. SPICE output showing 3-pulse memory echo (only envelope is shown).

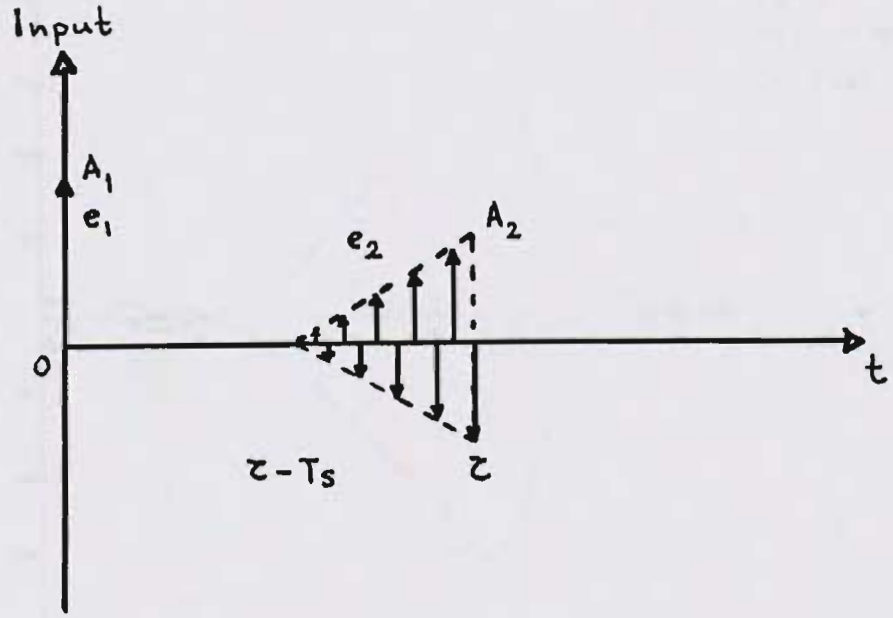

Figure 5.3. Input write-in sequence for non-time-inverted memory echo.

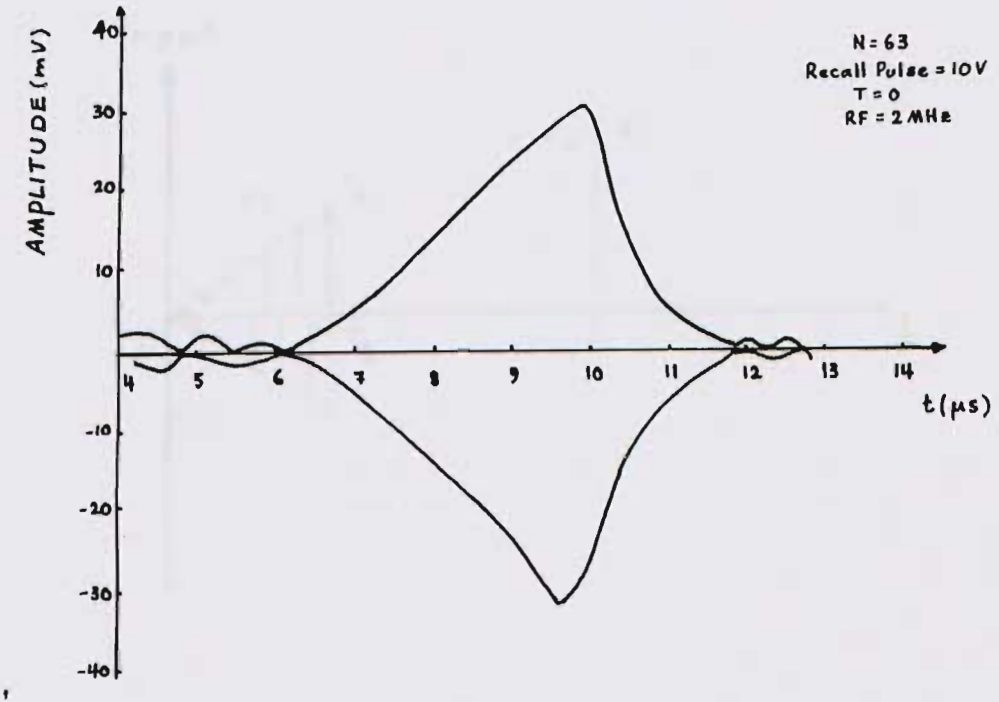

Figure 5.4. SPICE output for non-time-inverted memory echo (only envelope is shown).

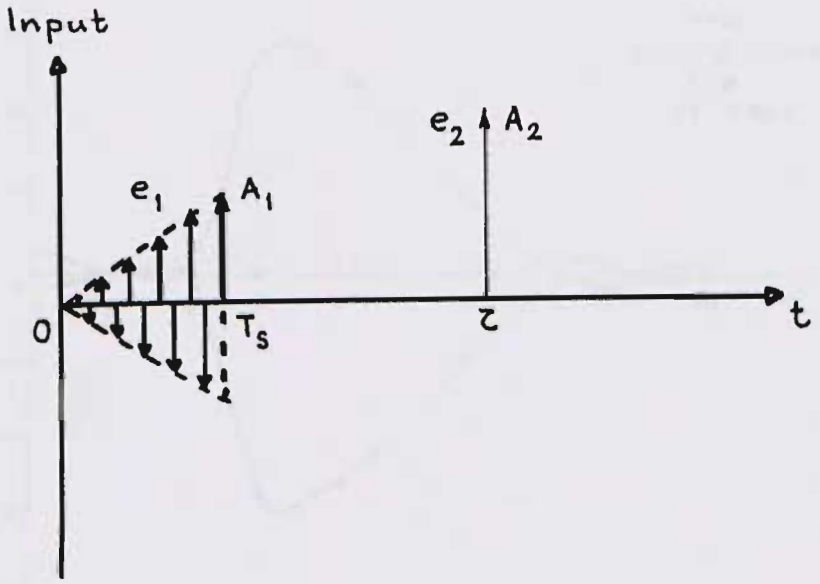

Figure 5.5. Input write-in sequence for time-inverted memory echo.

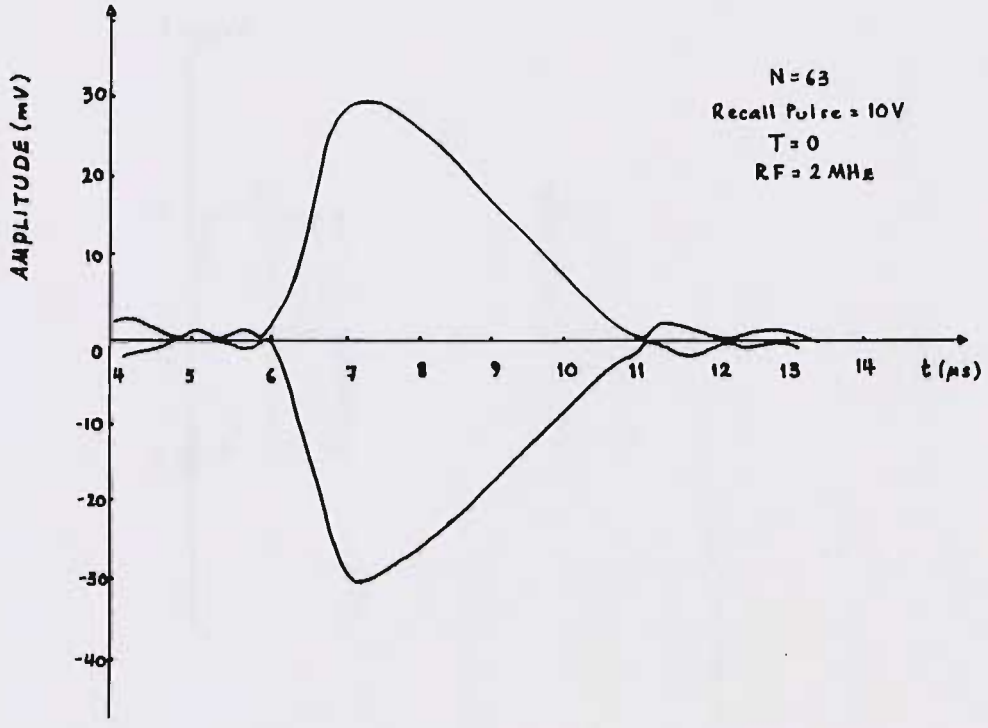

Figure 5.6. SPICE output for time-inverted memory echo (only envelope is shown).

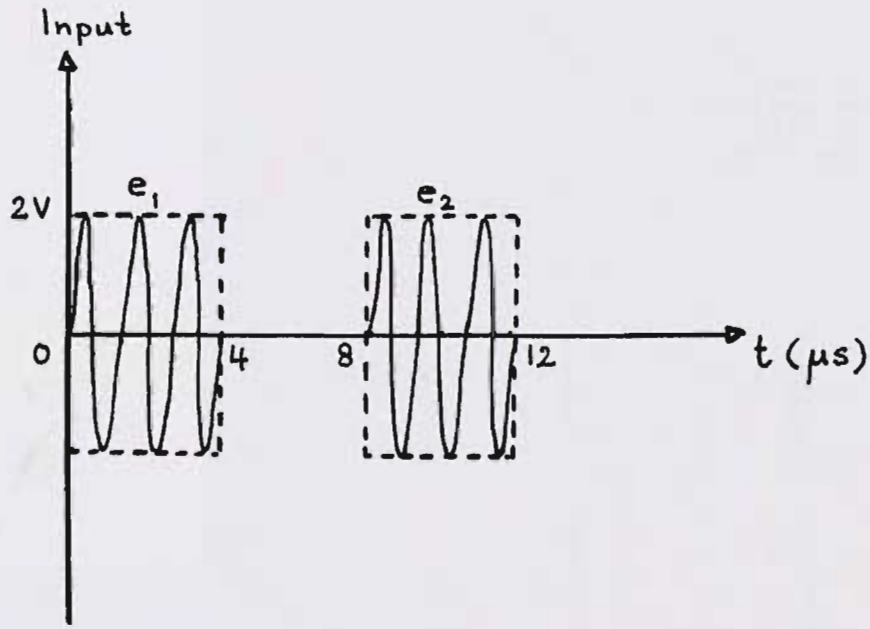

Figure 5.7. Input write-in
for static echo correlator.

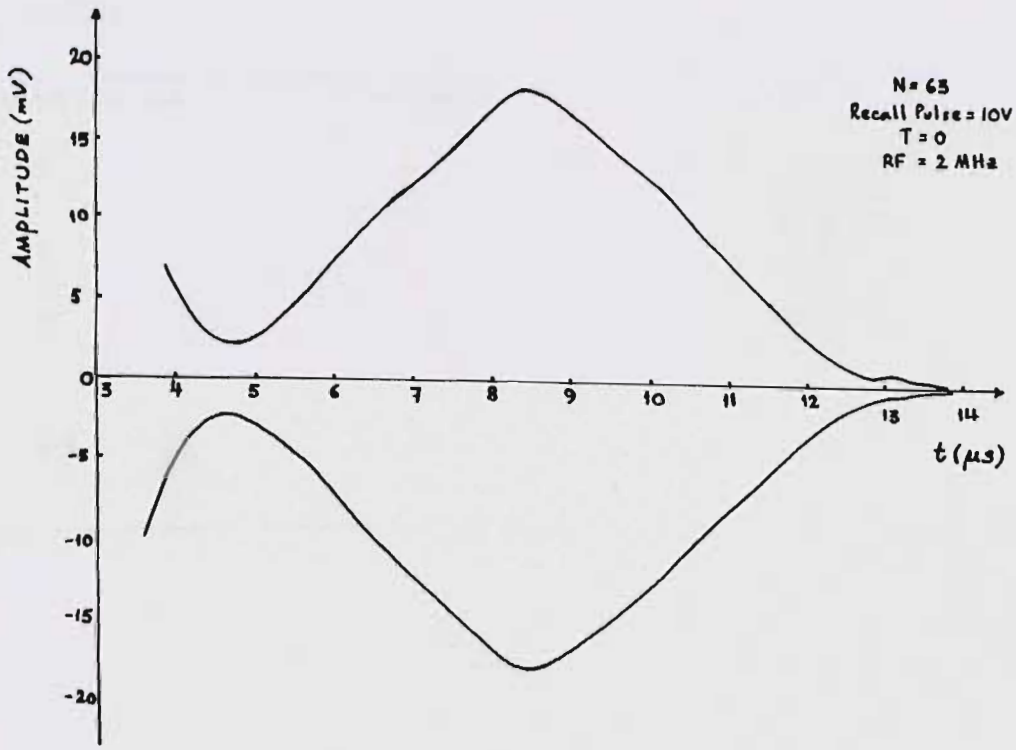

Figure 5.8. SPICE output for static echo correlator (only envelope is shown).

Table 5.1

Values of a_1 for 3-pulse memory echo write-in

N=63; f_c=2MHz; τ=10μs; $V_1:V_2$=1:10; Δf_c=25KHz.

Resonator no.	$\cos i\Delta\omega_c\tau$	$a_1(\omega_0)$
1	0	-833.32
2	-1	-666.66
3	0	-833.32
4	+1	-1000.0
5	0	-833.32
6	-1	-666.66
.	.	.
.	.	.
.	.	.
63	0	-833.32

Table 5.2

Values of a_1 for non-time-inverted memory echo write-in

Resonator no.	$\lvert V_{in}(\omega_0)\rvert^2 (V^2 sec^2)$	Normalized $\lvert a_1\rvert$
k	$\times 10^{-12}$	
1	.2278	120.5
2	.3728	197.2
3	.4117	217.8
4	.2585	136.8
5	.2044	108.1
6	.3609	191.0
7	.4278	226.3
8	.2708	143.2
9	.2001	105.8
10	.3700	195.8
11	.4510	238.6
12	.2627	139.0
13	.1643	86.93
14	.3806	201.4
15	.5251	277.8
16	.3107	164.4
17	.1361	72.0
18	.3496	185.0
19	.5408	286.1
20	.3067	162.2
21	.1055	55.8
22	.4424	234.1
23	.7953	420.8
24	.4669	247.0
25	.0085	5.3
26	.4335	229.4
27	1.32	698.4
28	1.286	680.4
29	.361	191.0
30	.1425	75.1
31	1.167	613.7
32	1.891	1000.0

$\lvert a_1\rvert_k = \lvert a_1\rvert_{(N+1)-k}$.

Table 5.3

Values of a_1 for time-inverted memory echo write-in

Resonator no.	$\lvert V_{in}(\omega_0)\rvert^2(V^2s^2)$ $\times 10^{-12}$	Norm. $\lvert a_1\rvert$
1	.4136	219.0
2	.3728	197.4
3	.2687	142.3
4	.1969	104.2
5	.2323	122.8
6	.3436	182.0
7	.4278	226.4
8	.4169	220.6
9	.3249	172.0
10	.2183	115.3
11	.1790	94.7
12	.2626	139.2
13	.4250	224.9
14	.5166	273.5
15	.4286	227.0
16	.2390	126.5
17	.1361	72.0
18	.2069	109.5
19	.3795	200.5
20	.5402	285.7
21	.5915	313.2
22	.4425	233.9
23	.1461	77.2
24	.0386	20.4
25	.4447	233.9
26	1.12	592.6
27	1.32	698.4
28	.7363	389.4
29	.0898	47.5
30	.3313	175.1
31	1.32	700.5
32	1.89	1000.0

$\lvert a_1\rvert_k = \lvert a_1\rvert_{(N+1)-k}$.

Table 5.4

Values of a_1 for static-echo correlator with two r.f. square pulses as input write-in

Resonator no.	Norm. $\lvert a_1 \rvert$	Resonator no.	Norm. $\lvert a_1 \rvert$
1	0.75	17	46.4
2	0.0	18	31.5
3	0.85	19	3.83
4	0.46	20	2.36
5	0.95	21	5.31
6	9.7	22	0.0
7	17.6	23	7.91
8	11.3	24	5.27
9	1.28	25	13.0
10	0.73	26	167.5
11	1.51	27	406.6
12	0.0	28	375.7
13	1.84	29	70.4
14	1.08	30	52.93
15	2.28	31	633.4
16	24.2	32	1000.0

$\lvert a_1 \rvert_k = \lvert a_1 \rvert_{(N+1)-k}$.

CHAPTER VI

CONCLUSION

In conclusion of this dissertation, we discuss in this chapter some of the observed merits and limitations of SPICE as a tool for computer circuit simulation. We discuss its feasibility in the context of the experiments detailed in the preceding chapters, and present an approximate speed and cost estimate. We also present an overview of the scope of electronic holography and the parametric formalism as a fundamental model which explains all nonlinear echo phenomena in general, and provides simple means of deriving convenient quantitative expressions (of the triple product type) that can be visualized and interpreted with greater clarity than other existing formalisms. The possibilities of using SPICE to predict other nonlinear physical phenomena are also overviewed.

VI.1 Transient Analysis on SPICE

The SPICE simulation program operates on the basis of short computation intervals (TMAX) over which it updates the voltages and currents at all the circuit nodes. Essentially, TMAX is the amount by which time is incremented to evaluate

the node voltages and currents after that increment. It is necessary, therefore, to make the intervals short enough to enable the program to follow the fastest variation of the input or the response at any node accurately. A convenient rule of thumb that appeared to work in our experiments was to have at least 50 computation intervals per cycle of the average carrier in the ensemble.

Another interesting factor observed was the plotting interval (TSTEP). (TSTEP is the time interval over which the SPICE output values are plotted, and is kept larger than TMAX to save space and time.) It was found that if the response is periodic, then if the number of points plotted per cycle is insufficient, the resulting waveform plotted may turn out to be periodic as well, with a different period altogether. In other words, depending on the number of samples plotted per cycle, one might end up with a "stroboscopic" effect by which the wave plotted becomes quite different from that intended. To avoid this situation, one needs simply to make TSTEP small enough to accommodate at least 10 samples per cycle.

In our SPICE experiments, TMAX and TSTEP were selected as follows :

$TMAX < T_c/50 = 1/50f_c = 10ns$, for $f_c = 2MHz$.

$TSTEP < T_c/10 = 50ns$, for $f_c = 2MHz$.

In general, the smaller we make TMAX and TSTEP, the more accurate are the computation and plot. However, there are severe limitations to making TMAX too small. If TMAX is made too small, the computation time and cost increase linearly. Even worse, below a certain value of TMAX, the computer runs out of available memory space. In our SPICE experiments with large resonator ensembles (N=101 or greater), the memory region was increased to 2000K (which is the maximum available). Even then, one could compute only 5μs of circuit time with a TMAX of 1ns.

As far as real time SPICE computation is concerned, we found that on the average, the time required for SPICE calculations with 21 linear resonators was less than 10 minutes for a circuit time of 85μs. For any other ensemble size and circuit time, the real computation time may be linearly extrapolated.

Thus, for 101 resonators, one would expect approximately 1 minute of computer time per microsecond of circuit time. However, for an arbitrary R.F. input, it was necessary to construct the input by using several piecewise linear (PWL) statements in the program. This construction was found to take several additional minutes. Thus, a 20μs circuit computation with a 4μs input took about 47 minutes of computer time.

As pointed out in the preceding chapters, the ensemble size for most of the SPICE experiments was kept well under 101. A size of 63 or so, it turned out, was sufficient to illustrate the properties of the nonlinear system under investigation. A far larger ensemble size was required of the nonlinear damping system (in the range of thousands), and this was beyond the existing SPICE capability.

For large ensembles with 500 or more nodes, SPICE often gave an "EXCEEDS ALLOCATED MEMORY OF 60,000" error message, even for relatively short circuit intervals of 0-5μs. The following facts about the available SPICE system were later discovered :

(i) Increasing the memory space on the //EXEC SPICE card by setting REGION=2000K or higher does not help, because the SPICE software capability is limited to 536K. To increase the capability would involve massive alterations in the program software.

(ii) One may define an approximate figure of merit by:

F=((TSTOP-TSTART)/TSTEP)*N, where N is the number of nodes,

which determines whether or not a given SPICE program would have the right memory capability. The experimental value of this figure of merit was found to be F<40,000.

(iii) If one is interested in the temporal evolution of the voltage at a node at a time much later than t=0, one can safely let TSTART to be any value without any memory problem. This is because the SPICE program will do computations from t=0 all the way to TSTOP for transient analysis, but will only store the data from TSTART to TSTOP, and discard the data from t=0 to TSTART. Hence, the critical determinant for memory limitations is the interval (TSTOP-TSTART). Based on the above, one may therefore run large networks over predetermined short intervals (TSTOP-TSTART) satisfying the figure of merit F.

It is interesting to note that a nonlinear coupling experiment with 101 resonators, which had not run from 0-5μs due to memory limitations, was run successfully in 2μs intervals from 15-17μs, 17-19μs,... upto 29-31μs. Not only were memory problems eliminated using this procedure, but the outputs were also fairly continuous over the intervals.

In most of the SPICE experiments, however, this procedure was not required. The ensemble size, as mentioned earlier, was kept reasonably small, and the upper limit of circuit time was kept close to 2τ. This kept the programs free from memory limitations, and the computation costs within 200 dollars or less for fairly large circuits.

Some of the observed memory and time limitations of SPICE may be circumvented by using more recent and updated versions of SPICE now available. However, the SPICE package available to us was sufficient for explaining the properties of nonlinear signal storage, and in fact, it provided results in some cases which were not theoretically predicted but were later verified to be physically accurate (such as instability in nonlinear capacitor circuits; the high level splitting of anharmonic echoes; and the very slow rise of the output in nonlinear coupling experiments when terminated by very large time constant filters). These findings attest to the high reliability of SPICE in accurately modeling *fairly complex circuits.*

VI.2 Scope of Electronic Holography as a General Model for Nonlinear Signal Storage

As stated in the Introduction, prior to the parametric interaction model based on electronic holography proposed by Korpel, there were several models in the nonlinear echo literature which attempted to explain various aspects of nonlinear echo behavior. Some of these were very well suited for dynamic echoes (such as the electroacoustic interaction model), predicting two-pulse as well as multiple echoes, and

even echo pulses with different frequencies than the applied R.F. Others offered useful descriptions of the possible mechanisms behind the generation of the memory echo (such as the orientation model and the dislocation nonlinearity model). However, most of these models appear to be inadequate in some respect, and do not explain both dynamic and static echoes under a common principle. Based on our SPICE modeling experiments, it appears safe to state that the parametric interaction model provides a single phenomenological scheme with which both types of nonlinear echoes (dynamic and static) may be described. Thus, dynamic echoes are the result of (typically) the modulation of a parameter of the system of resonators or eigenmodes at 2ω (for a cubic nonlinearity), brought about by phase conjugation. Static echoes, on the other hand, result from a permanent alteration of the resonator coupling constants following the write-in process, and are then regenerated by using a recall pulse in a manner similar to optical holography. Both phenomena, it turns out, may be described by appropriate triple product formalisms in time.

Another respect in which the parametric model goes beyond other existing models is that it may be extended to include more general write-in signals than pulses. This, as we have seen, not only leads to generalized storage and

recall of arbitrary signals, but also predicts the possibility of useful signal processing such as non-time-inverted and time-inverted recall, convolution and correlation of finite-duration signals.

As a final note, it needs to be stated that the parametric model provides very useful mathematical tools with which one may readily verify nonlinear echo phenomena, without having to resort to extremely complicated systems of vector and scalar nonlinear differential equations.

Considering the overall success of the SPICE experiments with nonlinear resonator circuits, one can extend its use to other nonlinear systems as well. Nonlinear transmission lines may be simulated to study the propagation of guided waves leading to such phenomena as solitary waves. SPICE could also be used to simulate certain nonlinear differential equations by setting up appropriate circuit models.

APPENDIX A

DERIVATION OF NONLINEAR LARGE SIGNAL CAPACITANCE

Starting with (2.1), we can show that:

$$i=dQ_c/dt=C_0 d(V-f(V))/dt=C_0(1-3a_3V^2)dV/dt. \tag{A.1}$$

Now, let

$$i=\mathrm{Re}(I_0 e^{j\omega t})=(1/2)I_0 e^{j\omega t}+(1/2)I_0^{*} e^{-j\omega t}, \tag{A.2a}$$

and,

$$V=\mathrm{Re}(V_0 e^{j\omega t})=(1/2)V_0 e^{j\omega t}+(1/2)V_0^{*} e^{-j\omega t}. \tag{A.2b}$$

Then, using (A.1), we have:

$$(1/2)(I_0 e^{j\omega t}+I_0^{*} e^{-j\omega t})=C_0(1-(3/2)a_3(V_0 e^{j\omega t}+V_0^{*} e^{-j\omega t})^2)\times$$
$$\times(1/2)(j\omega V_0 e^{j\omega t}-j\omega V_0^{*} e^{-j\omega t}). \tag{A.3}$$

Equating the coefficients of exp(jωt) in (A.3), we get:

$$I_0=j\omega C_0V_0-(3/2)a_3j\omega C_0V_0|V_0|^2+(3/4)a_3j\omega C_0V_0{}^*V_0^2$$

$$=j\omega C_0V_0-(3/4)j\omega C_0V_0a_3|V_0|^2 . \qquad (A.4)$$

Or, $(I_0/V_0)=j\omega C_{1s}=j\omega C_0(1-(3/4)a_3|V_0|^2)$. (A.5)

Hence, $C_{1s}=C_0(1-(3/4)a_3|V_0|^2)$, (A.6)

which is the required result.

APPENDIX B

STABILITY ANALYSIS FROM INJECTED CHARGE APPROACH

Starting from

$$f(V)=a_3V_{oi}^{\ 3}, \tag{B.1}$$

we can show that the charge in the capacitor is given by :

$$Q_i=C_0V_{oi}-C_0a_3V_{oi}^{\ 3}. \tag{B.2}$$

We next find :

$$dQ_i/dV_{oi}=C_0-3C_0a_3V_{oi}^{\ 2}=0. \tag{B.3}$$

This gives $V_{oi}^{\ 2}=1/3a_3$ at extremum. (B.4)

Also, $d^2Q_{oi}/dV_{oi}^{\ 2}=-6C_0a_3V_{oi}<0$, if a_3, $V_{oi}>0$. (B.5)

Hence the extremum is a maximum.

Using (B.4) in (B.1) we finally get :

$$Q_{imax}=C_0V_{oi}(1-a_3V_{oi}^{\ 2})=2C_0/(3(3a_3)^{1/2}). \tag{B.6}$$

APPENDIX C

VALIDITY OF APPROXIMATE TRANSFER FUNCTION AS $Q_0 \to \infty$

We are to show that :

$$j\omega L/(R(1-\omega^2 LC_0)+j\omega L) \to (\pi/RC_0)(\delta(\omega+\omega_0)+\delta(\omega-\omega_0)), \qquad (C.1)$$

where $RC_0 \to \infty$, and $\omega_0^2 = 1/LC_0$.

Let $f(t) \to F(\omega)$ be the input.

Then the system response will be :

$$V_0(t) = (1/2\pi) \int_{-\infty}^{\infty} F(\omega) j\omega L e^{j\omega t} /(R(1-\omega^2 LC_0)+j\omega L) d\omega. \qquad (C.2)$$

We can rewrite (C.2) as :

$$V_0(t) = (-1/2\pi RLC_0) \int_{-\infty}^{\infty} F(\omega) j\omega L e^{j\omega t} /(\omega^2 - \omega_0^2 - j\omega\omega_0/Q_0) d\omega. \qquad (C.3)$$

The integral in (C.3) has two complex poles. For simplicity, if we let $Q_0 \to \infty$ as $RC_0 \to \infty$ in (C.3), then the poles are determined easily as :

$$\omega_{1,2}=+\omega_0. \qquad (C.4)$$

Since these poles lie on the real axis, we can apply the Cauchy residue theorem to evaluate (C.3), using (C.4). This, after some algebra, leads to :

$$V_0(t)=(1/2RC_0)(F(\omega_0)e^{j\omega_0 t}+F(-\omega_0)e^{-j\omega_0 t}) . \qquad (C.5)$$

Next, if we use (2.26) to find $V_0(t)$, we get :

$$V_0(t)=(1/2\pi)\int_{-\infty}^{\infty}(\pi/RC_0)(\delta(\omega+\omega_0)+\delta(\omega-\omega_0))F(\omega)e^{j\omega t}\,d\omega.$$

Or,

$$V_0(t)=(1/2RC_0)(F(-\omega_0)e^{-j\omega_0 t}+F(\omega_0)e^{j\omega_0 t}), \qquad (C.6)$$

which is identical to (C.5).

Hence, in the limit as $Q_0\to\infty$, (2.26) is a valid approximation for (2.21).

APPENDIX D

RESPONSE TO ANHARMONIC NONLINEARITY

(a) Nonlinear response to two delta pulses

Using (2.38) in (2.39), we have :

$$V_{NL}(t)=(NW/W_b)\mathrm{Re}\Big(A_1\int_{\omega_c-W_b/2}^{\omega_c+W_b/2} e^{j\omega t}\, e^{-j\alpha a^2 t}\, d\omega$$

$$+A_2\int_{\omega_c-W_b/2}^{\omega_c+W_b/2} e^{j\omega(t-\tau)}\, e^{-j\alpha a^2 (t-\tau)}\, d\omega\Big) . \qquad (D.1)$$

Now, using (2.37b), we get :

$$e^{-j\alpha a^2 t} = e^{-j\alpha W^2 (A_1^2+A_2^2)t}\, e^{-2j\alpha W^2 A_1 A_2 t\cos\omega\tau}$$

$$= e^{-j\alpha W^2 (A_1^2+A_2^2)t}\, e^{-jb_1\cos\omega\tau} , \qquad (D.2)$$

and, similarly,

$$e^{-j\alpha a^2(t-\tau)} = e^{-j\alpha W^2(A_1^2+A_2^2)(t-\tau)} e^{-jb_2\cos\omega\tau} ,$$

(D.3)

where $b_1 = 2\alpha W^2 A_1 A_2 t$, (D.4a)

and $b_2 = 2\alpha W^2 A_1 A_2 (t-\tau)$. (D.4b)

Using (D.2) and (D.3) in (D.1), and using the identity :

$$e^{-jz\cos\phi} = \sum_{n=-\infty}^{\infty} (-j)^n e^{jn\phi} J_n(z) , \quad (D.5)$$

we obtain :

$$V_{NL}(t) = (NW/W_b)\mathrm{Re}\Big(A_1 e^{-j\alpha W^2(A_1^2+A_2^2)t} \times \sum_{n=-\infty}^{\infty} (-j)^n J_n(b_1) \int_{\omega_c-W_b/2}^{\omega_c+W_b/2} e^{j\omega(t+n\tau)} d\omega$$

$$+A_2 e^{-j\alpha W^2(A_1^2+A_2^2)(t-\tau)} \times \sum_{n=-\infty}^{\infty} (-j)^n J_n(b_2) \int_{\omega_c-W_b/2}^{\omega_c+W_b/2} e^{j\omega(t+(n-1)\tau)} d\omega\Big).$$

(D.6)

Now, eq.(D.6) can be rewritten as :

$$V_{NL}(t)=(NW/W_b)\mathrm{Re}\Big(A_1 e^{-j\alpha W^2(A_1^2+A_2^2)t}\sum_{n=-\infty}^{\infty}(-j)^n J_n(b_1)\times$$

$$\times\int_{-W_b/2}^{W_b/2} e^{j\omega(t+n\tau)}\, e^{j\omega_c(t+n\tau)}\, d\omega$$

$$+A_2 e^{-j\alpha W^2(A_1^2+A_2^2)(t-\tau)}\sum_{n=-\infty}^{\infty}(-j)^n J_n(b_2)\times$$

$$\times\int_{-W_b/2}^{W_b/2} e^{j\omega(t+(n-1)\tau)}\, e^{j\omega_c(t+(n-1)\tau)}\, d\omega\Big).$$

(D.7)

Carrying out the integrations in (D.7), we obtain :

$$V_{NL}(t)=NW\mathrm{Re}\Big(A_1 e^{-j\alpha W^2(A_1^2+A_2^2)t}\times$$

$$\times\sum_{n=-\infty}^{\infty}(-j)^n J_n(b_1)e^{j\omega_c(t+n\tau)}\,\mathrm{sincf}_b(t+n\tau)$$

$$+A_2 e^{-j\alpha W^2(A_1^2+A_2^2)t}\times$$

$$\times\sum_{n=-\infty}^{\infty}(-j)^n J_n(b_2)e^{j\omega_c(t+(n-1)\tau)}\,\mathrm{sincf}_b(t+(n-1)\tau)\Big),$$

(D.8)

which is the required result.

(b) Nonlinear response to general signal followed by a recall pulse

The four integrals in (2.55) are :

$$I_1=\mathrm{Re}\left((NWA_2/W_b)e^{j\omega_c(t-\tau)}e^{-j\alpha A_2^2 W^2(t-\tau)}\times\right.$$
$$\left.\times\int_{-W_b/2}^{W_b/2}e^{j\Omega(t-\tau)}d\Omega\right)$$
$$=NWA_2\cos(\omega_c(t-\tau)-\alpha A_2^2 W^2(t-\tau))\,\mathrm{sincf}_b(t-\tau). \qquad (D.9)$$

$$I_2=\mathrm{Re}\left((-j\alpha(t-\tau)NW^3/4W_b)A_2e^{j(t-\tau)(\omega_c-\alpha A_2^2 W^2)}\times\right.$$
$$\left.\times\int_{-W_b/2}^{W_b/2}|G(\Omega)|^2 e^{j\Omega(t-\tau)}d\Omega\right)$$
$$=(N\alpha W^3 A_2(t-\tau)/4W_b)\sin((\omega_c-\alpha A_2^2 W^2)(t-\tau))\times$$
$$\times\int_{-W_b/2}^{W_b/2}|G(\Omega)|^2 e^{j\Omega(t-\tau)}d\Omega. \qquad (D.10)$$

$$I_3=\mathrm{Re}\left(\left(-j\alpha(t-\tau)NW^3A_2^2/2W_b\right)e^{j(t-\tau)(\omega_c-\alpha A_2^2W^2)}\times\right.$$

$$\left.\times\int_{-W_b/2}^{W_b/2}G(\Omega)e^{j\Omega t}\,d\Omega\right)$$

$$=\left(N\alpha W^3A_2^2(t-\tau)\pi/W_b\right)\sin\left(\left(\omega_c-\alpha W^2A_2^2\right)(t-\tau)\right)g(t). \qquad (D.11)$$

$$I_4=\mathrm{Re}\left(\left(-j\alpha(t-\tau)NW^3A_2^2/2W_b\right)e^{j(t-\tau)(\omega_c-\alpha A_2^2W^2)}\times\right.$$

$$\left.\times\int_{-W_b/2}^{W_b/2}G^*(\Omega)e^{j\Omega(t-2\tau)}\,d\Omega\right)$$

$$=\left(N\alpha W^3A_2^2(t-\tau)\pi/W_b\right)\sin\left(\omega_c(t-\tau)-\alpha A_2^2W^2(t-\tau)\right)g(2\tau-t).$$

(D.12)

APPENDIX E

DERIVATION OF EQUATIONS (2.64A) AND (2.66)

(a) Derivation of eq.(2.64a) for anharmonic nonlinearity, one resonator

Under the assumption $A_2 >> A_1$, for $t > \tau^+$, (2.62) may be written as :

$$V_0(t) \sim (A_2/RC_0) e^{-(t-\tau)/2RC_0} u(t-\tau) \mathrm{Re}(e^{j(\omega_0+\Delta\omega)(t-\tau)}). \qquad (E.1)$$

Using (2.37) and (2.38) with the definitions (2.63a) and (2.63b), we can write :

$$e^{j(\omega_0+\Delta\omega)(t-\tau)} = e^{-j\alpha(A_1'^2 + A_2'^2)(t-\tau)} \times \sum_{n=-\infty}^{\infty} (-j)^n J_n(b) e^{j\omega_0(t+(n-1)\tau)}, \qquad (E.2)$$

where $b = 2\alpha A_1' A_2' (t-\tau)$. (E.3)

Using (E.2) in (E.1) we get :

$$V_0(t) \sim (A_2/RC_0)e^{-(t-\tau)/2RC_0}u(t-\tau)\times$$

$$\times \mathrm{Re}\left(e^{-j\alpha(A_1'^2+A_2'^2)(t-\tau)} \sum_{n=-\infty}^{\infty} (-j)^n J_n(b) e^{j\omega_0(t+(n-1)\tau)}\right),$$

(E.4)

which is the required result.

(b) Derivation of eq.(2.66) for anharmonic nonlinearity, N resonators

We first introduce m=-n+1 in (2.65), and replace the summation over n from n=-∞ to n=-1 in order to concentrate on the response centered in the region t>2τ.

Then (2.65) becomes :

$$V_{0,NL}(t) \sim (A_2/RC_0)e^{-(t-\tau)/2RC_0}u(t-\tau)\mathrm{Re}\left(e^{-j\alpha(A_1'^2+A_2'^2)(t-\tau)}\times\right.$$

$$\left.\times \sum_{i=1}^{N} \sum_{m=2}^{\infty} J_{1-m}(b)(-j)^{1-m} e^{j(\omega_c-((N+1)/2)\Delta\omega_c+i\Delta\omega_c)(t-m\tau)}\right).$$

(E.5)

Interchanging the summation in (E.5), we first write :

$$\sum_{i=1}^{N} e^{j(\omega_c-((N+1)/2)\Delta\omega_c+i\Delta\omega_c)(t-m\tau)} = e^{j(\omega_c-((N+1)/2)\Delta\omega_c)(t-m\tau)} \times$$

$$\times F(t-m\tau)e^{j((N+1)/2)\Delta\omega_c(t-m\tau)} .$$

$$= e^{j\omega_c(t-m\tau)} F(t-m\tau) , \qquad (E.6)$$

where F(x) is defined by (3.5b).

Using (E.6) in (E.5) we get :

$$V_{0,NL}(t) \sim (A_2/RC_0)e^{-(t-\tau)/2RC_0} u(t-\tau)\mathrm{Re}(e^{-j\alpha(A_1'^2+A_2'^2)(t-\tau)} \times$$

$$\times \sum_{m=2}^{\infty} J_{1-m}(b)(-j)^{1-m} e^{j\omega_c(t-m\tau)} F(t-m\tau)), \qquad (E.7)$$

which is the required result.

APPENDIX F

DERIVATION OF ANHARMONIC FREQUENCY SHIFT AND OTHER PARAMETERS FROM SPICE CIRCUIT MODEL

We have,

$$C_{ls}=C_0(1-(3/4)a_3|V_0|^2), \tag{F.1}$$

and, $$\Delta C=-(3/4)a_3|V_0|^2C_0. \tag{F.2}$$

Now, $$\omega_{ls}=(1/(L(C_0+\Delta C)))^{1/2}$$

$$=(1/LC_0)^{1/2}(1+\Delta C/C_0)^{-1/2} \tag{F.3}$$

$$\sim\omega_{ss}(1-\Delta C/2C_0), \text{ if } \Delta C<<C_0. \tag{F.4}$$

Hence, $$\Delta\omega=\omega_{ls}-\omega_{ss}=-(\Delta C/2C_0)\omega_{ss}. \tag{F.5}$$

Or, using (F.2), $$\Delta\omega=(3/8)a_3|V_0|^2\omega_{ss}. \tag{F.6}$$

Thus, if we let $$\Delta\omega=-\alpha a^2, \tag{F.7}$$

it immediately follows that :

$$\alpha=-(3/8)a_3\omega_i=\alpha(\omega_i) \ . \tag{F.8}$$

To derive the input instability criteria, we start with :

$$a_3|V_0|^2<0.25. \tag{F.9}$$

Let $Q_0=(1/2)I_0\Delta T$ (F.10)

be the input charge.

Using (F.10) in (F.9), and substituting $I_0=V_{in}/R$, we can show that :

$$V_{in}^2<R^2C_0^2/a_3\Delta T^2 \ , \qquad \text{(F.11)}$$

where V_{in} is the peak value of the input.

APPENDIX G

ESTIMATION OF PARAMETERS FOR SPICE NONLINEAR ECHO EXPERIMENT

The linear response amplitude at $t=2\tau$ can be obtained from (2.24) as :

$$V_L(2\tau)=(A_2/RC_0)e^{-\tau/2RC_0}F(\tau). \qquad (G.1)$$

The nonlinear amplitude at $t=2\tau$ can be written as :

$$V_{NL}(2\tau)\sim(-A_2N/RC_0)e^{-\tau/2RC_0}J_1((2\alpha A_1A_2\tau/R^2C_0^2)e^{-3\tau/2RC_0}). \qquad (G.2)$$

In order to ensure that the nonlinear echo can be seen above the tail of the linear response at $t=2\tau$, we must have :

$$|V_{NL}(2\tau)|>>|V_L(2\tau)| \ . \qquad (G.3)$$

This leads to :

$$J_1((2\alpha A_1A_2\tau/R^2C_0^2)e^{-3\tau/2RC_0})>>(1/N)F(\tau). \qquad (G.4)$$

We also need $A_2>>A_1$.

Let us denote the argument of J_1 in (G.4) as y.

Suppose $A_2=pA_1$. (G.5)

Using (F.8) and (F.11), we can write :

$$V_{in}^2<R^2C_0^2/(-8\alpha/3\omega_c)\Delta T^2. \quad (G.6)$$

Or, $$\alpha V_{in}^2<-3R^2C_0^2\omega_c/8\Delta T^2 \quad . \quad (G.7)$$

Putting $V_{in}=V_2$, and remembering that

$$V_2=2A_2/\Delta T, \quad (G.8)$$

we can rewrite (G.7) as :

$$|\alpha A_2^2|<|3R^2C_0^2\omega_c/32|=M. \quad (G.9)$$

Hence we need $|\alpha A_2^2|/M<1$. (G.10)

Typical Design Set

Let $\tau=T/3\sim14\mu s$.

Then $F(\tau)=\sin7\pi/\sin(\pi/3)=0$.

Thus, from (G.4), $J_1(y)>>0$.

Hence we can choose $0.631<y<1.84$.

Picking $y=0.631$, we get :

$e^{-3\tau/2RC_0}\sim0.708$, $e^{-\tau/2RC_0}\sim0.891$.

Now, we can write y as :

$$y=2\alpha A_2^2 \tau e^{-3\tau/2RC_0}/pR^2C_0^2 . \qquad (G.11)$$

Hence,

$$|\alpha A_2^2|=pR^2C_0^2 y/2\tau e^{-3\tau/2RC_0}. \qquad (G.12)$$

The R.H.S. of (G.12) is evaluated as :

$$|\alpha A_2^2|\sim 11.25\times10^{-5}p.$$

Since $M=(3/32)R^2C_0^2\omega_c=3.963\times10^{-3}$ sec for f_c=2MHz.

Hence, $|\alpha A_2^2|/M=2.83\times10^{-2}p<1.$

Or, $p<35.$

Choosing p=10, $V_2=10V_1=10V$, T=0.1μs, we get :

$$|\alpha|\sim 45\times10^{8}V^{-2}s^{-1}.$$

Hence, $|a_3|\sim 954.$

The above completes the calculation of design parameters.

APPENDIX H

ANALYSIS OF TIR ECHO IN NONLINEAR COUPLING CASE

(a) Time Inverted Recall of R.F. Square Wave

From the sampled r.f. square wave of Fig.3.8(b), we can show that there are a total of $(2(T/T_c)+1)$ input pulses, each of strength A_1.

Now, in order to find the appropriate 2-pulse nonlinear coupling echo component when the first pulse is applied at $t=iT_c/2$ (where i is an integer), and the second pulse at $t=\tau$, we first consider the following expression for the dependent source f(V) :

$$f(V)\propto a_3\left((A_1/RC)e^{-(t-iT_c/2)/T_d}\cos\omega_0(t-iT_c/2)\right.$$

$$\left.+(A_2/RC)e^{-(t-\tau)/T_d}\cos\omega_0(t-\tau)\right)^3. \qquad (H.1)$$

Pulling out the appropriate nonlinear term responsible for the 2-pulse echo, we get from (H.1) after some algebra :

$$f(V)\propto(3/2)a_3A_1A_2^2/R^3C_0^3)e^{-3(t-iT_c/6-2\tau/3)/T_d}\times\cos\omega_0(t-iT_c/2)(1+\cos2\omega_0(t-\tau)). \qquad (H.2)$$

Retaining the relevant term in (H.2), and assuming that the resonator ensemble rejects the $3\omega_0$ term, we obtain :

$$f(V)\propto(3/4)(a_3A_1A_2^2/R^3C_0^3)e^{-3(t-iT_c/6-2\tau/3)/T_d}\times$$

$$\times\cos\omega_0(t-2\tau+iT_c/2)\ . \qquad (H.3)$$

For N resonators with a frequency distribution given by :

$$\omega_j=\omega_c-((N+1)/2)\Delta\omega_c+j\Delta\omega_c, \qquad (H.4)$$

we obtain the macroscopic response to two pulses as :

$$V_0^{2p}(t)\sim(3/4)(a_3A_1A_2^2/R^3C_0^3)e^{-3(t-iT_c/6-2\tau/3)/T_d}\times$$

$$\times F(t-2\tau+iT_c/2)\cos\omega_c(t-2\tau+iT_c/2), \qquad (H.5)$$

where the superscript 2p refers to a two pulse echo.

For the actual TIR system, we need to sum (H.5) over all the pulses of the sampled signal. Thus, summing over i, we finally obtain :

$$V_0^{TIR}(t)\sim\sum_{i=0}^{2(T/T_c)}(-1)^i(3/4)(A_1A_2^2/R^3C_0^3)a_3\times$$

$$\times e^{-3(t-iT_c/6-2\tau/3)/T_d}F(t-2\tau+iT_c/2)\cos\omega_c(t-2\tau+iT_c/2),$$

$$(H.6)$$

which is the required result. Note that the factor $(-1)^i$ is used to account for the sign of the pulses.

(b) Time Inverted Recall of R.F. Sawtooth

From Fig.3.12(b), we can show that the amplitude of the ith sampling pulse is given by :

$$A_i = BV_p t/T \quad \text{(analog)}$$

$$= kV_p iT_c/2T, \quad i=0,1,\ldots,2T/T_c, \quad \text{(sampled)} \qquad \text{(H.7)}$$

where $B=\Delta T/2$ (ΔT=duration of pulse).

Thus, to obtain the TIR response to a sawtooth input, we need to modify eq.(H.6) as follows :

$$V_0^{TIR}(t) \sim \sum_{i=0}^{2T/T_c} (-1)^i (BV_p T_c/2T) i (3/4)(a_3 A_2^2/R^3 C_0^3) \times$$

$$\times e^{-3(t-iT_c/6-2\tau/3)/T_d} F(t-2\tau+iT_c/2)\cos\omega_c(t-2\tau+iT_c/2), \qquad \text{(H.8)}$$

which is the required result.

APPENDIX I

DERIVATION OF MACROSCOPIC NONLINEAR DAMPING RESPONSE

With the assumptions listed in chapter IV, we can express the output of the ith resonator as :

$$V_{0,nl}^{i} \sim (A_2/RC) e^{-t/RC} e^{\tau/RC} \times$$

$$\times e^{-\gamma(A_1'^2 + A_2'^2 + 2A_1'A_2'\cos\omega_{0,i}\tau)(t-\tau)} \cos\omega_{0,i}(t-\tau). \quad (I.1)$$

Next, assuming that $|2\gamma(t-\tau)A_1' A_2'| << 1$, (I.2)

we can expand part of the exponential in (I.1) to obtain :

$$V_{0,nl}^{i} \sim (A_2/RC) e^{-((1/RC)+\gamma(A_1'^2 + A_2'^2))(t-\tau)} \times$$

$$\times (1-2\gamma A_1'A_2'(t-\tau)\cos\omega_{0,i}\tau)\cos\omega_{0,i}(t-\tau), \quad (I.3)$$

retaining only the linear part of the expansion.

Defining P(t) and Q(t) as given by eq.4.23(a) and (b), we can rewrite (I.3) as :

$$V_{0,nl}^{i} \sim P(t)\cos\omega_{0,i}(t-\tau) - (1/2)Q(t)(\cos\omega_{0,i}t + \cos\omega_{0,i}(t-2\tau)). \qquad (I.4)$$

The overall macroscopic response for an ensemble of resonators is obtained by summing (I.4) over i. Thus, we have :

$$V_{0,nl} \sim P(t)\sum_i \cos\omega_{0,i}(t-\tau) - (1/2)Q(t)\sum_i \cos\omega_{0,i}t - (1/2)Q(t)\sum_i \cos\omega_{0,i}(t-2\tau) \ , \qquad (I.5)$$

which leads to the required result.

LIST OF REFERENCES

1. E.L.Hahn, "Spin Echoes," Phys.Rev., vol.80, no.4, pp.580-594, Nov.15, 1950.

2. N.S.Shiren, R.L.Melcher, D.K.Garrod, and T.G.Kazyaka, "Echo phenomena in piezoelectric crystals," Phys.Rev.Lett., vol.31, no.13, pp.819-821, Sept.24, 1973.

3. Ya.Ya.Asadullin, V.M.Berezov, V.D.Korepanov, and V.S.Romanov, "Anomalous relaxation of stimulated echo in piezoelectric crystals," JETP Lett., vol.22, no.5, pp.132-133, Sept.5, 1975.

4. K.Fossheim, K.Kajimura, T.G.Kazyaka, R.L.Melcher, and N.S.Shiren, "Dynamic polarization echoes in piezoelectric powders," Phys.Rev.B, vol.17, no.3, pp.964-997, Feb.1, 1978.

5. D.Cheeke, and A.A.Lakhani, "Orientation dependence of the memory echo in piezoelectric powders," Solid-State Commun., vol.25, no.5, pp.289-291, 1978.

6. A.Korpel, and M.Chatterjee, "Nonlinear echoes, phase conjugation, time reversal, and electronic holography," Proc.IEEE, vol.69, no.12, pp.1539-1556, December 1981.

7. R.M.White, "Energy echoes," J.Appl.Phys., vol.37, no.4, pp.1693-1696, March 1966.

8. R.G.Brewer, "Coherent optical transients," Phys.Today, vol.30, no.5, pp.50-59, May 1977.

9. R.L.Melcher, and N.S.Shiren, "New class of polarization echoes," Phys.Rev.Lett., vol.34, no.12, pp.731-733, Mar.24, 1975.

10. R.L.Melcher, and N.S.Shiren, "Polarization echoes and long time storage in piezoelectric powders," Phys.Rev.Lett., vol.36, no.15, pp.888-891, Apr.12, 1976.

11. A.Korpel, "A simple description and demonstration of parametric echoes," J.Appl.Phys., vol.49, no.12, pp.6125-6131, Dec.1978.

12. D.Gabor, "Holographic model of temporal recall," Nature, vol.217, p.584, Feb.10, 1968.

13. D.Gabor, "Improved holographic model of temporal recall," Nature, vol.217, pp.1288-1289, Mar.30, 1968.

14. H.C.Longuet-Higgins, "Holographic model of temporal recall," Nature, vol.217, p.104, Jan.6, 1968.

15. T.R.Meeker, and A.H.Meitzler in Physical Acoustics, W.P.Mason, Ed., vol.1, part A, chapter 2, Academic Press, New York, 1964.

16. N.N.Krainik, S.N.Popov, and G.A.Smolenskii, "Phonon (electroacoustic) echo in crystals," Sov.Phys.Acoust., vol.22, no.1, pp.83-84, Jan.-Feb., 1976.

17. R.L.Melcher, and N.S.Shiren, "Echo storage in piezoelectric powders," in 1975 Ultrason.Symp.Proc., IEEE Cat. no.75, CHO 994-4SU, pp.672-673.

18. A.R.Kessel, "On the mechanism of the long time phase memory in piezoelectric powders," Ferroelectrics, vol.22, no.1 & 2, pp.759-761, 1978.

19. A.Korpel, and V.Ramaswamy, "Ferroresonant effect caused by nonlinear capacitors," Proc.IEEE, vol.52, p.82, Jan. 1964.

20. J.W.Goodman, Introduction to Fourier Optics. New York: McGraw-Hill, 1968.

21. A.Yariv, Introduction to Optical Electronics, second edition. Holt, Rinehart and Winston, 1976.

22. K.Kajimura, K.Fossheim, T.G.Kazyaka, R.L.Melcher, and N.S.Shiren, "Dynamic polarization echo in powders," Phys.Rev.Lett., vol.37, no.17, pp.1151-1154, Oct.25, 1976.

23. S.N.Popov, N.N.Krainik, and G.A.Smolenskii, "Three pulse phonon (electroacoustic) echo with large relaxation time," JETP Lett., vol.21, no.9, pp.253-254, May 5, 1975.

24. V.M.Berezov, and V.S.Romanov, "Role of the dislocation mechanism in the polarization-echo phenomenon," JETP Lett., vol.25, no.3, pp.151-152, Feb.5, 1977.